Title

Phenotypic studies in mice deficient in methylenetetrahydrofolate reductase and methionine synthase and their use as models for the pathophysiology of vitamin B12 deficiency

Author

Wang, Nan

Publication Date

2009

Peer reviewed|Thesis/dissertation

Phenotypic studies in mice deficient in methylenetetrahydrofolate reductase and methionine synthase and their use as models for the pathophysiology of vitamin B_{12} deficiency

By

Nan Wang

A dissertation submitted in partial satisfaction of the

requirements for the degree of

Doctor of Philosophy

in

Molecular and biochemical nutrition

in the

Graduate Division

of the

University of California, Berkeley

Committee in charge:

Professor Barry Shane, Chair
Professor Nancy Amy
Professor Gary Firestone

Fall 2009

ABSTRACT

Phenotypic studies in mice deficient in methylenetetrahydrofolate reductase and methionine synthase and their use as models for the pathophysiology of vitamin B_{12} deficiency.

By

Nan Wang

Doctor of Philosophy in Molecular and Biochemical Nutrition
University of California, Berkeley
Professor Barry Shane, Chair

Vitamin B_{12} and folate are substrates and cofactors for various enzymes involved in one carbon metabolism, which is important for DNA/RNA synthesis, amino acid interconversions and the methylation cycle. Two enzymes, methylene-tetrahydrofolate reductase (MTHFR) and methionine synthase (MS) play pivotal roles determining the direction of one carbon flow. MTHFR catalyzes the intracellular synthesis of 5-methyl-THF from 5, 10-methylene-THF. MS is one of two B_{12}-dependent mammalian enzymes and catalyzes the remethylation of homocysteine to methionine and the concurrent demethylation of 5-methyl-THF to THF.

MTHFR knockout mice show a variable phenotype with reduced survival. The MS knockout is early embryonic lethal. MTHFR/MS double knockout mice survive and have similar phenotypes as MTHFR null mice, which proved that the MS null mice die from extreme folate deficiency due to a “methyl-folate trap”.

The common phenotypes shared by the MTHFR null and MS/MTHFR double null mice include retarded growth, hyperhomocysteinemia and a significantly low SAM/SAH ratio. Histological studies revealed cerebellum neuropathology and impaired male reproductive system in knockout mice. Microarray analysis showed that the expression of many genes was altered in MTHFR null and MS/MTHFR double null mice. Several subsets of induced or repressed genes encoded proteins involved in iron metabolism, lipid metabolism, SUMOylation, growth hormone/IGF pathway, stress responses, etc.

We also studied some of the consequences of vitamin B_{12} deficiency in wild type, MTHFR null and MS heterozygous mice. B_{12} deficiency resulted in increased plasma homocysteine, elevated plasma total cholesterol and triglyceride, and significantly up-regulated hepatic ApoC1 and ApoC3 expression in wild type and MS heterozygous mice. MTHFR null mice maintained lower plasma cholesterol and triglycerides, repressed hepatic ApoC1/C3 expression on both B_{12}-deficient and sufficient diets, despite their very high plasma homocysteine, which indicated that the elevated homocysteine was not responsible for the changes in blood lipid profiles found in B_{12}-deficient wild type or MS heterozygous mice.

Both folate deficiency and vitamin B_{12} deficiency can result in megaloblastic anemia, but the latter also causes subacute combined disease (SCD), a chronic demyelination disease, but its underlying mechanism is not understood. Although SCD occurs in B_{12} deficient humans and

other primates, it has never been observed in rodents placed on B_{12}-deficient diets. In animals with defective MS or MTHFR, the effects of B_{12} deficiency on myelin turnover were quantitatively studied by measuring the kinetics of synthesis and turnover of galactocerebroside (GalC), a myelin lipid, using a GC/MS stable isotope method. Vitamin B_{12} deficiency significantly decreased initial myelination rates in MS heterozygote and young wild type mice, and significantly inhibited remyelination after cuprizone-induced demyelination in adult MS heterozygotes and wild type mice. The MTHFR null mouse had a lower apparent remyelination rate compared with MS heterozygote and wild type mice, but remyelination in the MTHFR null was not affected by vitamin B_{12} deprivation.

We also investigated the effect of replacing folic acid with 5-methyl-THF in mice null for both MTHFR and MS. In this artificial "methyl folate trap" situation, MS/MTHFR double null mice developed megaloblastic anemia, and some of them showed a mild myelin defect with increased expression of TNF-α and NF-κB. The existence of megaloblastic macrocytic anemia and an early-phase neuropathy in MS/MTHFR double null mice fed on 5-methyl-THF implies that the accumulation of methyl-folate that occurs in the methyl folate trap plays a direct mechanistic role and is at least partly responsible for the development of both symptoms of vitamin B_{12} deficiency.

The final part of my study focused on differences in folate-related biochemical metabolites in inbred mouse strains and the identification of genes variants or modifier genes associated with these differences. Mouse brain and liver SAM and SAH, plasma homocysteine and cysteine, liver and plasma total folate were measured. Some showed significant differences among inbred mouse strains. Genomic loci associated with metabolite differences were identified by quantitative trait loci analysis and are now available for further scanning for modifier gene polymorphisms.

DEDICATION

I would like to sincerely thank my advisor, Dr. Barry Shane, for his guidance, support, and encouragement during my graduate studies at UC Berkeley. He has guided me to develop an independent thinking and provided a foundation for me to grow as a biologist. I would also like to thank my committee members, Dr. Nancy Amy and Dr. Gary Firestone, for reviewing my dissertation and providing valuable suggestions. My sincere thanks also go to Shane lab members, especially Dr. Su Yan and Dr. Lindsay Lee, as well as the undergraduate students, Yixiao Chen, Joanna Pak and Chris Chung, who have assisted me to finish this large amount of work. I also greatly appreciate people from Dr. Hellersteine lab for providing the method for stable isotope labeling and sharing the instruments, Dr. Stela Masle for helping with the folate-related genetic variances analyses and Dr. Seung-min Lee for generously supplied animal tissues of inbred mouse strains.

I am very grateful to my husband, Xiang Lu, and my father, Weijun Wang, for their love and support. Specially, I would like to delicate this work to my deceased mother, Lixin Han and wish her rest in peace.

TABLE of CONTENTS

LIST of ABBREVIATIONS

Ado-Cbl……5'-deoxyadenosyl cobalamin
AS…… association score
BHMT……...…betaine-homocysteine methyltransferase
BrdU……..…….5-bromo-2-deoxyuridine
Cbl ……cobalamin
CBS…….cystathionine β-synthase
CN-Cbl…… cyanocobalamin
CNS……...… central nervous system
CSF…….…… cerebrospinal fluid
DHFR…….. …dihydrofolate reductase
dNTP……deoxyribonucleotide triphosphate
dTMP……deoxythymidylate
dUMP…….deoxyuridylate
FAD……flavin adenine dinucleotide
FPGS……..folylpoly-γ-glutamate synthetase
GalC…….galactocerebroside
Hcy……...homocysteine
IF…….intrinsic factor
MAT……methionine adenosyltransferase
Me-Cbl……..methyl-cobalamin
MMA…….methylmalonyl CoA
MS…….methionine synthase
MSR……..methionine synthase reductase
MTHFD……..methylenetetrahydrofolate dehydrogenase
MTHFR……..methylene-tetrahydrofolate reductase
MUT…….....methylmalonyl CoA mutase
NTDs……neural tube defects
OH-Cbl…….hydroxocobalamin
PABA……..4-Aminobenzoic acid
PBS……...phosphate buffered saline
PLP……pyridoxal phosphate

$PteGlu_n$……...pteroylpolygultamic acid (with “n” glutamates)
QTL……quantitative trait locus
SAM……...S-adenosylmethionine
SAH……S-adenosylhomocysteine
SCD ……..subacute combined degeneration
SHMT……serine hydroxymethyltransferase
SNP……single-nucleotide polymorphism
TC II ……..transcobalamin II
TGX……total gastrectomy
THF……...5,6,7,8-tetrahydropteroylglutamate (tetrahydrofolate)
TS …….thymidylate synthetase

LIST of FIGURES

LIST of TABLES

INTRODUCTION

Folate and Vitamin B12: History and Chemistry

Folic acid is a water-soluble B vitamin. In 1931, Lucy Wills first found that liver and yeast extracts prevented anemia in pregnant women. Day, Stokstad and Manning independently reported an anti-anemia growth factor from yeast that was necessary for monkeys and chicks (Hoffbrand, 2001). This factor was first isolated from spinach and named "folic acid" (*folium*, Latin for leaf) by Mitchell and colleagues in 1941 (Mitchell, 1941). Stokstad isolated the pure crystalline folic acid in 1943, and identified its chemical structure as pteroylpolyglutamic acid (Stokstad, 1990).

Many reduced derivatives of folic acid occur in nature and biological systems, and folate is the generic name for all of them. Folate is composed of a pteridine moiety, a para-aminobenzoyl (PABA) moiety and one or more glutamic acid residues, as shown in Fig 1. The reduced derivative tetrahydrofolate (THF) is the bioactive form of folate, and accepts and donates one carbon moieties in one carbon metabolism. These can be attached at the N-5 and/or N-10 positions and can be at the oxidation state of methanol (5- methyl-), formaldehyde (5,10-methylene-) or formate (5- or 10-formyl-, 5,10-methenyl-). Folic acid, the oxidized form, does not occur naturally, and is only found in supplements and fortified foods. The active co-enzymatic forms of the folate are polyglutamate derivatives which can contain up to 11 glutamate residues in γ–peptide linkage (Foo, 1982). Polyglutamate chain lengths of three or greater are required for folate retention by tissues, while the pteroylmonoglutamate derivatives are the absorbed and transported forms (Shane, 1989).

Vitamin B12 is also a water-soluble B vitamin. The history of the discovery of vitamin B12 was related to efforts to treat a disease, pernicious anemia. Combe described the first case of pernicious anemia in 1824 and related it to a dysfunction of the digestive system. Later, clinical symptoms of pernicious anemia were described by Combe and Addison (Jacobs, 1959). Until the early 1900s, this disease was considering incurable. In 1925, George Whipple discovered that ingesting large amounts of liver greatly benefited the recovery from the anemia in dogs (Whipple, 1929). The next year, Minot and Murphy reported that water-soluble isolates of liver cured pernicious anemia in humans, for which they received the Nobel prize, and initiated studies on the presumed "anti-pernicious anemia factor" from liver extracts (Minot and Murphy, 1926). In 1948, Rickes, Smith and Parker, working separately, isolated vitamin crystalline B12 and the molecular structures of cobalamins were determined by Hodgkin and her team using X-ray crystallography in 1955 (Nockolds, 1967).

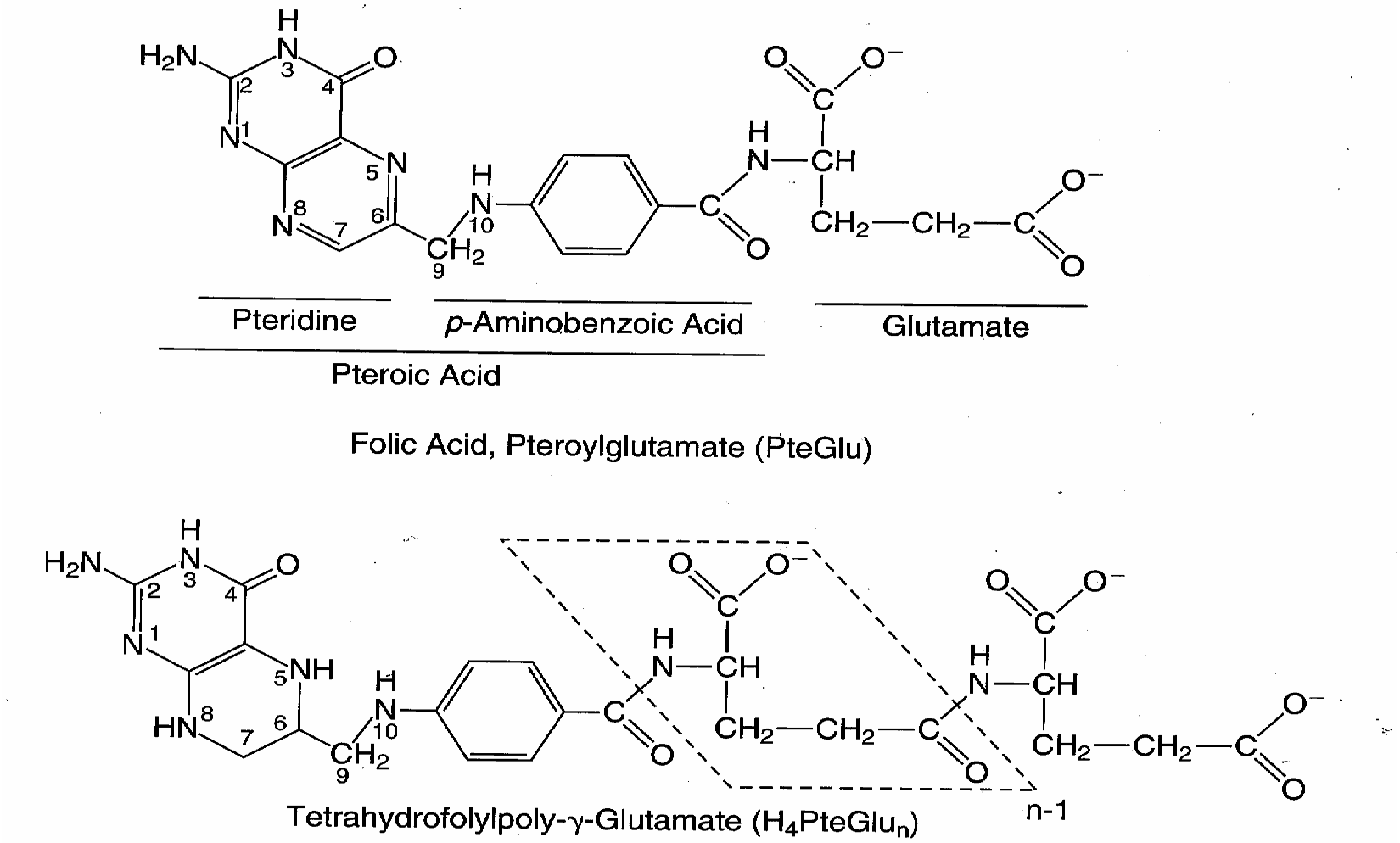

Figure 1. Structure of Folic Acid and THF-poly-Glutamate. One-carbon substitutions occur at N-5 or N-10 in folate derivatives.

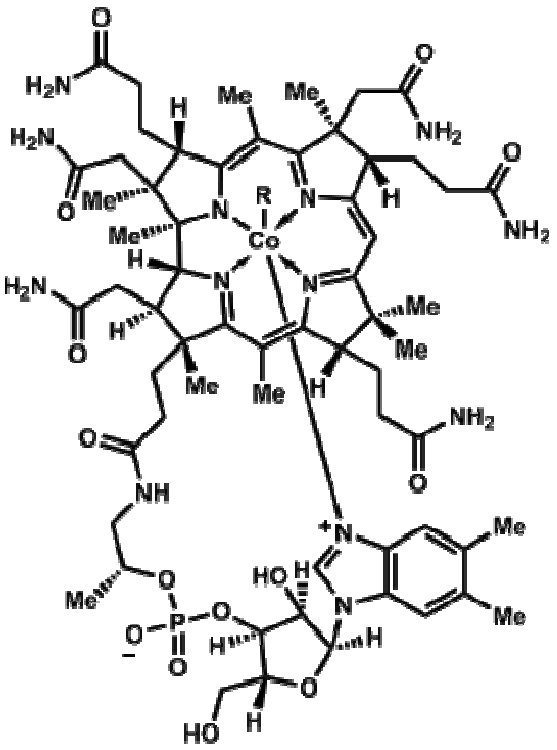

Figure 2. Structure of a cobalamin molecule. R = CN, OH, Me or 5'-deoxyadenosyl.

Vitamin B12 has the most complicated chemical structure among all vitamins, as shown in Fig 2. The structure is composed of a corrin ring bound to a central cobalt atom. A corrin ring is similar to the porphyrin ring found in heme, chlorophyll, and cytochromes (Roth, 1996). The central cobalt ion has six coordination sites: four of them are provided by the corrin ring, and the fifth by a dimethylbenzimidazole group (Bunge, 1956). The sixth coordination site is variable and therefore the center of reactivity. In cyanocobalamin, the common synthetic cobalamin found in fortified food and supplements, a cyano (-CN) moiety is bonded to cobalt. In mammalian cells, this cyano moiety can be replaced by a hydroxyl group (-OH), a methyl group (-Me) or a 5'-deoxyadenosyl group (-Ado). Me-Cbl and Ado-Cbl are the coenzyme forms.

Human absorption and transport of folate and vitamin B12

Folates are synthesized by microorganisms and plants, humans obtain folate from the diet. Most dietary folates are polyglutamate derivatives. Prior to absorption, polyglutamates are deconjugated to monoglutamates by a brush border γ-glutamylhydrolase (glutamate carboxypeptidase II, GCPII) (Devlin, 2000). In many other mammalian species, folylpolyglutamates are hydrolyzed by a soluble γ-glutamylhydrolase secreted from the pancreas and present in the intestinal juice (Rosenberg, 1976). Folates are charged molecules and their hydrophilic nature prevents them crossing the cell membranes by passive diffusion. Therefore, highly specific transporters are required to mediate intestinal folate absorption and the transport of folates into cells. A transmembrane protein, the reduced folate carrier (RFC; official gene symbol SLC19A1) had been recognized as the major intestinal transporter of folates for decades. RFC is a member of the solute carrier superfamily and an anionic exchanger; it transports folates

at physiological pH (Sirotnak, 1999). Recently, another folate transporter was identified – the proton-coupled folate transporter (PCFT; SLC46A1). PCFT also belongs to the solute carrier superfamily and functions better at an acidic pH (Zhao. 2009). Because the site of folate absorption, the duodenum and jejunum brush-border membranes, has an acid microclimate with a pH of 5.8–6.0, PCFT is now considered as playing the major role in intestinal folate absorption. Folic acid is transported across the intestinal mucosa as effectively as reduced folates, and PCFT has similar affinity for folic acid and reduced folates, while RFC is specific for reduced folates. Folate monoglutamates absorbed across the intestine enter the portal circulation and are transported to the liver, where they are metabolized to polyglutamates and retained or are metabolized to 5-methyltetrahydrofolate (5-methyl-THF) monoglutamate and released into the systemic circulation and distributed to systemic tissues. Because of this metabolism and release, 5-methyl-THF is the predominant folate in plasma. RFC is the predominant transmembrane carrier in peripheral tissues, while a subset of tissues, including the liver, also expresses PCFT. Some tissues also express a folate receptor, also known as folate binding protein, which mediates folate internalization by endocytosis (Salazar, 2007). Four isoforms of the folate receptor have been identified, encoded by separate genes.

Once transported into tissues, 5-methyl-THF is metabolized to THF. THF is a good substrate for the enzyme folylpolyglutamate synthetase (FPGS), which catalyzes the conversion of folates to polyglutamate derivatives.

Cobalamins are exclusively synthesized by microorganisms and dietary B12 is almost exclusively obtained from animal products. The absorption of cobalamins is complicated and involves multiple factors. Protein bound cobalamins are released in the stomach by the action of pepsin and gastric acid. Free cobalamins are then bound to R-proteins to form a B12-R protein complex (Sourial, 1992). Gastric parietal cells secrete another important factor, a glycoprotein named intrinsic factor (IF). In the duodenum, the B12-R-protein complex is digested by proteases. B12 is released and then binds to IF and form a B12-IF complex (Festen, 1991). The formation of this complex is critical for B12 absorption because IF is recognized by a receptor (cubulin) located at the distal end of the ileum (Seetharam, 2003). This receptor only recognizes the B12-IF complex, not B12 itself. Classical pernicious anemia results from an autoimmune disease that destroys parietal cells in the stomach, the cells that produce IF and stomach acid.

The receptor bound B12-IF complex enters the intestinal mucosal cell by endocytosis and the B12 disassociated from IF under the acidic conditions of the endosome and lysosome. B12 is transported out of the lysosome by a specific transporter and is subsequently bound to transcobalamin II (TC II). TC II and other proteins, such as haptocorrin (HC, also referred to as transcobalamin I, TC I) facilitate the transport of cobalamins in blood to various tissues (Russell-Jones, 1999). Although most of the circulating B12 is associated with TC I, B12 associated with TC II is removed from the circulation much more rapidly and TC II is the major provider of B12 to tissues. The TC-II/B12 complex is taken up into cells by receptor-mediated endocytosis. Megalin has been identified as the TCII receptor as it recognizes the TC II/B12 complex and internalizes it (Barth, 2001). Although megalin, which has a wide specificity for protein ligands, may be involved in B12-TCII uptake in fetal tissues and some adult tissues, a specific TCII receptor, which appears to be the major one in adult tissues, has recently been identified (Quadros, 2009). Within the cell, the B12-TC-II complex is degraded within lysosomes, and free

cobalamin is released and converted into either Me-Cbl in the cytosol or to Ado-Cbl in the mitochondria, the two important cofactors for mammalian cells.

Absorption of dietary vitamin B12 requires good coordination of stomach, pancreas and small intestine. Any problem with one of these organs may result in a vitamin B12 deficiency. While the incidence of classical pernicious anemia in the elderly, as assessed by circulating antibodies to intrinsic factor has been estimated at 2-5 percent, malabsorption of B12 is quite common in the elderly, and has been estimated to range from 5-40 %, depending on the diagnostic procedure used, and undiagnosed B12 deficiency is remarkably common in this age group (Baik, 1999).

Gastric parietal cell atrophy, which also leads to decreased acid production, is very common in the elderly, often caused by *H. pylori* infection; therefore, elderly have a particularly high risk for B12 deficiency (Whittingham, 2005). In many cases the problem is an inability to absorp food B12 and the absorption of crystalline B12, the form found in fortified foods, is normal.

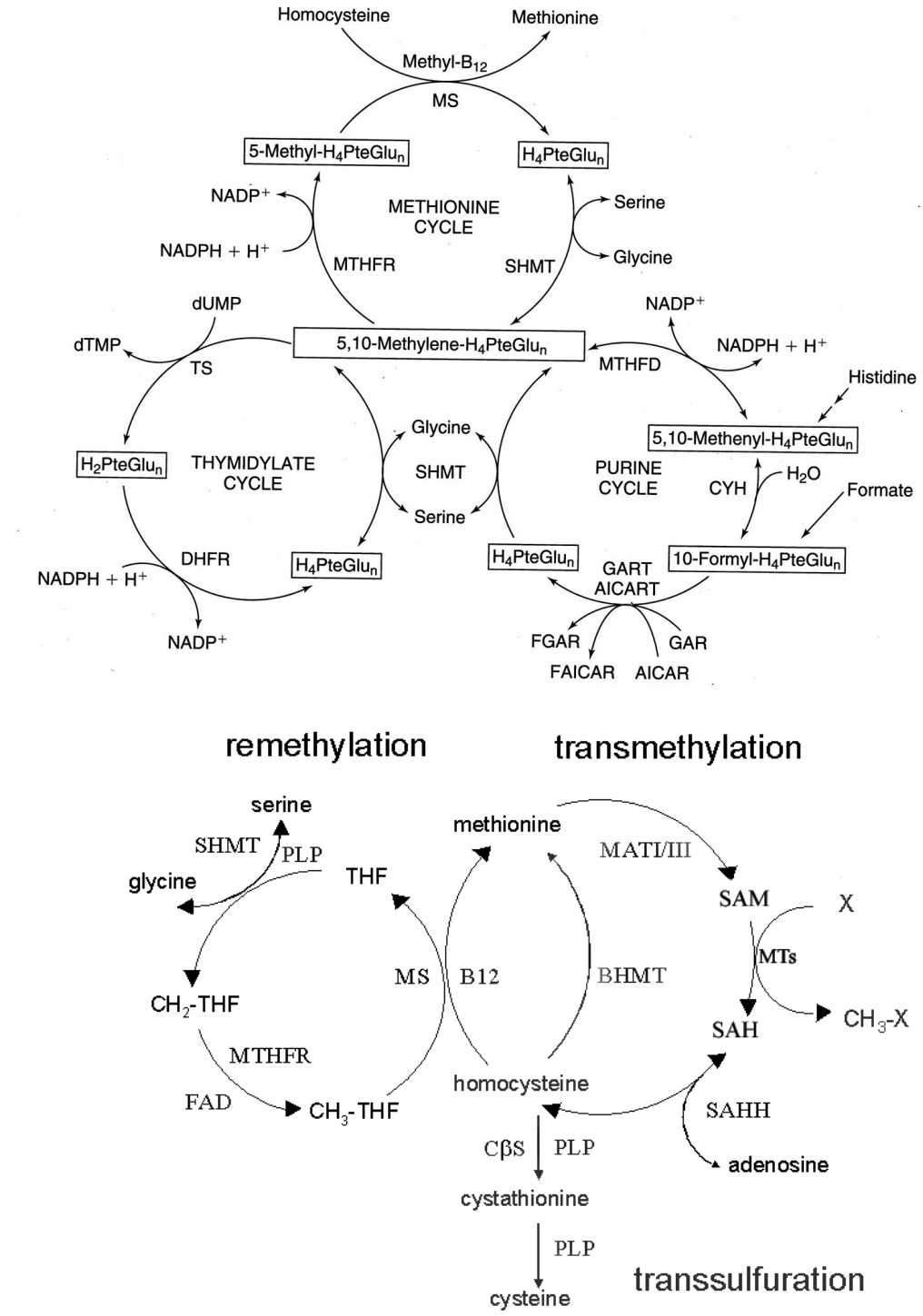

Figure 3. Metabolic reactions of folate-mediated one-carbon metabolism. MS: methionine synthase; MTHFR: methylene-tetrahydrofolate reductase; SHMT: serine hydroxymethyltransferase; TS: thymidylate synthetase; DHFR: dihydrofolate reductase; MTHFD: methylenetetrahydrofolate dehydrogenase; CYH: methenyltetrahydrofolate cyclohydrolase; GAR: glycinamide ribonucleotide; AICAR: aminoimidazole

carboxamide ribonucleotide; FGAR: formylglycinamide ribonucleotide; FAICAR: formylaminoimidazole carboxamide ribonucleotide; GART: GAR formyltransferase; AICART: AICAR formyltransferase; MATI/III: methionine adenosyltransferase I/III; SAM: adenosylmethionine; SAH: adenosylhomocysteine; CBS: cystathionine β-synthase; MT: methyltransferase; BHMT: betaine-homocysteine methyltransferase; SAHH: adenosylhomocysteine hydrolase.

Folate and Vitamin B12 functions

Folate and nucleotide synthesis

Folate is necessary for DNA synthesis because it is required for synthesis of purines and the conversion of dUMP to dTMP. 10-Formyl-THF is the one-carbon donor for the C-2 and C-8 positions of the purine ring; the reactions are catalyzed by AICART and GART, respectively. Thymidylate synthetase catalyzes the transfer of the one-carbon group from 5,10-methylene-THF to the 5'-position of dUMP and its reduction to a methyl group to generate dTMP.

Because dNTPs are the substrates for DNA polymerases and have short half-lives, the fidelity of DNA replication and repair synthesis is critically dependent on maintenance of the correct balance of dNTPs. During folate deficiency, an imbalance in dNTP pools can delay replication fork progression, induce uracil misincorporation and promote genomic instability. Excessive incorporation of uracil in DNA not only leads to point mutations, but may also result in the generation of single- and double-stranded DNA breaks, chromosome breakage, and micronucleus formation (Blount, 1994).

Folate and methylation

The methylation of homocysteine to reproduce methionine requires 5-methyl-THF as the methyl donor. The reaction is catalyzed by methionine synthase (MS; EC 2.1.1.13), a vitamin B12-dependent enzyme. 5-Methyl-THF is generated from 5,10-methylene-THF, catalyzed by methylene-tetrahydrofolate reductase (MTHFR; EC 1.5.1.20). The remethylation of homocysteine to methionine is important for the synthesis of S-adenosylmethionine (SAM). SAM serves as the proximal methyl donor for more than 100 methylation reactions. Cellular methyl acceptors include phospholipids, proteins, histones, neurotransmitters, RNA and DNA.

DNA methylation has received wide attention, because of its close relationship with chromatin structure and segregation and gene expression. DNA methylation is a conspicuous feature of vertebrate genomes. Approximately 4% of total cytosines are methylated, representing about 5×10^7 5-methylcytosine (5-mC) residues per diploid nucleus. All 5-mC is present in the dinucleotide CpG, although only 70-80% of the potentially methylatable sites are actually in a methylated form (Cooper, 1989). DNA contains short stretches in which the frequency of the CG sequence is higher than other regions called CpG islands. CpG islands are consistently nonmethylated and they are often located around the promoters of housekeeping genes or other genes frequently expressed in a cell (Bird, 1992). Also, because of the existence of a maintenance methylase, the DNA methylation pattern can be inherited from parent cells to the daughter cells, which allows each type of cell to have its own methylation pattern so that a unique set of proteins may be expressed to perform functions specific for this cell type (Li, 1993). In human tumors, global DNA hypomethylation and transcriptional silencing of tumor

suppressor genes by CpG island promoter hypermethylation has been widely identified, such as cell-cycle inhibitor $p16^{INK4a}$; the p53-regulator $p14^{ARF}$; the DNA repair genes hMLH1, BRCA1 and MGMT; the cell-adherence gene E-cadherin and the estrogen and retinoid receptors (Supić, 2009; Murao, 2006; Kim, 2004).

Both DNA synthesis and DNA methylation patterns affect DNA and chromosome stability. Folate-sensitive fragile sites were initially found as chromosomal fragile sites that contain nonrandom breaks and gaps, which appear in metaphase chromosomes under cell culture conditions that induce folate depletion and dNTP imbalance (Butler, 1988). A rare folate-sensitive fragile site on the X chromosome is a major genetic cause of mental retardation (Ho, 1988). These fragile sites are unstable, showing increased recombination, translocations, sister chromatin exchanges, and intrachromosomal gene amplification and deletions (Reidy, 1988).

Folate and Serine-Glycine interconversion

Serine hydroxymethyltransferase (SHMT), a PLP-containing enzyme, catalyzes the reversible conversion of serine to glycine, along with the transfer of formaldehyde to THF to generate 5,10-methylene-THF. There are two isozymes of SHMT in mammalian tissues, one in the cytosol and one in the mitochondria, and they are encoded by separate genes. Recent studies suggest that mSHMT is mainly responsible for supplying the β-carbon of serine that is used as the one-carbon source for folate metabolism, while the cSHMT more likely plays a role to generate serine from glycine for gluconeogenesis in the liver and kidney (Gregory. 2000). Some of the cSHMT is associated with a complex that translocates to the nucleus during the S phase of the cell cycle together with other enzymes involved in thymidylate synthesis (Woeller, 2007).

Metabolic functions of vitamin B12

There are only two mammalian enzymes known to require vitamin B12 as a cofactor, methylmalony CoA mutase and methionine synthase.

Mitochondrial methylmalonyl CoA mutase (MUT; EC 5.4.99.2) requires adenosylcobalamin (Ado-Cbl) as cofactor. This mutase catalyzes the isomerization of methylmalonyl CoA (MMA) to succinyl CoA, the final step in the metabolism of propionate to succinyl CoA. Propionyl CoA is derived from the catabolism of branch chain amino acids, the catabolism of odd chain fatty acids, and from fermentation of fiber in the gut.

Vitamin B12 and methylation

A second enzyme that requires vitamin B12 as the cofactor is cytoplasmic methionine synthase (MS). As described previously, MS catalyzes the methylation of homocysteine to methionine with simultaneous conversion of 5-methyl-THF to THF and uses Me-Cbl as its cofactor for this reaction. MSs are highly conserved, large (about 140-kDa) monomeric Zn metalloproteins and consist of three domains: a catalytic domain that contains the binding sites for 5-methyl-THF and homocysteine; a B12 domain, where the MeCbl cofactor is tightly bound; and an activation domain (Chen, 1997). MS is essential for the provision of SAM, the universal donor of methyl groups, as well as the provision of THF for use in nucleotide synthesis, which is

critical for folate metabolism. In this regard, vitamin B12 is required by all biofunctions of folates.

Folate - vitamin B12 interrelationships: "Methyl folate trap" hypothesis

Two of the enzymes mentioned previously, MTHFR and MS, are the pivotal enzymes explaining the interrelationship of folate and vitamin B12 deficiency by the "methyl folate trap" hypothesis. This hypothesis was first advanced in early 60's by two independent groups (Noronha, 1962; Herbert, 1962) to explain the identical anemia of folate and B12 deficiency and postulates that B12 deficiency induces a functional folate deficiency. This hypothesis postulates that in B12 deficiency, methionine synthase, the enzyme which converts 5-methyl-THF into THF, is inactive; while MTHFR, the enzyme that catalyzes the biosynthesis of 5-methyl THF is thermodynamically irreversible in vivo, because of a high ratio of cytosolic NADPH/$NADP^+$, as well as a lack of SAM allosteric inhibition on MTHFR (Kutzbach, 1967). Thus all folates are trapped as 5-methyl-THF leading to a lack of cofactors for other folate-dependent reactions, such as purine and dTMP synthesis. Also, as 5-methyl-THF is a very poor substrate for folylpoly-γ-glutamate synthetase (FPGS), cellular folate retention is decreased, leading to an absolute folate deficiency in tissues (Chen, 1996). The final result of the "methyl folate trap" is severe deficiency of active folate and abortive DNA synthesis, which has been ascribed to uracil misincorporation into DNA (Metz, 1968).

Folate and vitamin B12 deficiency

Because the important role of folate in DNA/RNA synthesis, its deficiency especially impairs fast growing cells, such as erythroid cells and cells in the GI tract. In humans and other primates, folate deficiency leads to impaired cell division and causes a megaloblastic, macrocytic anemia. Fast growing cancer cells have a high requirement for folate, so folate antagonists that impair folate metabolism, such as methotrexate (MTX), have been found widespread clinical use as anti-cancer agents for years (Hitchings, 1965).

Folate deficiency also increases chromosome instability and gene mutations. Many epidemiological studies have suggested that individuals who had a low dietary intake of folate had a higher risk of developing cancers, such as breast cancer and colorectal cancer, etc, compared to those with sufficient folate intake (Sellers, 2001; Sanderson, 2007).

It has been suggested for decades that inadequate maternal folic acid status is associated with a higher incidence of neural tube defects (NTD) of newborns (Butterworth, 1996). NTDs are the major birth defect in humans, and occur when the spinal cord fails to close properly during the fourth week of gestation. The clinical manifestation is spina bifida or anencephaly. It has been reported that peri-conceptual supplementation with folic acid significantly reduces the incidence of NTD, by greater than 70 percent (Locksmith, 1998). It is thought that a subset of women is prone to this condition because they have a higher folate requirement in pregnancy, as folate deficiency per se will not induce NTDs. Therefore, to lower the incidence of NTDs, the Food and Drug Administration (FDA) mandated the folate fortification of all enriched grain products in the United States by January 1998 (Rader, 2002).

Poor folate status also increases body homocysteine levels directly. Homocysteine has received considerable attention recently as mild hyperhomocysteinemia was found to be a risk factor for fetal neural tube defects (NTD) and cardiovascular disease (Selhub, 2008). Hyperhomocysteinemia has pathogenic effects on the vasculature, including toxicity to the vascular endothelium, enhanced proliferation of smooth muscle cells, thrombogenic effects and an increase in oxidative stress (Lentz, 2005).

Patients suffering from vitamin B12 deficiency develop pernicious anemia, which has two major symptoms, macrocytic anemia which is hematologically indistinguishable from folate deficiency, and neurological complications. Large doses of folate can cause hematological remission in these patients, as the macrocytic anemia of B12 deficiency is caused by a secondary folate deficiency. However, folate supplementation fails to correct the neurological lesions due to prolonged vitamin B12 deprivation. Subacute combined degeneration (SCD) of the spinal cord is a hallmark of B12 neuropathy and demyelination is a major pathological sign (Metz, 1992). The mechanism behind the neurological manifestations of B12 deficiency is not understood, and has been a major focus of my research.

Neurological manifestations of B12 deficiency

Several experimental animal models have been used to investigate the B12 deficiency neuropathy, including the monkey, fruit bat and pig. Studies have involved dietary deprivation of Cbl or repeated N_2O exposure, or by a combination of both (Dinn, 1978; Duffield, 1990; Weir, 1988). Pathological demyelination in the spinal cord similar to human SCD has been successfully induced in these animals. However, rodents do not develop a neuropathology (or anemia) on a B12-restricted diet, possibly because it is very difficult to completely remove B12 from the diet or to prevent B12 utilization from gut microbial synthesis in rodents. The only reported similar neuropathy as human SCD in rodents was induced by total gastrectomy in rats (Scalabrino, 1990). This extreme model eliminates gastric production of intrinsic factor which is required for B12 absorption, but also affects the digestion and absorption of many other nutrients, as discussed later.

Studies have also been done targeting enzymes involved in B12 absorption and transportation. Cubilin is the endocytic receptor for the intrinsic factor-B12 complex. A null mutation in cubilin caused early embryonic lethality, due to failures in visceral endoderm and somite formation (Smith, 2006). However, even if cubilin null mice had survived through embryonic development, they would still not be a suitable model for B12 deficiency because of cubilin's multiple functions: besides the intrinsic factor-B12 complex, cubilin is a receptor for apolipoprotein A-I (apoA-I)/high density lipoprotein (HDL), albumin, transferrin, vitamin D-binding protein and other proteins (Barth, 2001).

All current animal models are only partially useful for studying B12 deficiency effects and are not practical for addressing the underlying mechanism of B12 neuropathy.

Research has also been focused on the only two mammalian enzymes known to use B12 as a co-enzyme: MUT and MS. The question, which of these two enzymes plays a pivotal role in the neurological manifestation of B12 deficiency, has been debated over decades. The possibility

that B12 plays additional and thus far unrecognized roles can also not be excluded.

Some researchers studied the correlation between demyelination and the increase in methylmalonyl-CoA caused by methylmalonyl-CoA mutase dysfunction. Methylmalonyl-CoA (MMA) is a competitive inhibitor of malonyl-CoA in fatty acid biosynthesis and can substitute for malonyl-CoA in fatty acid biosynthesis (Frenkel, 1974). Because the myelin sheath is in continual flux, the MMA-induced inhibition of fatty acid synthesis may result in the eventual destruction of the sheath. Incorporation of MMA into fatty acids results in branched-chain fatty acids being produced that may severely alter the architecture of the normal membrane structure of nerve cells. However, this Adenosylcobalamin Hypothesis is at odds with observations on children with inherited Methylmalonic Aciduria (Rosenblatt, 1990). These children have inherited mutations of Ado-Cbl synthesis (CblA and CblB mutants) and accumulate MMA. They usually manifest muscular hypotonia and mental retardation, but demyelination typical of Cbl neuropathy is not observed.

Other evidence strongly suggests that MS is the locus responsible for the neuropathy and defective methylation may be the direct cause. First, fruit bats and monkeys treated with nitrous oxide, which inactivates MS, develop SCD of the spinal cord, and the onset of SCD can be delayed by concomitant methionine administration (Dinn, 1978). Second, inhibition of myelin basic protein (arginine) methyltransferase results in a lack of compact myelin formation in cultured cerebral cells from embryonic mice (Amur, 1986). Furthermore, administration of cycloleucine to mice was shown to produce neurological changes that were histologically indistinguishable from SCD (Small, 1981). Cycloleucine is an analogue of methionine that inhibits the biosynthesis of SAM. Also, in patients under B12 treatment, remyelination is associated with a return of CSF SAM levels to normal (Bottiglieri, 1994).

There are, however, some potential confounders to this Defective Methylation Hypothesis of B12 neuropathy. First, the concentrations of methionine and SAM were not affected by the defective MS activity in rats or pigs after N_2O administration (Lumb, 1983; Weir, 1988). Stronger evidence against this hypothesis has come from observations on patients with defective MTHFR. MTFR is upstream of MS and is the committed activity that directs the one carbon flux into methionine synthesis. A MTHFR defect would also severely impact the methionine remethylation cycle. If the demyelination in B12 deficiency is solely due to low SAM, MTHFR defects should result in similar effects. Clinical records showed that MTHFR defective patients rarely show the SCD symptoms observed in B12 deficiency. Severe MTHFR deficiency is the most common inborn error of folate metabolism. The major laboratory findings are hyperhomocysteinemia and hypomethioninemia. Because methylene-THF, the substrate for thymidylate synthase, as well as other folate derivatives except for methyl-THF are not deficient, patients with severe MTHFR deficiency do not develop megaloblastic anemia. Clinical presentation can occur at any age from the neonatal period to adulthood, although most cases have been described in infants (Rozen, 1996). A common feature is thrombosis, probably mediated through elevated levels of homocysteine. The predominant neurological findings included apnea, developmental delay and seizures, but only rare cases have reported demyelination as in B12 deficiency (Bottiglieri, 2005).

Previous research on the MTHFR null mouse is also consistent with the observations seen in human MTHFR mutants. These MTHFR gene knockout mice will be discussed in detail later. However, briefly, the MTHFR null mouse manifests some neuropathology, including dilated lateral ventricle and a dramatically under-developed cerebellum, but does not exhibit the demyelination that is a hallmark of the B12 deficiency induced SCD found in humans.

The exact underlying mechanism responsible for B12 neuropathy still remains unclear. The aim of my study was to further investigate the phenotypes of genetic mouse models, such as the MS and MTHFR knockouts, and to evaluate the effects of vitamin B12 deficiency and 5-methyl-THF administration on these models. It was hoped that these studies would lead to a better understanding of the relationship between impaired one-carbon metabolism and multiple diseases, with particular emphasis on the B12 deficiency neuropathy.

Chapter I: Development and characterization of the MTHFR/MS double knockout mouse.

Considerable research has been carried out on folate remethylation enzymes, especially on MTHFR because of its pivotal function in one-carbon metabolism. As the rate-limiting step in methionine remethylation, MTHFR regulates balance between one carbon used for DNA synthesis and for methionine/SAM synthesis and methylation reactions. SAM is an allosteric inhibitor of MTHFR: the mammalian enzyme has an additional regulatory C-terminal domain not found in the E.*coli* protein, and this domain is the binding site for SAM.

A single nucleotide polymorphism in MTHFR (677C→ T) which causes an amino acid change from alanine to valine has been well studied (van der Linden, 2006; Kim, 2009; Trabetti, 2008). The frequency of the C667T polymorphism varies among racial and ethnic groups. The homozygous (T/T) genotype accounts for ~12% of Caucasian and Asian populations; a much lower incidence of T/T genotype is found in the African-American population (Bailey, 1999). The C677T polymorphism produces a thermolabile MTHFR phenotype due to the reduced stability of the enzyme by facile loss of its cofactor FAD, and the variant human enzyme can be stabilized both by folate and FAD. Mild hyperhomocysteinemia is prevalent among homozygous 677TT MTHFR subjects. A meta-analysis showed that the mean total plasma homocysteine concentration is 25% higher in the individuals with T/T genotype than the C/C genotype (Brattstrom, 1998). A higher homocysteine level is a risk factor for vascular diseases and also for fetal neural tube defects. Several studies indicated that T/T genotype individuals are at higher risk of cardiovascular disease and NTD, especially when dietary folate is insufficient. However, recent studies have reported a protective effect of the T allele of MTHFR in colon cancer and adult acute lymphocytic leukemia risk (Pereira, 2006).

Another well-studied enzyme in folate metabolism is MS because it is the key junction of folate metabolism and B12 metabolism. Mutations in the human MS gene are responsible for the rare autosomal recessive disease of cobalamin metabolism known as cblG (Rosenblatt, 1989). Patients with this disorder have homocysteinemia, homocysteinuria, and hypomethioninemia, and suffer from megaloblastic anemia similar to that of folate or B_{12} deficiency, and may or may not manifest some degree of neural dysfunction and mental retardation.

A2756G is a common polymorphism in the MS gene that results in lower enzyme activity and is associated with elevated homocysteine (Matthews, 2007). The frequency of the heterozygous MS A2756G is around 15% in Caucasian population, and the homozygous variant accounts for 2-3% in the same population. Studies have suggested that pregnant women with the MS (A2759G) polymorphism (heterozygous and homozygous) have a higher risk of Down syndrome offspring (Gueant, 2003). The MS polymorphism is also associated with increased risk of colorectal adenoma, especially under low methionine intakes (Goode, 2004). It has been reported that individuals carrying at least one copy of the variant allele of MS presented a 2.3 fold increased risk of developing bladder cancer than their control group (MS 2759A/A) (Ouerhani, 2007).

To better understand the homocysteine remethylation process and the molecular interaction between variant enzymes and the corresponding phenotypes, a number of genetically modified animal models have been generated, including the MTHFR and the MS knockouts.

MTHFR knockout mice were generated by Dr. Rima Rozen and colleagues at McGill University in Canada (Chen, 2001). In the MTHFR knockout mouse, exon 3 was disrupted via insertion of the neomycin phosphotransferase (*neo*^{r}) gene. Mice deficient in MTHFR showed a variable phenotype with reduced survival, and exhibited hyperhomocysteinemia and decreased methylation capacity, with neuropathology and aortic lipid deposition. Supplementation with betaine rescues MTHFR null mice from postnatal death, and improves their somatic development (Schwahn, 2004).

Heterozygous MS knockout mice were previously generated by our lab (Swanson, 2001). An MS knockout construct was designed in which 3.5 exons of the gene were replaced by a PGK promoter/neomycin resistance cassette. The deletion corresponded to amino acids 101 to 254 in the human enzyme, a region which, by analogy with the *E. coli* protein, is responsible for homocysteine binding. Heterozygous MS knockout mice have slightly elevated plasma homocysteine compared to wild-type mice, but otherwise seem to be indistinguishable. Homozygous MS knockout embryos survive through implantation but die soon thereafter (E5-6). Nutritional supplementation during pregnancy failed to rescue embryos that were completely null in MS.

Because of the differences in survival of the MTHFR and MS nulls, we hypothesized that the MS null mice die from abortive DNA synthesis due to extreme folate deficiency during early embryonic development, which is caused by the formation of a “methyl folate trap”. Other possibilities, such as essential nutrient deficiency, or abnormal remethylation and high homocysteine as being responsible for the early embryonic lethality seemed unlikely, as homocysteine remethylation should be equally impaired in the MTHFR null. An additional possibility, that MS serves an additional unrecognized function during development was also possible.

Therefore, to test this hypothesis, we developed the MS/MTHFR double knockout mouse and characterized its phenotype. The aim of this study was to better understand the interrelationship of folate and vitamin B12 and their roles in one-carbon metabolism and in disease development.

MATERIAL AND METHODS

1.1. Body weight and general outcome

Animals and Diets

Mice heterozygous for the disruption of the MTHFR gene (Chen, 2001) were a gift from Dr. Rima Rozen at McGill University in Canada. Mice heterozygous for the disruption of the MS gene (Swanson, 2001) were previously generated in our lab. MTHFR null mice were bred from heterozygote. MS/MTHFR double null were bred from MS heterozygote versus MTHFR heterozygote or null. Genotyping for the wild type and targeted MTHFR and MS alleles was performed by PCR (Chen, 2001; Swanson, 2001). Unless otherwise specified, all gene interrupted mice were fed on modified AIN-93G diet with 1% succinyl sulfathiazole *ad libitum*. Succinyl sulfathiazole is an antibiotic that reduces gut flora responsible for synthesis of a significant amount of folic acid and vitamin B12. By adding this antibiotic, the amount of folate and B12 available to the experimental mice were controlled. The final concentration of folic acid, vitamin B12, methionine, cysteine in the above diet were 2mg, 25μg, 3.9g and 4.9g per kilogram diet, respectively (Reeves, 1997). 0.25% betaine was added into the drinking water during mating, pregnancy and lactation when MTHFR or MS/MTHFR double nullizygote pups were potentially delivered.

After the feeding periods, the mice were fasted overnight and anesthetized under isoflurane. Blood was collected from the hearts into heparin treated eppendorf tubes. Blood, obtained from the heart, was centrifuged and the plasma was stored at -80 ^{o}C. Liver, brain, spinal cord, kidney, and testes samples were either frozen in liquid nitrogen immediately and stored at -80 ^{o}C until used, or fixed in 4% paraformaldehyde in PBS buffer (pH 7.4) and embedded in paraffin. The protocols used complied with the Guideline for Animal Experimentation of the University of California, Berkeley.

Body weights of the mice were measured weekly or monthly throughout the experimental period.

1.2. Histology studies

1.2.1. Hematoxylin-Eosin staining

Mouse tissues were dissected, fixed in 4% Para formaldehyde and embedded into paraffin. 8μm tissue slices were cut with a microtone machine. Mouse tissue slides were deparaffinized with xylene for 3 x 3 min, then rehydrated through a series of ethanol washes: 100%, 95%, 70%, 50% then distilled water, each for 3 minutes. Slides were stained in Hematoxylin solution for 20 seconds, rinsed in distilled water, then incubated with 0.2% ammonium hydroxide in PBS to maintain Heme staining, followed by another water wash. After incubation with 50% ethyl alcohol for 3 min, slides were counterstained with 1% Eosin for 1 min. 95% and 100% ethyl alcohol were used to dehydrate the sections. After incubation with 2 x 3 min xylene, slides were mounted with resinous medium and checked microscopically.

1.2.2. Luxol fast blue

Paraffin sections at 8 μm were deparaffinized, hydrated to 95% ethyl alcohol and incubated in 0.1% luxol fast blue solution in a 56^{o}C oven for 2 hours. Excess stain was rinsed off with 95% ethyl alcohol. Slides were rinsed with distilled water and differentiated with 0.05% lithium carbonate solution and 70% ethyl alcohol successively for 20 seconds each. Slides were then rinsed in distilled water and counterstained with 0.1% cresyl violet solution for 40 seconds. Slides were rinsed again and differentiated in 95% ethyl alcohol for 10 seconds. 2 x 5 min 100% alcohol and 2 x 5 min xylenes were used to dehydrate the slides, which were then mounted with resinous medium.

1.2.3. Red O lipid staining

Frozen coronary artery sections were cut at 8mm and air dried to the slides. The sections were fixed in formalin and briefly washed with running tap water for 5 minutes. After rinsed with 60% isopropanol, sections were stained with freshly prepared Oil Red O solution (0.3% W/V Oil Red O in 60% isopropanol) for 15 minutes and rinsed again. Nuclei was lightly stained with haematoxylin 5 dips. Finally the sections were rinsed with distilled water and mounted in aqueous mountant.

1.3. Metabolite assays

1.3.1. Homocysteine

Plasma homocysteine was measured according to a previously described method (Durand, 1996). Plasma (50 μl) was treated with 0.6mol/l tri-n-butylphosphine in dimethylformamide (50 μl) for 30min at 4 ^{o}C. Proteins were then precipitated with 0.6mol/l cold perchloric acid containing 1 mmol/l EDTA (300 μl), left at room temperature for 10 min after thorough mixing, and centrifuged at 2000xg for 10minutes. The supernatant was mixed with 10ul of 1.55mol/l NaOH, 125 μl of 0.125 mol/l borate buffer (pH 9.5) containing 4mmol/l EDTA and 50 μl of a 1mg/ml solution in the borate buffer of the derivatization reagent SBDF. Complete derivatization of thiols was performed in a shaking water bath at 60 ^{o}C for one hour. After cooling on ice, samples were analyzed by HPLC. The following isocratic conditions were used for HPLC analyses: 0.1mol/l acetate buffer, pH 4.0, containing 2% methanol, degassed and filtered through 0.45 μm membranes with a flow rate of 1.2ml/min for 14 min. Separation was carried out with an analytical reverse phase column (C18). The fluorescence intensities were measured with a 385 nm excitation and a 515 nm emission. Homocysteine standards were used to identify the elution peaks and for the preparation of the standard curve. All analyses were performed and repeated using plasma samples from at least 6 different mice for each experimental group. (All chemicals were obtained from Sigma)

1.3.2. SAM and SAH assay

SAM and SAH were determined by HPLC by a modification of a previously described method (Fell, 1985). Frozen tissues were thawed in 0.4M ice-cold perchloric acid and then homogenized on ice with a polytron homogenizer. Homogenates were centrifuged at 10,000g for

10minutes at 4 ^{o}C and the supernatants were collected and stored at -80 ^{o}C until they were analyzed. The supernatant of each sample was filtered through 0.45 μm filters (Millipore) and then loaded onto a C18 column (250 x 4.6nm) fitted with a matched guard column operated by a Varian Vista 5500 chromatography system connected to an ultraviolet detector. Absorption of eluted compounds was monitored at 254 nm. A two-buffer elution system was used: mobile phase A and B, both contain 10 mM ammonium formate, 4 mM 1-heptanesulfonic acid (pH 4.0). Mobile phase B also contains 50% acentonitrile by volume. Elution of SAM and SAH was achieved at a flow rate of 1 ml/min with the following parameters: 0-0.5 min, 100%A; 0.5-20 min, linear gradient to 75% A and 25% B; 20-30 min, 25% B; 30-50 min, 100% A. SAM and SAH standards were used to identify the elution peaks and for the preparation of the standard curve. SAM and SAH values were normalized to tissue weight. All analyses were performed and repeated using tissue samples from at least 6 different mice for each experimental group. (All chemicals were obtained from Sigma)

1.3.3. Assay and identification of folate derivatives

1.3.3.1. Plasma and liver total folate with microbiological assay

Cryoprotected culture of *Lactobacillus rhamnosus* (formerly known as *L. casei*) was used for the assay. All reagents to be used were filtered immediately before use. (6-R,S)- 5-formyltetrahydrofolate (leucovorin, calcium salt, Sigma) was used as the folate standard and its exact concentration was determined by measuring absorbance at 282nm and calculated using an extinction coefficient of 28,200/mol.

Mouse liver was removed after overnight fasting and weighed. 5 volumes of 5% sodium ascorbate buffer, pH 4.2 was added to the liver and the mixture was homogenized and incubated for 90 min at 37 ^{o}C (protect from light) to allow the hydrolysis of folylpolyglutamates to the monoglutamate derivatives catalyzed by an endogenous lysosomal-glutamylhydrolase. The sample was then centrifuged at 20,000 g for 20 min. The supernatant was removed and stored until used.

The assay was performed in a 96-well microplate. Each well contained 155μL assay buffer (0.1 M potassium phosphate solution, pH 6.3 ontaining 1 mg/mL of ascorbic acid), 120μL *L. casei* medium and 20μL *L. rhamnosus* cryoprotected bacteria. 5μL of samples were then added to each well to make final volume 300μL. The plate was placed in a plastic bag, sealed to prevent evaporation and incubated for 16 – 20 hours at 37°C. Content of each well was mixed and O.D. (representing light scattering) read at 595 nm using water as a reference blank.

Plasma folate assay was similar except no hydrolysis step was required as plasma contains only folate monoglutamates. 5 μL thawed plasma was added to each well in the assay.

Folate concentrations were calculated using a standard curve (logarithm fitting curve) established with leucovorin standard and presented as nmol/g or nmol/L.

1.3.3.2. Liver folate derivatives analysis using HPLC combined with microbiological assay.

Mice were injected with sterile 25μCi ^{3}H-folic acid in 0.9% NaCl intra-peritoneally. Liver folate derivative determination was performed as described by Horne (Wilson, 1984) with the following modification. 24 hours after ^{3}H-folic acid i.p., mouse liver was removed, weighed and minced. 10 vol. of extraction buffer was pre-heated to 100°C and added. Extraction buffer contained 2% (w/v) sodium ascorbate, 10mM 2-mecaptoethanol, 50mM Hepes buffer and 50mM Ches buffer, pH 7.85. The vials were heated for 10 minutes at 100°C in the dark and cooled on ice. The liver was then homogenized with a Polytron homogenizer at 0°C. The homogenate was centrifuged at 30,000g for 30 min in a refrigerated ultracentrifuge. The supernatant was removed and further centrifuged for another 15 minutes. Any material floating on the top surface was removed and the remaining supernatant was stored at -20°C under N_2.

Rat plasma was used as the source of neutral glutamyl hydrolase. Rat plasma was dialyzed against PBS containing charcoal to remove any folate present and the dialyzed preparation was added to the liver extract (1:4 v/v). A drop of toluene was added to the vial and vials were incubated at 37°C for 3 hours in the dark. The vials were then heated at 100°C for 5 minutes to precipitate plasma proteins. After centrifuge at 18,000g for 4 minutes, the supernatant was removed and stored at -20°C under N_2.

100 ul folate extract (treated with rat serum conjugase) from mouse liver was injected onto the HPLC column. HPLC was first run under a concave gradient (setting 7 for 40-min duration) where solvent B composition increased from 15% to 25%, and then a convex gradient (setting 5 for 30-min duration) where solvent B composition increased from 25% to 30%. Solvent A contained 5mM tetrabutylammonium phosphate (TBAP) and 5mM 2-mecaptoethanol in water; solvent B contained the same solutes but in 1:1 mixture of water and 95% ethanol. The flow rate was set as 1 ml/min and absorbance of eluates was monitored at 280nm. Fractions were collected into liquid scintillation vials (1ml/vial). 100 μl was removed to store and use in microbiological assay as previously described (1.3.3.1), another 900 μl was mixed with 6.1 ml liquid scintillation fluid and count for tritium in a Beckman LS6000 using program 1.

1.3.4. Cobalamin derivatives

Cobalamin derivatives were identified using a previously described method by Dr. Kitchens (Frenkel, 1980) which was modified as follows. Mice were injected with sterile ^{57}Co-cyancobalamin in 0.9% NaCl intra-peritoneally 24 hours before sacrifice. Approx. 1g tissue was weighed and a 5 fold volume of 80% ethanol was added. Homogenized liver was incubated at 70°C for 20 minutes. After centrifuged at 5000g for 20 minutes at 4°C, the supernatant was removed and store on ice. Equal amount of 80% ethanol as above was added to the sediment and incubated at 70°C for 20 minutes. After another centrifugation, the supernatant was combined with previous one. All extractions were vacuum dried until their final volumes decreased to about 20% of original. 1ml ddH_2O was added to dilute each sample and extracts were loaded onto a Sep-Pak C18 cartridge (pre-wet with 5ml acetonitrile and 10ml ddH_2O). The cartridge was washed with 10ml ddH_2O and then eluted with 2ml 50% acetonitrile. The eluate was dried under vacuum at 40°C until the final volume was less than 800 μl and stored at -20°C until used.

100μl of the above extract was injected on to a C18 HPLC column. A gradient system was used to elute cobalamins which consisted of 0.05 M phosphoric acid titrated to pH 3.0 with

concentrated ammonium hydroxide (solvent A) and acetonitrile (solvent B). Acetonitrile concentration was increased from 5 to 30% linearly in 20 min and maintained at 30% for 8 min. Flow rate was set as 1ml/min and cobalamins were detected by UV absorbance at 254nm. Eluted fractions were collected every 0.5min and their ^{57}Co radioactivity was monitored in a gamma spectrometer.

1.3.5. Methyl-malonyl CoA assay

Plasma methyl-malonyl CoA content was kindly measured by Dr. Jacob Selhub (Tufts University) using an LC-MS assay.

1.4. MS tissue distribution

1.4.1. Western Blot

Mouse tissues were removed, weighed and homogenized in 1x RIPA buffer. Mouse primary cultured astrocytes were generously supplied by the Napoli lab (UCB). Cells were disrupted in 1x RIPA buffer by sonication. Homogenates or cell lysates were centrifuged at 14,000xg for 10 minutes at 4^{o}C, and pellets were discarded. Protein concentrations in the supernatant were determined by the Bradford assay (Bio-Rad, CA). Aliquots of protein extracts were stored at -80^{o}C.

Equal amount of total protein (10 μg) were mixed with two volumes of gel loading buffer (250mM Tris-HCl, pH 8.0, 20% beta-mercaptoethanol, 40% glycerol, 8% SDS, 1.2mg/ml bromophenol blue), heated for 5 min at 95 ^{o}C, and resolved on 15% polyacrylamide gels. Proteins were transferred onto nitrocellulose membranes (Fisher Sci.). The membranes were blocked for one hour in TBS buffer containing 5% nonfat dry milk and 0.1% Tween-20 at room temperature. Anti-methionine synthase primary monoclonal antibody (Abcam) was diluted 1:500 in blocking buffer according to the manufacture's recommendations. Primary antibody binding were performed at 4 ^{o}C overnight with constant shaking. Secondary donkey anti-goat antibody conjugated with horseradish peroxidase (Chemicon) was applied at 1:2000 dilutions, and binding was carried out at room temperature for one hour. Chemifluorescence detection was performed with ECL (Amersham) following the manufacture's instruction. β-actin was used as an internal loading control of the western assay.

1.4.2. In-situ Hybridization

Mouse MS was amplified by polymerase chain reaction (PCR) using a pair of primers, 5'-GGAATTCCAGAGGATCATGGTGCTAGACG- 3' and 5'-CCTTGGCAATGTCAGGCT- 3'. The primers were designed to amplify *mtr* based on the known sequence [NM_001081128] and there was an *Eco*RI site (5'-GGAATTCC-3') included in the forward primer which facilitated further digestion.

Both sense and antisense RNA probe were prepared using a DIG RNA labeling kit (Roche). The PCR product was digested with *Eco*RI and *Bam*HI and subcloned into pBluescript® II phagemid vectors (Stratagene). These plasmids were linearized with *SalI* before transcription

with T3 RNA polymerase to generate approximately 0.6 kb antisense or sense probes. Frozen sections (4 mm) placed on slides were treated with 2 mg/ml proteinase K in PBS for 30 min, 0.1 M triethanolamine–HCl (pH 8.0) for 1 min and 0.25% acetic anhydride in triethanolamine for 10 min before rinsing in distilled water for 5 min. The hybridization mixture consisted of approximately 3 ng RNA probe suspended in a solution containing 10% dextran sulfate, 54% deionized formamide, 13 Denhardt's solution, 0.33 M NaCl, 2.7 mM EDTA, 1 mg/ml of yeast tRNA. Tissue sections were hybridized with a digoxigenin-labeled antisense RNA probe. To confirm specificity of the observed signals, hybridization was also performed with a sense-strand probe derived from the same region. Slides were hybridized at 50°C for 16 h in a humid chamber. After hybridization, hybridized digoxigenin-labeled probes were used from a detection kit (Boehringer-Mannheim).

1.5. Brain lipid analysis

1.5.1. Brain lipid extraction

Approx. 100 mg of brain was weighed out into 2ml microcentrifuge tubes and a 6 fold volume of 2:1 chloroform–methanol with 0.5% BHT was added. The samples were homogenized with a Polytron homogenizer and incubated on a rotating rack for 15min. After centrifuged at 10000g for 10 min, the supernatant was transferred to a screw cap vial and stored at -20C.

1.5.2. Brain lipid analysis using 2-dimension thin layer chromatography

Myelin lipids were separated by thin layer chromatography (TLC) using 20-cm^2 silica gel H plates (250 μm). The first solvent system (diethyl ether: benzene: ethanol: acetic acid = 40:50:2:0.2 by volume) was allowed to run two-thirds of the height of the TLC plate. After drying the plates under low negative pressure in a chamber, a second solvent system (diethyl ether:hexane = 6:94 by volume) was allowed to run the full course of the TLC. After drying, the plate was further run with the second dimension solvent system (chloroform:methanol:water = 65:25:4 by volume). The TLC plates were dried and the lipid spots were identified by iodine staining.

1.6. Cell proliferation and apoptosis

1.6.1. BrdU Immunohistochemistry

BrdU was dissolved in PBS (10mg/ml) and filtered through a 0.2μm membrane. Mice were injected with BrdU intra-peritoneally at 50mg/kg body weight once per day for three consecutive days. Mice were sacrificed three days after the last injection. Mouse brain was dissected, fixed in 4% Para formaldehyde and embedded in paraffin. 7μm tissue slices were cut with a microtone machine. Mouse brain slides were deparaffinized with xylene for 5 minutes twice, then 20 minutes once. After the last xylene wash, slides were rehydrated through a series of ethanol washes: 100%, 90%, 70%, 30% then PBS. To denature and retrieve the antigen, slides were submerged in 400 ml 10mM citrate buffer pH6. The slides were microwaved (8oo watt) for 2 times 5 minutes with a 5 min wait between treatments. The slides were allowed to remain in the hot buffer for 30 minutes.

Slides were then incubated in 0.3% H_2O_2 in methanol for 10 minutes, rinsed with PBS two times and circled with a PAP pen. They were blocked for 20 minutes at room emperature with blocking solution (PBS with 0.5% Triton-X 100, 3% rabbit serum). Primary anti BrdU antibody (Sigma) was diluted 1:500 in PBS with 0.5% Tween 20 and 3% rabbit serum. The primary antibody solution added to slides and incubated overnight at 4 ℃ in a humidified chamber.

The following day, the slides were washed 3 times with PBS. The secondary antibody was added (Sigma HRP conjugated rabbit anti-mouse IgG) 1:100 in PBS with 1.5% rabbit serum. After incubation for 1 hour at room temperature, the slides were washed 3 times in PBS and then developed with Sigma Fast DAB with metal enhancer.

1.6.2. TUNEL assay for apoptosis

Terminal transferase dUTP nick end labeling (TUNEL) assay was performed following the manufacture's instruction (Boehringer-Mannheim). In brief, formalin fixed brain sections were rehydrated with water and permeabilized with a solution containing 0.1% Triton X-100 and 0.1% sodium citrate for 8 min. Sections were then washed 3 times with PBS, labeled with TUNEL reaction mixture, washed with PBS again and finally mounted with HydroMount. One slide treated with DNase I after the first wash was used as a positive control, while two slides treated with buffer without enzyme were used as negative controls. TUNEL signals were monitored with a confocal microscope setting 540nm (green) as the excitation wavelength and 580nm (red) as the detection wavelength.

1.7. Microarray study for gene expression

1.7.1. RNA isolation

Wild type, MTHFR null and MS/MTHFR double null P(1) pups from breeding mice fed on antibiotics-containing AIN-93G diet for 6 months were used to isolate RNA. Whole brains, ranging from the olfactory bulb to the cerebellum, or liver sections (around 150mg) from the same anatomic position were excised and frozen immediately in liquid nitrogen. Total RNA was isolated using Trizol (Invitrogen) following the manufacture's instruction. Isolated total RNA was further purified with RNeasy mini kits (Qiagen) according to the manufacture's instructions and quantified using a spectrometer. Only samples with an A260/A280 between 1.8 and 2.1 were considered suitable for use. Aliquots of total RNA was stored in 70% ethanol at -80 ^{o}C.

1.7.2. Reverse transcription

65ug of above total RNA samples were used to synthesize cDNA. Reverse transcription was performed using Superscript II reverse transcriptase (Invitrogen, Carlsbad, CA) primed by both random hexamers and oligo dT (Invitrogen, Carlsbad, CA) in the presence of aminoallyl dUTP. The resulting amino-modified cDNA was labeled using Cy3 or Cy5 fluorescent dyes (Amersham Biosciences, Piscataway, NJ).

1.7.3. cDNA Microarray

The cDNA microarrays were produced by the Stanford functional genomics facility and named “Mouse Exonic Evidence Based Oligonucleotide (MEEBO) Arrays”. MEEBO arrays consists of 38,784 70mer probes, which includes 30,125 constitutive exonic probes, 4,201 alternatively spliced / skipped exonic probes, 196 non coding RNA probes, 372 BCR / TCR genic / regional probes, 13 mitochondrial probes, 37 transgenic / cassette probes and 358 murine viral probes. (See http://www.microarray.org/sfgf/meebo.do)

The Cy3- and Cy5- labeled cDNAs were mixed prior to hybridization to MEEBO microarrays. Hybridization was performed at 65°C for 16 ~ 20 hours. Microarray images were obtained by scanning slides using an ArrayWoRx Biochip Reader (Applied Precision, Issaquah, WA). Images were quantified using GenePix 3.01 (Molecular Devices, Sunnyvale, CA) to obtain average hybridization signal intensity for each spot and background of surrounding area.

1.7.4. Data Analysis

Spot intensity values for each array were analyzed using an exploratory differential gene expression analysis algorithm. Spot intensities were normalized by non-parametric regression smoothing (super smoother, *supsmu*, also known as *lowess*), by which data were grouped into subsets of equal size (print tip groups) and then regression smoothers were applied to the median absolute residual against median of log2-transformed Cy3 for each box plot group. Log2-transformed normalized ratios were used for subsequent data analysis to identify candidate genes for differential expression. A general α-outlier model for residuals was adapted and smoothed simultaneous tolerance intervals (STIs) were applied to account for heteroscedasticity of residual variance. Candidate genes were analyzed for their association with biological functions and/or diseases by Ingenuity Pathways Analysis (Ingenuity Systems, Redwood City, CA).

1.8. Real-time quantitative PCR

RNA samples representing single animals were used to validate the expression profile of some of the genes obtained using the cDNA microarray. To remove contaminating genomic DNA, a DNase digestion was carried out by treating the total RNA (10 μg) with TURBO Dnase (Ambion) following the manufacture’s instructions. A minus reverse transcription (RT) control was performed and used for PCR with primers for glyceraldehyde-3-phosphate dehydrogenase (GAPDH) to check the removal of the contaminating genomic DNA from the total RNA samples. First-strand cDNA was synthesized from 1.5 μg DNase-treated total RNA using the SuperScript II reverse transcriptase (Invitrogen) with oligo dT (12-18) (Elimbio) as primers following the manufacture’s instructions. The cDNA samples obtained were then diluted 10 to 2000 times in RNase, DNase free water (GIBCO).

Primers were designed through the Invitrogen on-line primer design tool, Oligo Perfect™ Designer, and were based on cDNA sequences found in GeneBank. A valid primer set is defined as having a slope of -3.3 (±0.1) and a correlation coefficient (R_2 value) >0.95 for the standard curve of real-time PCR; at the same time, the PCR product is a single band which can be visualized on a 2% agarose gel. Primers used in the experiments are listed in Table 1-1. The final concentration of primer in the real-time PCR reaction was 315 nM.

Table 1-1. Primer sequences used in Real-time quantitative PCR to confirm microarray data.

Glyceraldehyde 3-phosphate dehydrogenase (GAPDH) F 5'-TTGATGGCAACAATCTCCAC-3' R 5'-CGTCCCGTAGACAAAATGGT-3'
Apolipoprotein A-IV (Apoa4) F 5'-TAGCATCCCCAAGTTTGTCC -3' R 5'-ACCCAGCTAAGCAACAATGC -3'
Ubiquitin-conjugating enzyme E2I (Ube2i or Ubc9) F 5'-GCTACAAAGCCAAAAGGGTG-3' R 5'-AGGGGTTTCAGGTGGAACTAA-3'
Ferritin heavy chain 1 (Fth1) F 5'-GGCAAAGTTCTTCAGAGCCA-3' R 5'-CATCAACCGCCAGATCAAC-3'
Ubiquitin carboxy-terminal hydrolase L1 (Uchl1) F 5'- GGACAGCTTCTCCGTTTCAG -3' R 5'- GGTACCATCGGGTTGATCC -3'
Cyclin E1 (Ccne1) F 5'- TCCACGCATGCTGAATTATC-3' R 5'- TTGCAAGACCCAGATGAAGA-3'
Low density lipoprotein receptor-related protein 1 (Lrp1) F 5'- TAGAAGTTTCCCGTCAGCCA -3' R 5'- CCTGAAGGGCTTTGTGGAT-3'
Solute carrier family 25, member 32 (Slc25a32) aka mitochondrial folate transporter/carrier (Mftc) F 5'- GTCCATCACTCACAGCGAAG-3' R 5'- GTACGAGAACCTGGTGGCTG -3'
Hepcidin antimicrobial peptide (Hamp) F 5'- TCTTCTGCATTGGTATCGCA-3' R 5'- GAGCAGCACCACCTATCTCC-3'

Glial fibrillary acidic protein (Gfap) F 5’- TTTCTCGGATCTGGAGGTTG -3’ R 5’- AGATCGCCACCTACAGGAAA-3’
Growth hormone (Gh) F 5’- CTTGAGGATCTGCCCAACAC-3’ R 5’- CCTCGGACCGTGTCTATGAG-3’
Insulin-like growth factor binding protein 1 (Igfbp1) F 5’- CTCTCAGAAAGCTCATCCGC-3’ R 5’- TGTGTACCAGAACCTGCTGC-3’
Methylenetetrahydrofolate dehydrogenase (NAD+ dependent), methenyltetrahydrofolate cyclohydrolase (Mthfd2) F 5’- CACTCTTCCACCTCCTGCTG -3’ R 5’- CCTACAGCCCTTCCACCTG-3’

Real-time PCR was performed using the ABI prism 7900 Sequence Detection System. SYBR Green I (Invitrogen) was used to detect double-stranded DNA generated during PCR amplification. PCR was performed in a 30ul reaction using Hot-start Taq from Allstar Scientific Company following the manufacture’s instructions. Amplification reactions were carried out using the following temperature profile: 50 ^{o}C, 2min; 95 ^{o}C, 10min; (95 ^{o}C, 20sec; 57 ^{o}C, 30sec; 70 ^{o}C, 30sec for 40 cycles).

The relative standard curve method was used to assess the amount of a particular gene in a group of samples (4 biological replicates for each group). In this method, the instrument software (SDS 2.0) calculates the quantity of transcript in each unknown sample based on the linear regression formula of the standard curve. For each sample, the quantity of the gene of interest (GOI) and the reference gene (Reference) are determined in triplicate, and from these values, the average transcript quantity (avg), the standard deviation of the average (stdev), and the coefficient of variation (CV) of the average is determined. Any single outlier point that has a value >17% CV is removed from the calculation. To determine the mRNA level in each unknown sample, the gene of interest is normalized to the reference gene.

RESULTS

Growth and overall outcome of MS/MTHFR double null mice fed on antibiotics-containing AIN-93G diet

	MTHFR +/+	MTHFR +/-	MTHFR -/-
MS +/+	349	39	43
MS +/-	659	54	90
MS -/-	0	0	32

Table 1-2. Breeding results of knockout mice. Numbers of neonates when MS heterozygotes were bred on MTHFR wild type, heterozygous and null backgrounds are showed.

MS nullizygotes die during early embryo development (about E5). We postulated that MS null mice die from extreme folate deficiency caused by a "methyl folate trap", and the survival of MTHFR/MS double knockout mice would confirm this hypothesis. The MTHFR knockout can block formation of the "methyl folate trap", which makes dietary folate retainable and functional, so MTHFR/MS mice were expected to survive and have a phenotype similar to MTHFR single null mice. Our breeding result proved this hypothesis correct and proved that MS does not have additional unknown functions during development. MS nulls only survived on the MTHFR null background and none were found on MTHFR +/+ or MTHFR +/- backgrounds. MS/MTHFR double null mice were delivered at close to the expected Mendelian frequency without sexual bias, suggesting that MS/MTHFR double null offspring did not undergo any significant increase in in utero losses beyond that observed in the MTHFR null.

Betaine supplement during breeding and lactation significantly improved the survival and growth of the double null mice, as it did the MTHFR null. Apparently, the matings between MS het/MTHFR null will generate the maximum amount of MS/MTHFR double null. However, such mating was extremely difficult, due to both the impaired fertility of the MTHFR null males and poor maternal behavior of the females. In this case, mating between MS het/MTHFR null and immediate transferring of new pups to wild type foster mothers became a common approach to produce the double null mice.

The double null embryo and P0 pups were indistinguishable from their double heterozygote littermates but they were soon apparently different in appearance, size, and general behavior. The overall survival of MS/MTHFR double null mice was approximately 30% at the age of 3 weeks, with nearly 3/4 of the deaths occurring during the first two postnatal weeks. The body sizes of the inborn double-knockout pups were very variable and mice that died in the first few weeks had severely retarded growth. They were usually with smaller body size and motor/gait abnormalities or severe tremors. The actual cause of death has not been determined but it was believed that the abnormality decreased milk/food supply from mothers and limited further weight gain. Mother mice showed apparent rejection towards weak knockout mice and decapitation during lactation were a very common phenomena. Even those knockout mice that

survived after the first 3 weeks were significantly smaller than their wild type littermates and also showed a retarded growth in the first few weeks. Figure 1-1 and 1-2 shows the group comparison of body weight from P(10) to P(50) at 10-day intervals. At each time point, knockout mice had lower body weight.

However, after the initial critical period of a few weeks, survival of the MS/MTHFR double null was relatively stable and the growth of knockout mice tended to be normal. In addition, several of our MS/MTHFR double null mice have survived nearly 2 years, indicating that longevity is possible. There was no significant long-term difference on the overall growth curve of MTHFR null and MS/MTHFR double null mice compared with wild type mice. However, with time, knockout mice showed more and more variation, especially after age of 10 months, as shown on figure 1-3 and 1-4. The range of body weight was from 24 grams to 39 grams in 16-month-old female knockout mice and from 29 grams to 41 grams in male knockout mice.

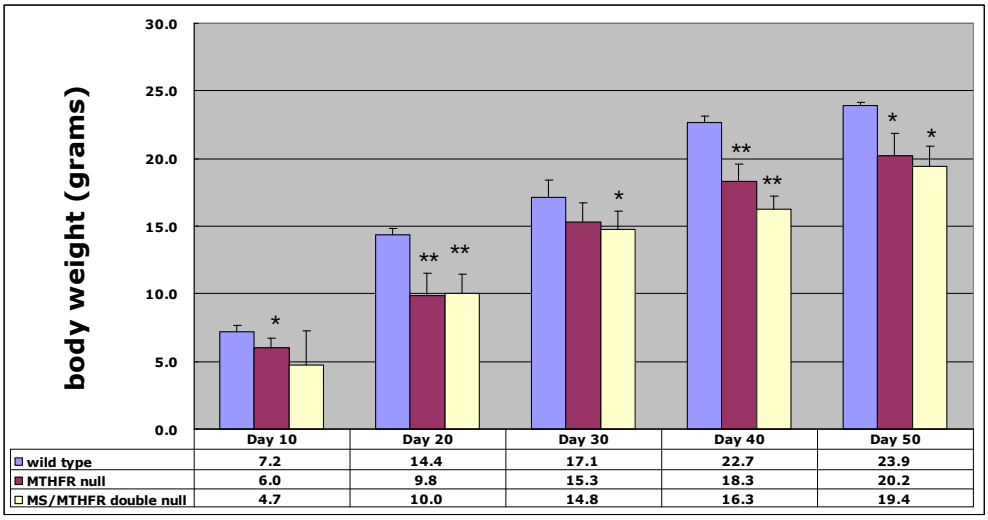

	Day 10	Day 20	Day 30	Day 40	Day 50
wild type	7.2	14.4	17.1	22.7	23.9
MTHFR null	6.0	9.8	15.3	18.3	20.2
MS/MTHFR double null	4.7	10.0	14.8	16.3	19.4

Figure 1-1. Body weight comparison of male wild type, MTHFR null and MS/MTHFR double null young mice. Each value represented data from 8 to 10 mice. * $P < 0.05$, ** $P < 0.01$ (Student's *t*- test) compared to WT mice of the same age.

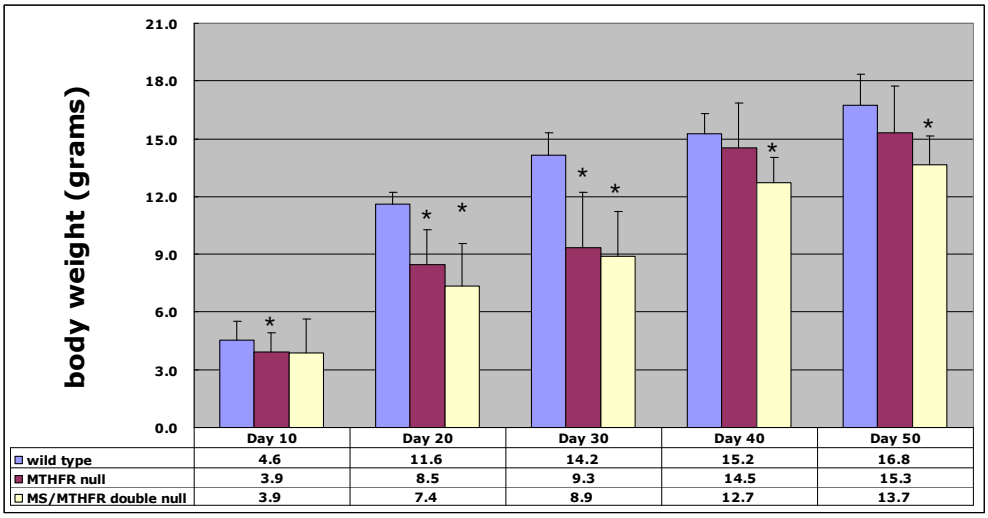

Figure 1-2. Body weight comparison of female wild type, MTHFR null and MS/MTHFR double null young mice. Each value represented data from 8 to 10 mice. * P < 0.05 (Student's *t*-test) compared to WT mice of the same age.

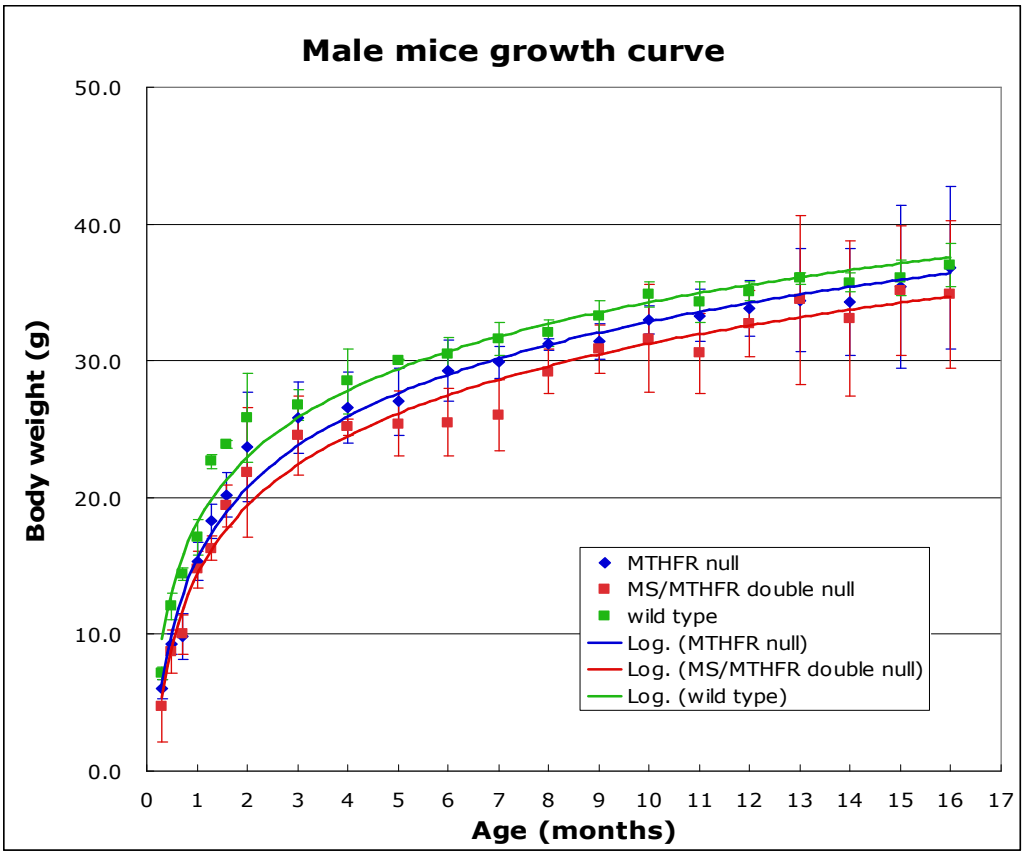

Figure 1-3. Growth curve of male wild type, MTHFR null and MS/MTHFR double null mice. Mean values ± SEM and their logarithmic trendlines are showed. Each value represented data from 8 to 10 mice.

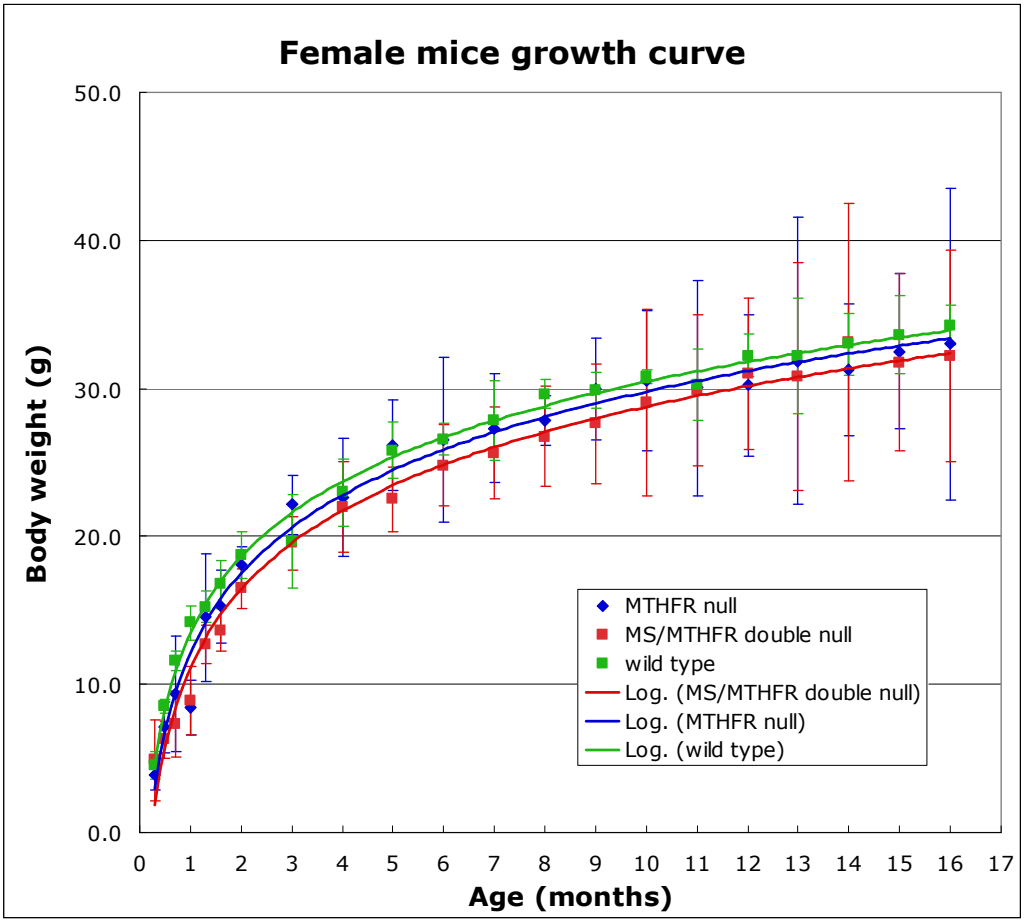

Figure 1-4. Growth curve of female wild type, MTHFR null and MS/MTHFR double null mice. Mean values ± SEM and their logarithmic trendlines are showed. Each value represented data from 8 to 10 mice.

Our lab had backcross bred MS and MTHFR defective mice to the C57Bl/6 background, however, when I bred the MS/MR het/het mice, there was only one double knockout mouse generated out of 152 mice which were born. This result prevented me from carrying out the following experiments on the pure C57Bl/6 background and indicated genetic background had significant impact on MS/MTHFR knockout outcome.

Brain abnormality and defective male reproductive system

Adult MS/MTHFR double null organs, except brain and testis, appeared grossly normal. We further analyzed internal adult organs using perfused fixed tissue sections that were stained with hematoxylin and eosin. There were no obvious differences between the wild-type and MS/MTHFR double null mice in liver, spleen, lung, kidney, heart and ovary duct (Figure 1-5, heart and lung not shown).

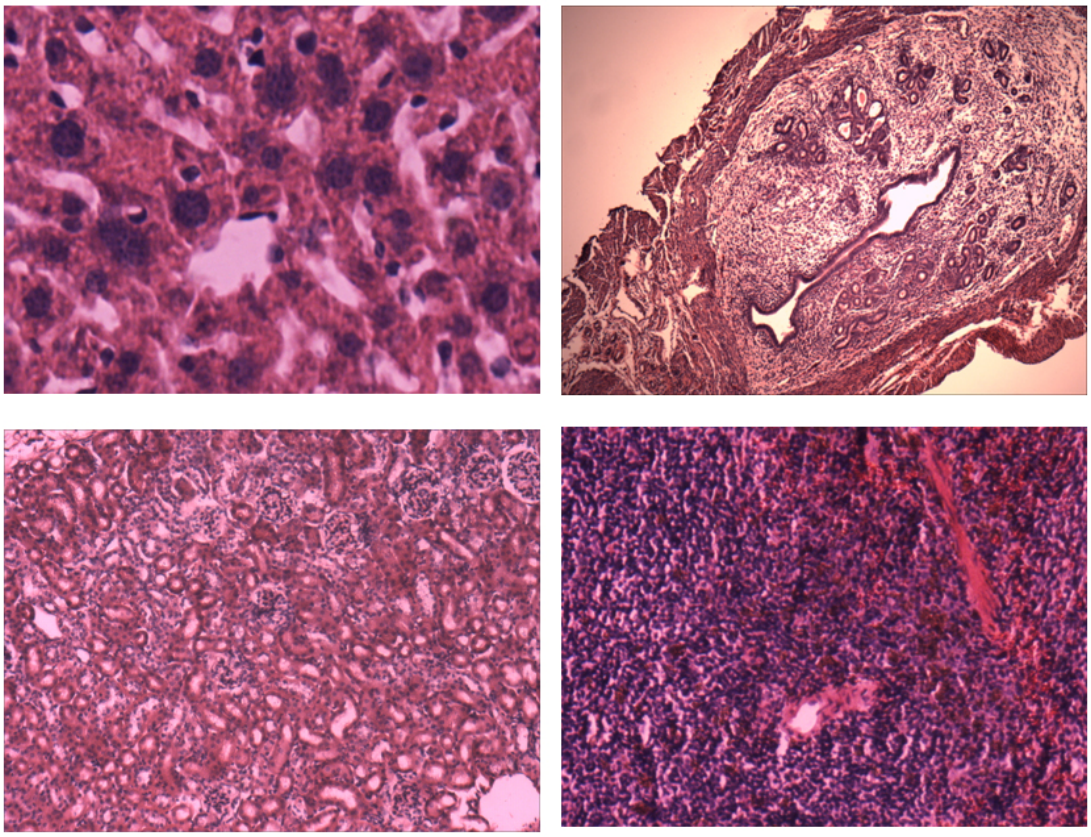

Figure 1-5. Histology of adult MS/MTHFR double null tissues. Paraformaldehyde fixed internal adult tissue sections of mice were stained with hematoxylin and eosin. There were no apparent abnormality in the liver (upper-left), ovary duct (upper-right), kidney (bottom-left) and spleen (bottom-right).

Demyelination is the major neurological symptom of vitamin B12 deficiency, so we examined myelin in the central nerve system of the knockout mouse carefully by Luxol Fast Blue staining. No myelin loss was revealed in CNS of double null mice fed on the antibiotic-containing AIN-93G diet (Figure 1-6).

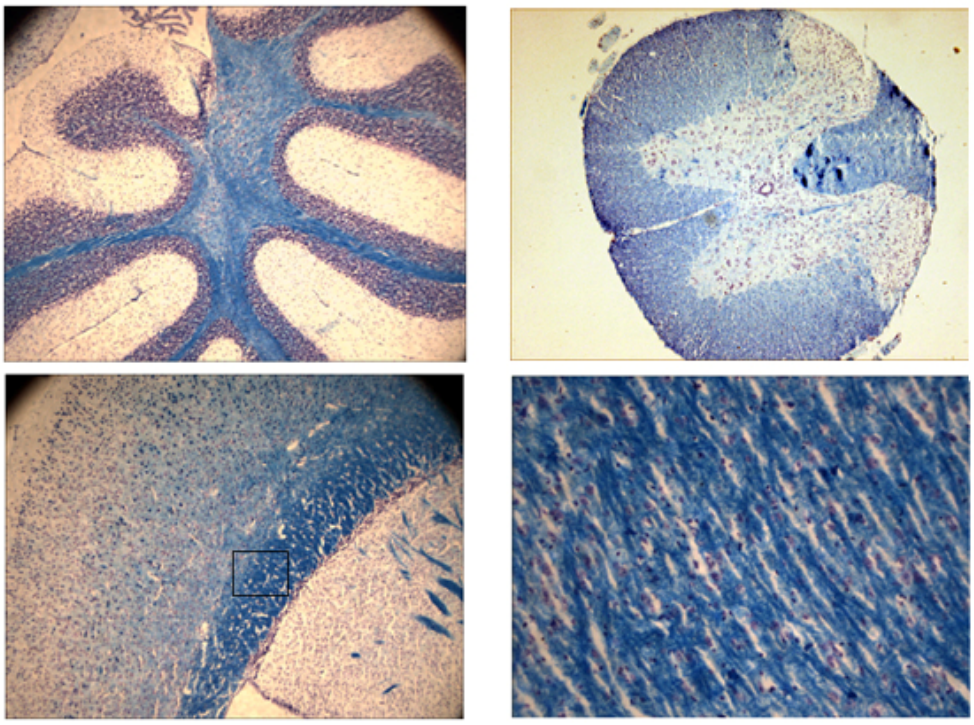

Figure 1-6. Luxol fast blue staining of CNS sections of MS/MTHFR double null mice. There was no apparent abnormality in the myelin at cerebellum (upper-left), spinal cord (upper-right), cerebrum cortex (bottom-left and magnified as bottom-right).

H&E staining did not reveal major defects in many tissues of the double knockout mouse. But we did observe several defects in the cerebrum, cerebellum and testis in knockout mice. Brain weight of postnatal day 120 (P120) MS/MTHFR double null male mice (n = 6) was approximately 74% of that of wild type animals (n = 7); mean ± standard deviation = 0.36 ± 0.04 g versus 0.48 ± 0.03 g (Figure 1-7).

Figure 1-7. Appearance of the whole brain of 4-month-old male wild type, MTHFR null and MS/MTHFR double null mice. (Above left to right)

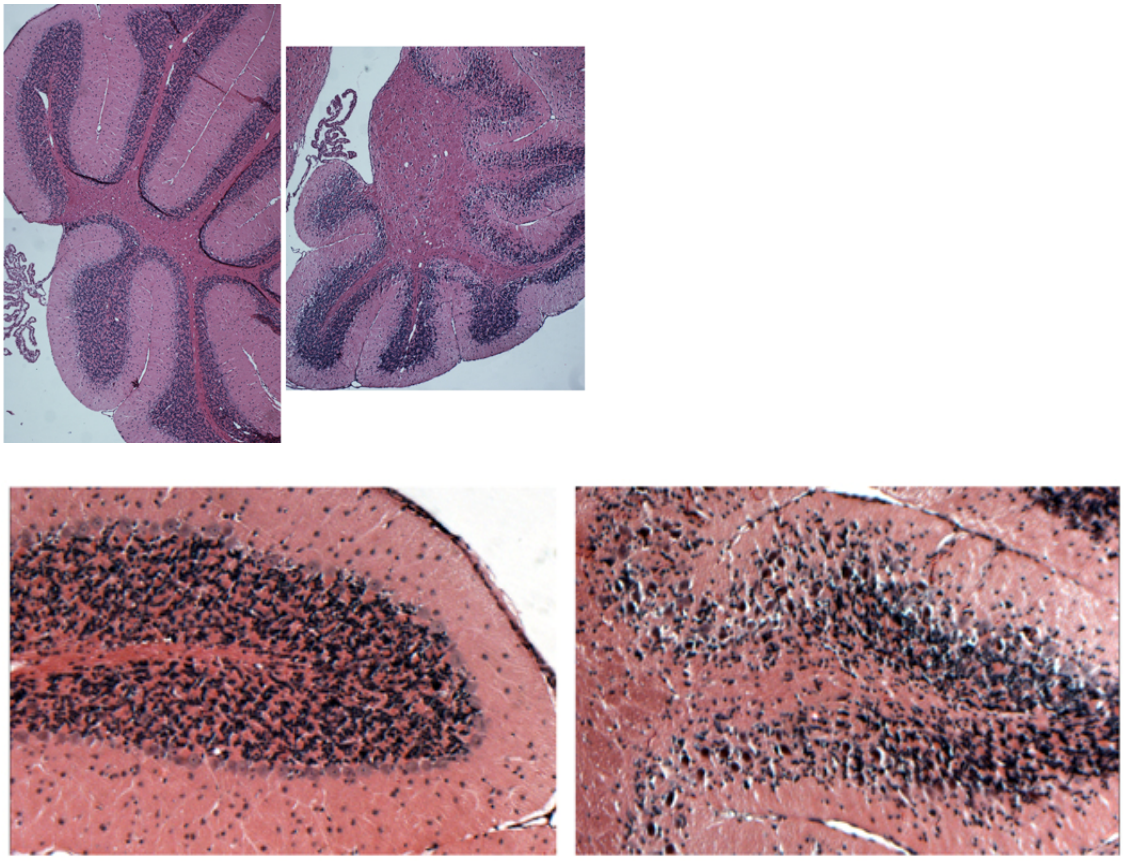

Figure 1-8. Cerebellum defects in MS/MTHFR double null mice. Near-midline sagittal brain sections of wild type and MS/MTHFR double null mouse were stained with hematoxylin and eosin and shown in left and right, respectively. Upper pictures showed a dramatically under-developed cerebellum in mutant mice. Bottom pictures showed a disrupted laminar structure at an anterior lobule of cerebellum in mutant mice; compared to the wild type, the granule cell layer of mutant cerebellum was partially missing or with dramatically reduced thickness and the Purkinje cells were less and very disorganized.

The overall brain structure in MS/MTHFR double null mice was intact, but the lateral ventricle in mutant mice was clearly enlarged. This is most likely due to the dramatically reduced size of the cerebellum and cerebral cortex. The cerebellum of MS/MTHFR double null animals was about only half the size of wild type and severely underdeveloped. All lobules were smaller and fissures were missing in mutant mice as compared to age-matched wild type animals (Figure 1-8). Bottom pictures showed a disrupted laminar structure at an anterior lobule of the cerebellum in mutant mice; compared to the wild type, the granule cell layer of mutant cerebellum was partially missing or with dramatically reduced thickness and the Purkinje cells were less and very disorganized.

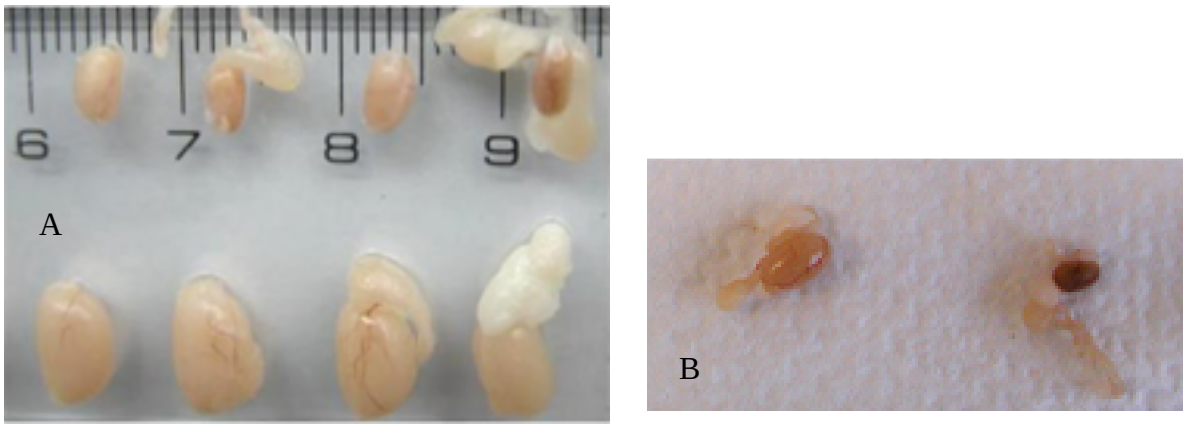

Figure 1-9. Testes appearance of wild type and knockout mice. A: comparison of the testis of 6-month-old male wild type (bottom) and MS/MTHFR double null (upper) mice. Mutant testis was smaller than wild type and these mice showed lower and remaining fertility. B: a testis of a sterile MS/MTHFR double null mouse (right) compared with another MS/MTHFR double null testis which was partially fertile.

MS/MTHFR double null male all had impaired fertility compared to wild type and there was considerable variation among mutant males. Figure 1-9 showed the testes appearance of wild type and mutant mice. Some mutant testis were half the size of wild type, but these mice still retain their fertility- just lower than wild type. About one third of mutant males were sterile and these mice had extremely small testis, about one eighth the size of wild type.

H&E staining revealed the internal structure of these testes (Figure 1-10). In mutant testis, decreased tubule diameter and germ cell numbers were clear visible; only a few tubules had been staged, and germ cells were absent in most tubules which showed predominantly vacuolization which only Sertoli cells appeared to contain.

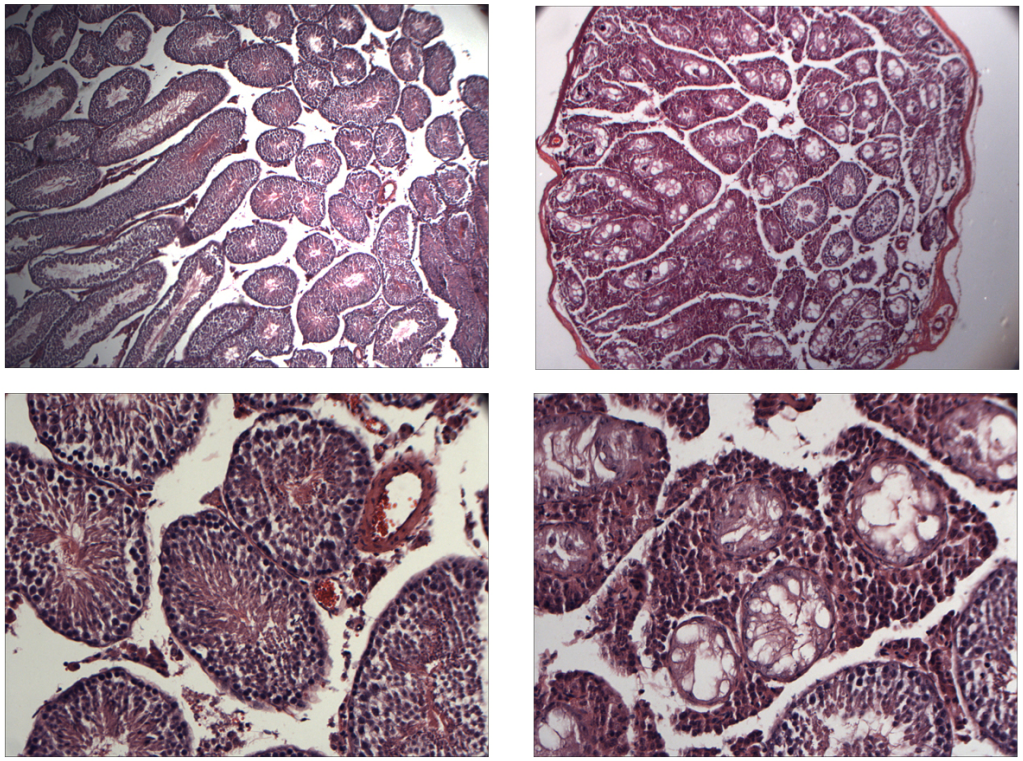

Figure 1-10. Histology of testis defects in knockout mice. Hematoxylin and eosin staining of paraformaldehyde fixed testis sections of 6-month-old wild type (left) and MS/MTHFR double null mice (right) are showed. In mutant testis, decreased tubule diameter and germ cell numbers were clear visible; only 4 tubules in this section had been staged, and germ cells were absent in all the other tubules which showed predominantly vacuolization.

Lipid deposition

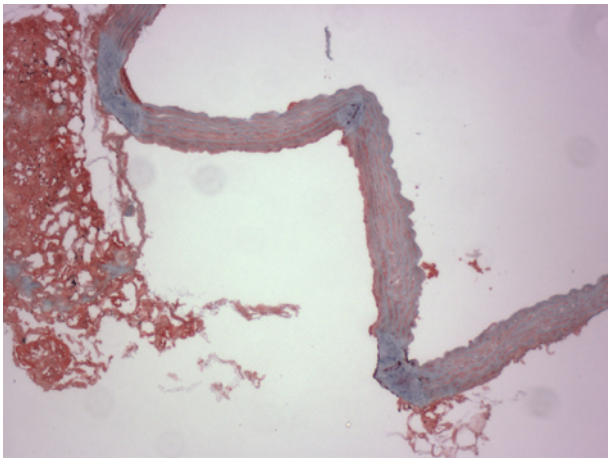

Figure 1-11. Red O lipid staining of coronary artery section of 6-month-old male MS/MTHFR double null mouse. No apparent plague was founded.

It was reported that MTHFR disruption would cause lipid deposition on the artery wall. However, we didn't observe clear plague on the coronary wall of MS/MTHFR double null mice (Figure 1-11).

Metabolic changes

Plasma homocysteine

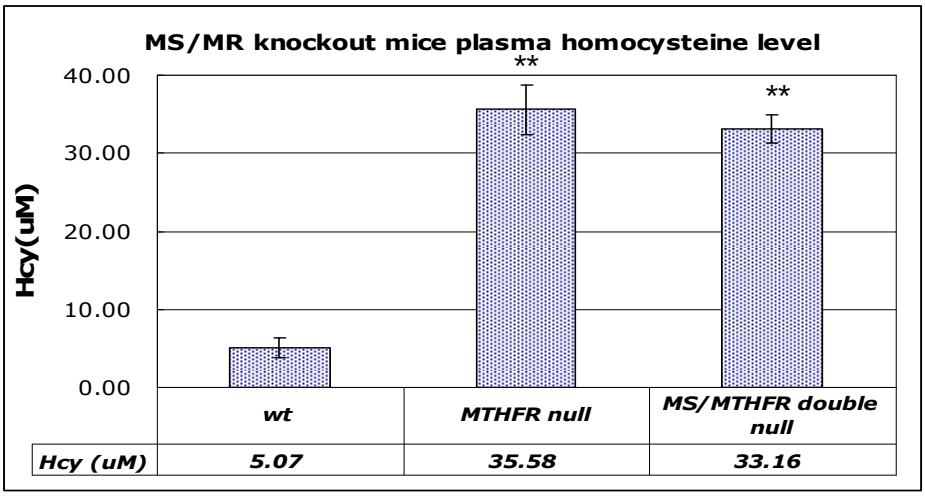

Figure 1-12. Plasma homocysteine level in 6-month-old male wild type, MTHFR null and MS/MTHFR double null mice. Each value represented data from 10 to 12 mice. ** $P < 0.001$ (Student's *t*-test) compared to WT mice of the same age.

Homocysteine exists in free and in protein-bound forms in circulation. The method we used to measure homocysteine combines both forms and results are presented as total homocysteine.

Plasma total homocysteine levels were significantly increased in MTHFR null and MS/MTHFR double null compared with wild type (Figure 1-12). The values were about 6.1 and 5.6 fold higher than wild-type in single and double null animals, respectively.

Tissue SAM and SAH

		SAM (nmol/g)	SAH (nmol/g)	SAM/SAH ratio
Brain	Wild type	8.1 ± 1.1	7.6 ± 1.1	1.1 ± 0.1
	MTHFR null	7.0 ± 0.4*	11.7 ± 2.5**	0.6 ± 0.1*
	MS/MR double null	5.7 ± 1.2**	9.0 ± 2.2*	0.7 ± 0.1*
Liver	Wild type	34.4 ± 2.0	19.9 ± 4.5	1.8 ± 0.3
	MTHFR null	13.1 ± 2.0**	33.3 ± 4.7**	0.4 ± 0.1**
	MS/MR double null	11.8 ± 2.1**	28.5 ± 6.4*	0.4 ± 0.1**
Kidney	Wild type	19.0 ± 2.1	15.8 ± 1.4	1.2 ± 0.2
	MTHFR null	25.1 ± 2.6*	21.3 ± 2.2*	1.2 ± 0.1
	MS/MR double null	21.5 ± 2.7	17.0 ± 3.1	1.3 ± 0.1
Testis	Wild type	10.4 ± 2.1	12.6 ± 1.0	0.8 ± 0.1
	MTHFR null	7.0 ± 0.3**	19.8 ± 0.4**	0.4 ± 0.0**
	MS/MR double null	7.0 ± 1.0*	16.4 ± 6.8*	0.5 ± 0.2*

Table 1-3. Tissue SAM and SAH in knockout mice. Data showed mean ± SEM concentration of tissue SAM, SAH (nmol/g) and SAM/SAH ratio in male wild type, MTHFR null and MS/MTHFR double null mice. Each datum represented 10–12 mice. * P < 0.05, ** P < 0.01 (Student's *t*-test) compared to WT mice of the same age.

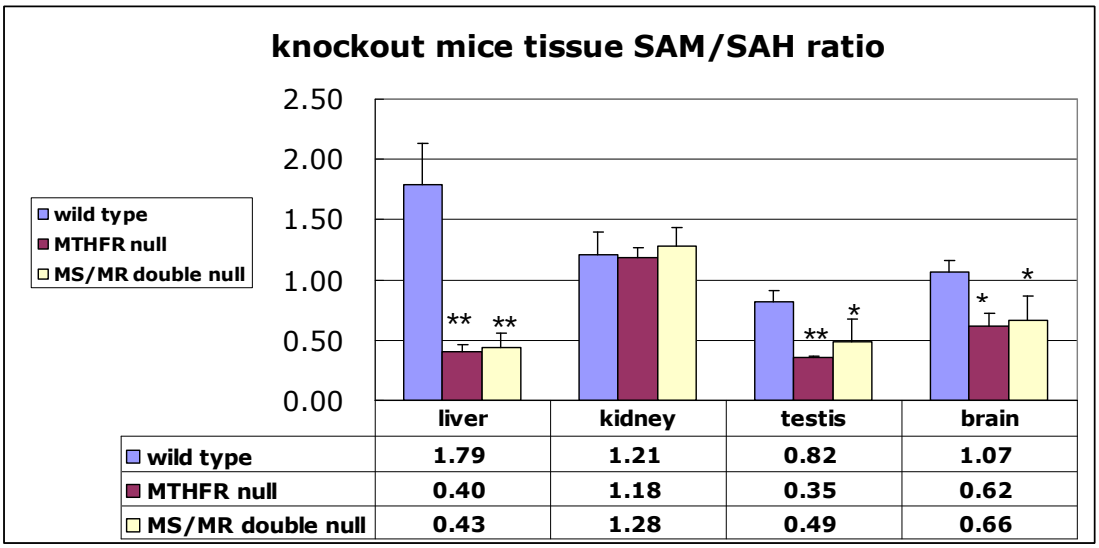

Figure 1-13. Tissue SAM/SAH ratios in 6-month-old male wild type, MTHFR null and MS/MTHFR double null mice. Each value represented data from 10 to 12 mice. * P < 0.05, ** P < 0.01 (Student's *t*-test) compared to WT mice of the same age.

Figure 1-13 and table 1-3 shows the changes in SAM and SAH levels and in the SAM/SAH ratio in the livers, kidney, testes and brains of MTHFR null or MS/MTHFR double null mice. The two types of knockout mice showed very similar patterns of SAM and SAH levels.

Compared to the other three organs, hepatic SAM and SAH showed the most significant change in the mutant mice. Hepatic SAM was dramatically decreased to only 1/3 as of wild type

while the SAH level was increased to at least 1.5 fold, which led to a considerate decrease in the SAM/SAH ratio compared to the wild type.

The change of SAM and SAH levels in the mutant brain and testis followed similar trend as in the livers, although less marked. SAM levels were significantly decreased in mutant mice while SAH levels were significantly increased, and the overall results were dramatically decreased SAM/SAH ratios.

It was very interesting that kidney SAM and SAH levels did not match the changes observed in liver, brain or testis. SAM levels were increased instead of decreased; SAH levels were increased as well, but both changes were not statistically significant. Kidney SAM/SAH ratios in the null mice were very similar to that in the wild-type.

The ratio of SAM/SAH is frequently used as an indicator of cellular methylation potential. The fact that a decreased SAM/SAH ratio existed in mutant brain and testis but not in kidney suggested a relationship between a disrupted methylation cycle and the pathological changes in these two organs.

MMA

Plasma methyl malonyl-CoA level did not show differences between wild type, MTHFR null or MS/MTHFR double null mice and all fell into a narrow range: from 300 to 350 pmol/ml (Figure 1-14).

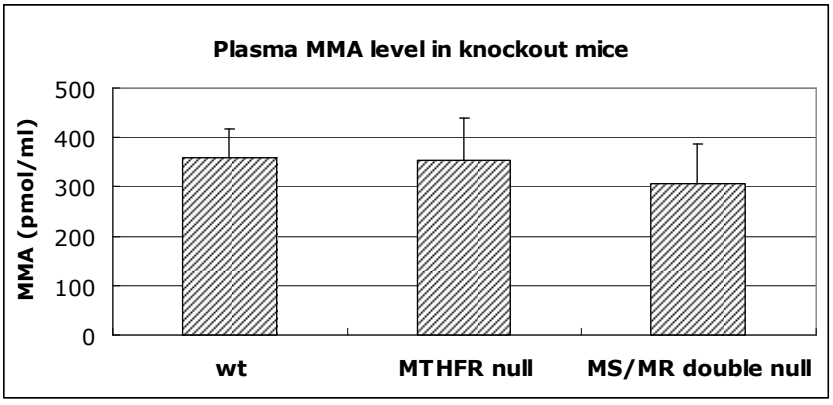

Figure 1-14. Concentration of plasma MMA in male wild type, MTHFR null and MS/MTHFR double null mice. Data were showed as mean ± SEM. Each bar represented data from 6–8 mice.

Folate derivatives

Wild type, MTHFR +/- and MTHFR -/- mice were fed an AIN-93G diet with 0.5 mg/kg or 5 mg/kg folic acid for 3 months, and their total liver and plasma folate content were determined by microbiological assay. The distribution of folate coenzymes in the liver was determined by HPLC-radioactivity analysis. Compared with mice fed with diet containing 0.5 mg/kg folic acid, those fed on a 5mg/kg folic acid diet had higher plasma folate (Figure 1-15). However, the amount of increase was affected by the genotype. In wild type mice, plasma folate

increased from 61.9 ng/ml to 203.5 ng/ml (3.3 fold); in MTHFR +/- and MTHFR -/- mice, plasma total folate increased 2.1 and 1.7 fold respectively, and these MTHFR defective mice had significant lower plasma folate compared with wild type when fed on 5 mg/kg folic acid diet. Unexpected, the opposite effects were seen in animals on the chow diet. MTHFR heterozygote and null mice had more plasma folate compared with wild type. This will need to be evaluated again but may have been due to inconsistency in the chow diet.

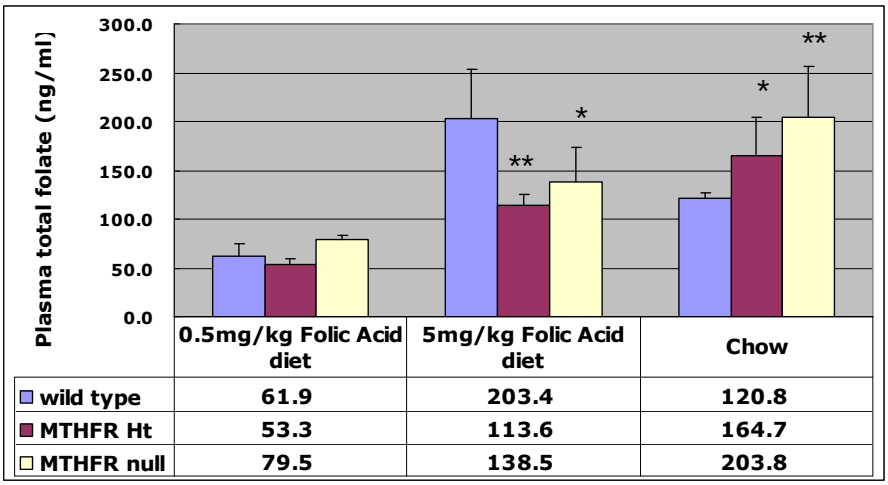

	0.5mg/kg Folic Acid diet	5mg/kg Folic Acid diet	Chow
wild type	61.9	203.4	120.8
MTHFR Ht	53.3	113.6	164.7
MTHFR null	79.5	138.5	203.8

Figure 1-15. Concentration of plasma total folate in wild type, MTHFR heterozygous and MTHFR null mice. Each bar represented data shown as mean ± SEM from 4–6 mice. * $P < 0.05$, ** $P < 0.01$ for comparison of mutant mice with the WT mice of the same diet (Student's *t*-test).

Liver total folate level did not change with folic acid content in the diet in the wild type mice. However, in MTHFR +/- or -/- mice, liver total folate increased by 27% and 20% respectively on 5 mg/kg folic acid diet compared with 0.5 mg/kg folic acid diet (Figure 1-16). Also, when dietary folate was low, wild type mice had more liver total folate than those with MTHFR mutant; when dietary folate was very high, the opposite phenomenon was observed. This showed that MTHFR +/- or -/- mice accumulated more folate in liver when the folate supply was more than sufficient. Mice fed on chow diet followed the similar tendency to the high folic acid diet.

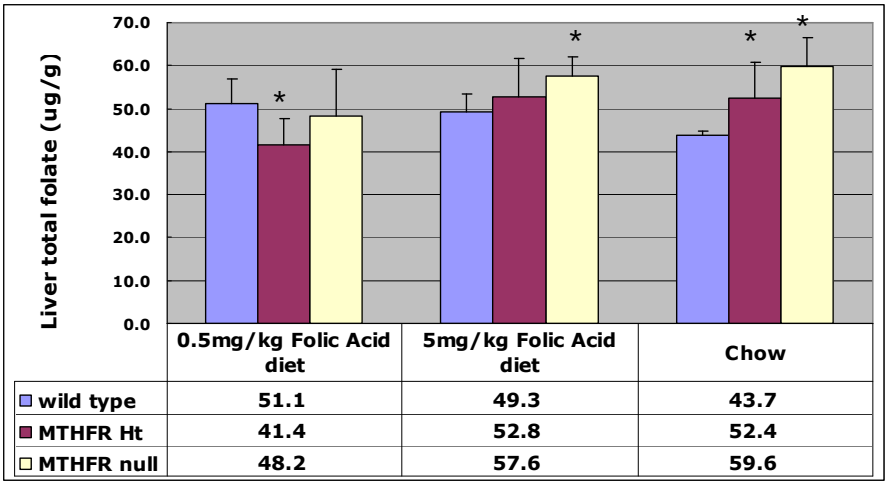

	0.5mg/kg Folic Acid diet	5mg/kg Folic Acid diet	Chow
wild type	51.1	49.3	43.7
MTHFR Ht	41.4	52.8	52.4
MTHFR null	48.2	57.6	59.6

Figure 1-16. Concentration of liver total folate in wild type, MTHFR heterozygous and MTHFR null mice. Each bar represented data shown as mean ± SEM from 4–6 mice. * $P < 0.05$ for comparison of mutant mice with the WT mice of the same diet (Student's *t*-test).

Folate enzyme distribution in liver was determined with a HPLC-radioactivity method. Liver folate was extracted and treated with dialyzed rat serum, which contained a conjugase to converted $PteGlu_n$ to their monoglutamate form. The different forms of folate were then separated by HPLC. Eluted fractions were monitored for folate by both radioactivity counting and microbiological assay. Experiment results from these two methods matched from each other and showed a common pattern (Figure 1-17). From wild type mouse liver, four major folate peaks were detected, 10-formyl-THF (10-HCO-H_4PteGlu), THF (H_4PteGlu), 5-formyl-THF (5-HCO-H_4PteGlu) and 5-methyl-THF (5-CH_3-H_4PteGlu) at retention time 25, 30, 35 and 51 minutes, respectively. Another small peak detected at retention time 10 min was determined as to be PABA-Glu, which may have resulted from folate degradation during handling.

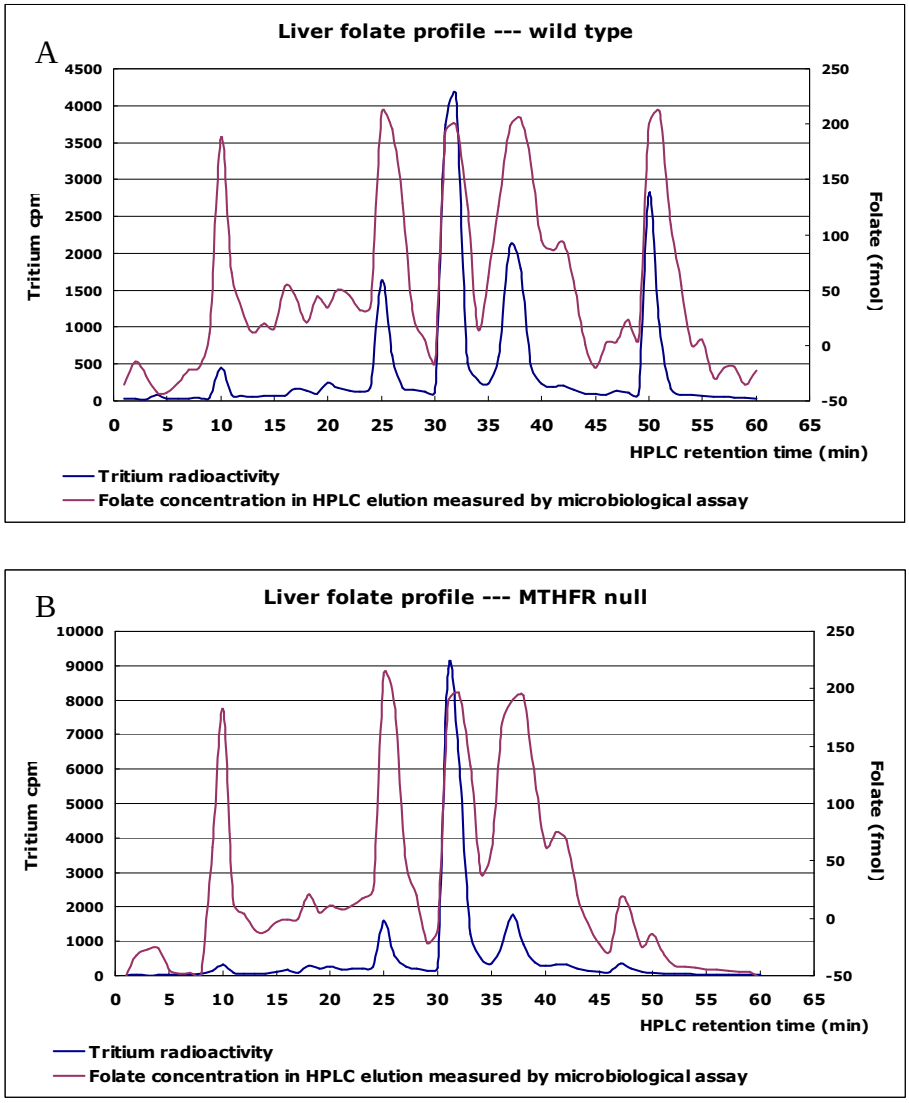

Figure 1-17. Representative profile of the separation and determination of liver folate coenzymes. Conjugase treated liver folate extract was separated by HPLC and fractions were then analyzed by both tritium radioactivity and microbiological assay, respectively. A: wild type. B: MTHFR null.

The quantitative percentage distribution of folate enzymes from HPLC elutes was determined by tritium radioactivity counting because of its better sensitivity and accuracy compared with microbiological assay. As shown on table 1-4, 24 hours after ^{3}H-folic acid injection, the percentages of each folate enzyme in wild type mouse liver were H_4PteGlu (44.6%), 5-CH_3-H_4PteGlu (24.8%), 5-HCO-H_4PteGlu (19.6%) and 10-HCO-H_4PteGlu (11.0%). In MTHFR +/- mouse liver, H_4PteGlu increased significantly and all the other forms decreased significantly compared to wild type mouse. Such a tendency was more obvious in MTHFR -/- mouse liver and the peak representing 5-CH_3-H_4PteGlu was totally absent. The fact that there was no injected ^{3}H-folic acid converted to 5-CH_3-H_4PteGlu in MTHFR -/- mouse liver proved that MTHFR knockout was complete. Very interestingly, when we monitored the eluted fractions with microbiological assay, there was a tiny amount of methyl-THF detected. This finding matched the previous results from the Rozen group, but after compared the results from tritium

radioactivity and microbiological assay, we decided that the former was more reliable than the latter and this tiny amount of methyl-THF might come from the potential contamination during the operation of the microbiological assay.

	Wild type	MTHFR Ht	MTHFR null
10-HCO-H_4PteGlu	11.0	5.8*	3.9**
H_4PteGlu	44.6	70.7*	88.4**
5-HCO-H_4PteGlu	24.8	10.0**	7.7**
5-CH_3- H_4PteGlu	19.6	13.5*	0.0 (ND)

Table 1-4. Percentage of individual tritium incorporated folate forms in total folates from liver of mice stratified by MTHFR genotype. Each number showed the percentage of individual PteGlu derivative in total liver folates eluted from the column. The distribution of folate derivatives in mouse liver was determined by HPLC-radioactivity analysis of conjugasetreated extracts prepared as described under Materials and Methods. The values reported represented the means of 5 samples. Symbols indicate a difference from the MTHFR wild type and knockout genotypes, ND, not detectable. * $P < 0.05$, ** $P < 0.01$ (Student's *t*-test) compared to WT mice.

Cobalamins

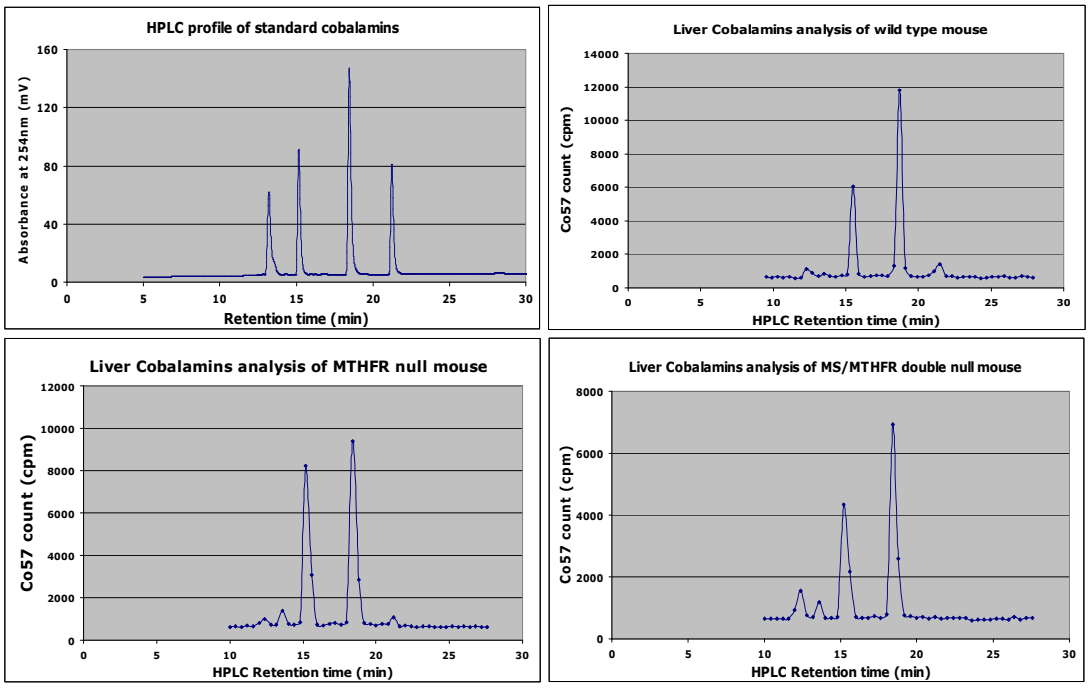

Figure 1-18. Separation profile of liver cobalamins by HPLC.

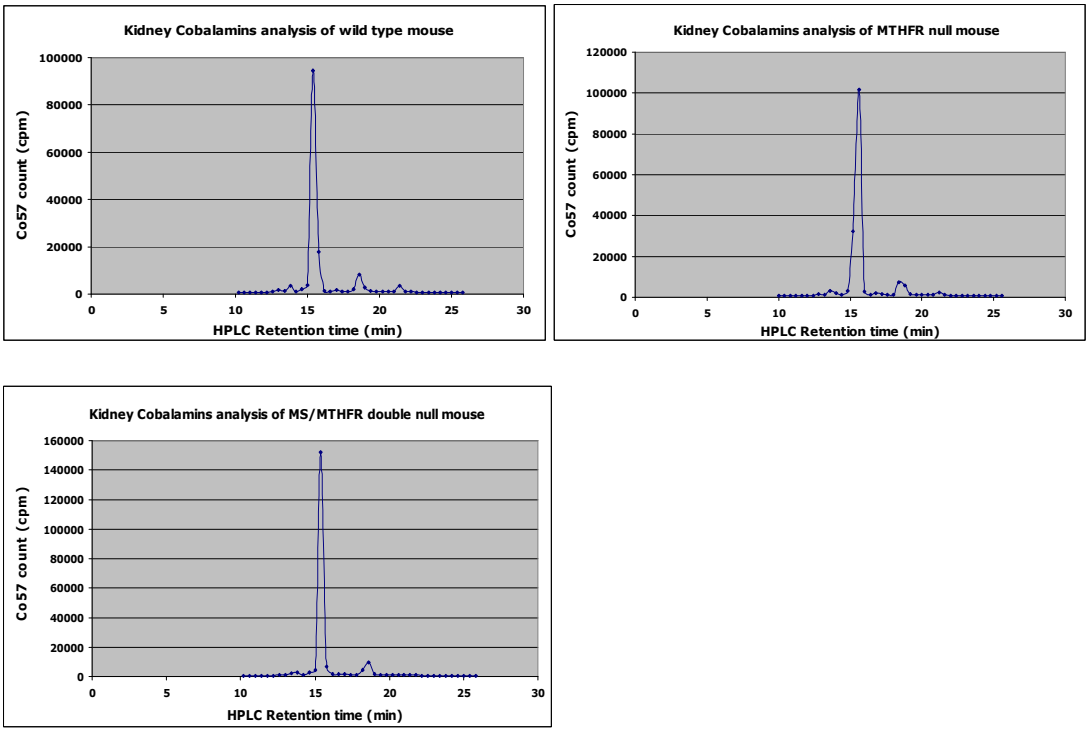

Figure 1-19. Separation profile of kidney cobalamins by HPLC.

Liver and kidney cobalamin coenzymes distribution in wild type, MTHFR null and MS/MTHFR double null mice was determined by a HPLC method combined with radioactive counting. Figure 1-18 and 1-19 show typical separation profiles.

24 hours after injection, most ^{57}Co-cyanocobalamin was excreted by the kidney. Liver accumulated about 10% of injected cyanocobalamin and 30-40% of this was unmetabolized while the remainder was converted it to other forms of cobalamins - mainly Ado-Cbl which accounted for 50-60% labeled liver cobalamin and small amount of Me-Cbl or OH-Cbl (Table 1-5). Liver's ability to convert cyancobalamin to its co-enzyme forms was significantly impaired in MTHFR null mice. In MS/MTHFR double null liver or kidney, an absolute absence of Me-Cbl was found, which proved that MS is the sole enzyme that catalyzes the transfer of the methyl group from methyl-THF to cob(I)alamin to form methylcob(III)alamin and the transfer of the methyl group from methylcob(III)alamin to homocysteine to generate methionine and cob(I)alamin. MS also plays a role in the general reduction of cob(II)alamin to cob(I)alamin catalyzed by methionine synthase reductase (MSR), so a reduction in Ado-Cbl level was also found in the double null mice.

		Wild type	MTHFR null	MS/MTHFR double null
Liver	OH-Cbl	3.7 ± 0.4	2.6 ± 1.1	5.3 ± 2.5*
	CN-Cbl	30.8 ± 2.8	43.9 ± 1.5**	40.1 ± 4.4*
	Ado-Cbl	60.3 ± 1.9	51.8 ± 3.2*	54.6 ± 6.9
	Me-Cbl	5.3 ± 1.4	1.6 ± 0.6**	N.D.
Kidney	OH-Cbl	2.2 ± 0.1	2.1 ± 1.0	1.3 ± 0.1**
	CN-Cbl	88.0 ± 0.3	90.2 ± 1.1	92.4 ± 0.6*
	Ado-Cbl	8.1 ± 0.1	7.0 ± 0.3	6.3 ± 0.5*
	Me-Cbl	1.7 ± 0.3	0.8 ± 0.3	ND

Table 1-5. Percentage of tissue cobalamins converted from exogenous ^{57}Co-Cyanocobalamin injection. Numbers (mean ± SEM) represented results from 3 mice of each genotype. ND, not detectable. * $P < 0.05$, ** $P < 0.01$ (Student's *t*-test) compared to WT mice.

MS distribution in mouse brain

Western blot and in situ hybridization of MS showed that MS had a very low abundance in mouse brain. MS heterozygote and MTHFR null mice had a significantly lower expression of MS protein compared to wild type (about 22% and 35% respectively). No MS protein was detected in MS/MTHFR double null brain or spinal cord, which indicated the MS knockout was complete. There was no MS protein detected in cultured astrocytes, other cell types not measured (Figure 1-20).

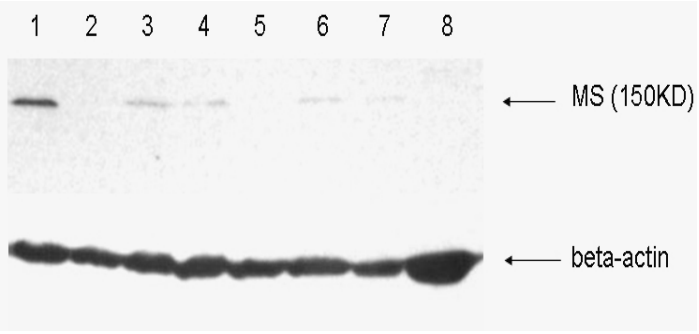

1. **Brain ─ wild type**
2. **Brain ─MS/MTHFR double null**
3. **Brain ─ MTHFR null**
4. **Brain ─ MS heterozygote**
5. **Spinal cord ─ MS/MTHFR double null**
6. **Spinal cord ─ MTHFR null**
7. **Spinal cord ─ MS heterozygote**
8. **Cultured astrocytes from wild type mouse brain**

Figure 1-20. Expression of MS in wild type or mutant mouse brain and spinal cord, and in primary cultured astrocytes.

In situ hybridization only detected very weak signals of MS RNA in hippocampus and olfactory bulb (data not shown), the only two regions in adult brains where cell proliferation exists, which indicated a potential function of MS in brain neurogenesis.

Apoptosis in brain cortex

Tissue sections were stained by TUNEL reaction and evaluated by morphometry using a confocal-microscope. The number of apoptotic nuclei was significantly increased in both the cortex and the spinal cord of the mutant mice (Figure 1-22).

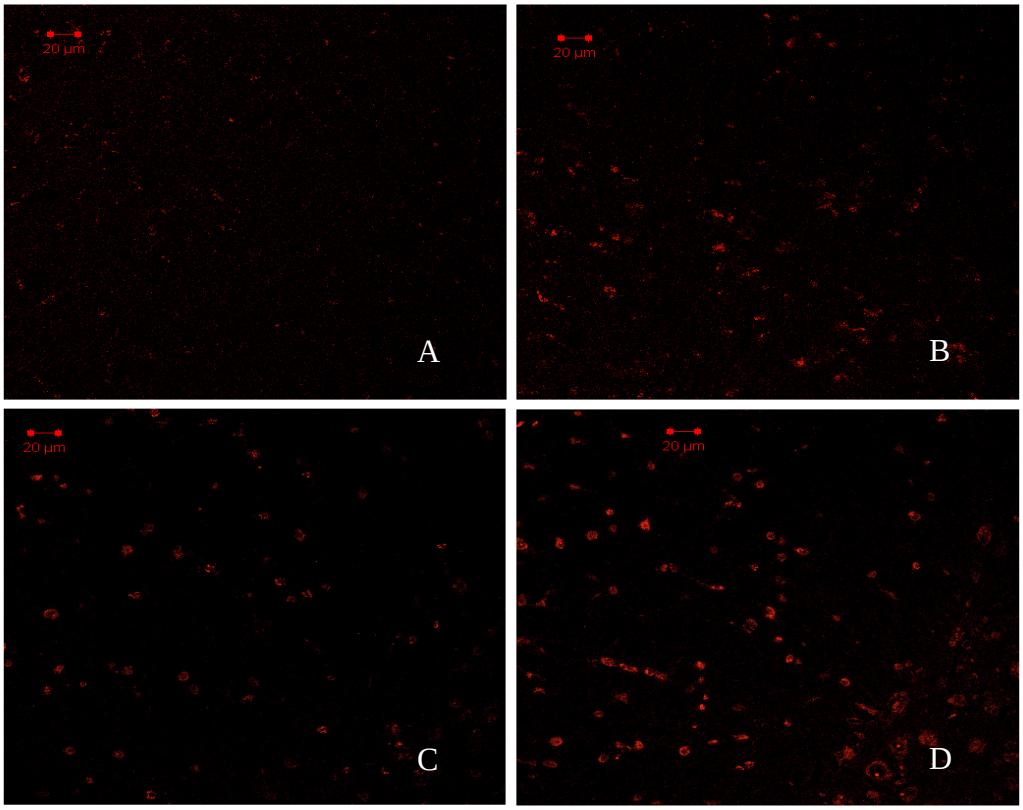

Figure 1-21. Apoptosis in MS/MTHFR double null brain and spinal cord. TUNEL analyses of cerebrum cortex and spinal cord at 6-month-old wild type (A and C) and MS/MTHFR double null (B and D) are shown. In wild type mice, apoptosis was rarely detectable, while in mutant mice, increased apoptosis was detected in both cortex and spinal cord, especially in white matter.

Impairment of neural cells proliferation in adult neurogenic regions

In the adult brain, some neurogenesis is still maintained in the ependymal/subependymal region of the lateral ventricles and the hippocampus dentate gyrus. We investigated cell proliferation in these regions by BrdU incorporation. BrdU was injected once daily over 3 consecutive days and the animals were killed 1 week after the first injection. A 1 week interval from the time of the first injection to the time of death allowed sufficient time for postmitotic oligodendrocyte progenitors to acquire properties of mature glia. In MS/MTHFR double mutants, the number of BrdU-positive cells was markedly reduced in the hippocampus germinative layer

(a 75% reduction) (Figure 1-23 A, B) and in the lateral ventricle (an 85% reduction) (Figure 1-23 C, D).

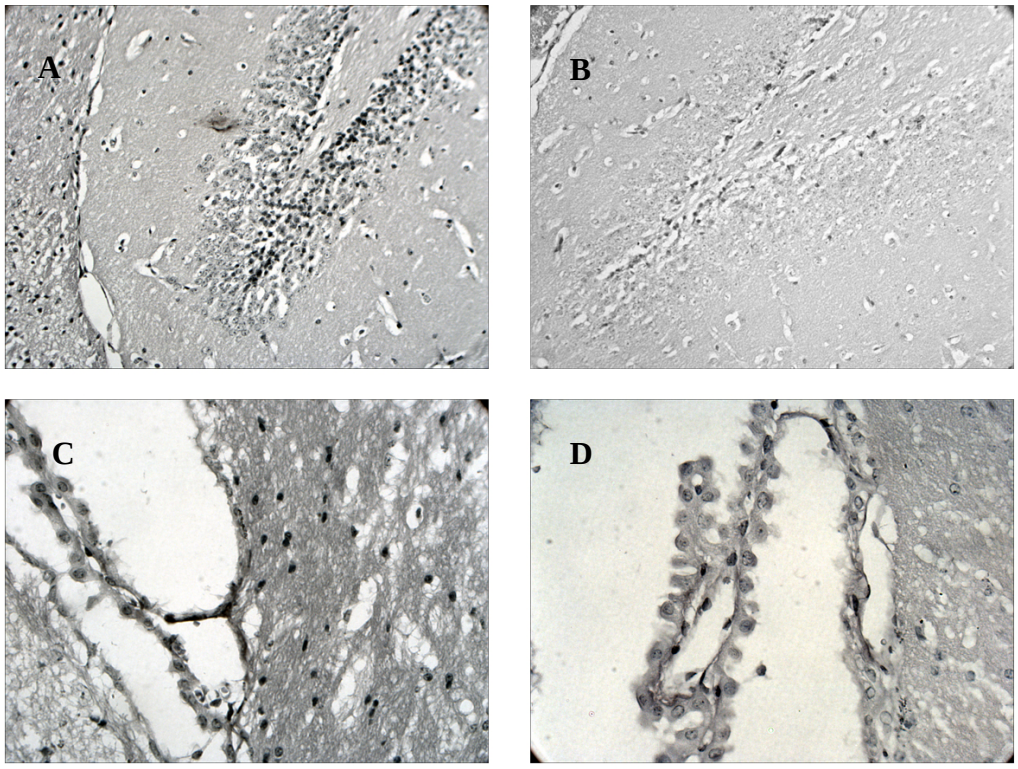

Figure 1-22. Brain cell proliferation in hippocampus and sub-ventricular zone of wild type mouse (A and C) and MS/MTHFR double null mouse (B and D). In MTHFR/MS mutants, the number of BrdU-positive cells was clearly reduced in both hippocampus dentate gyrus and in the lateral ventricle.

Brain lipid separation

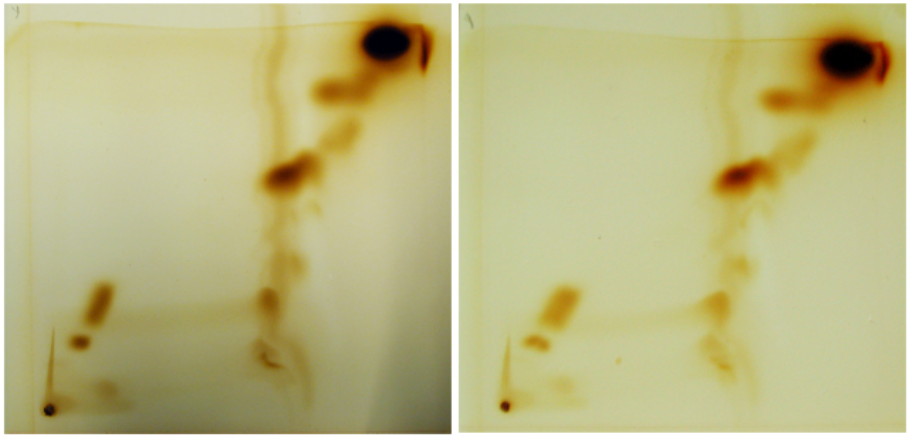

Figure 1-23. Two-dimension thin-layer chromatograph of brain lipids from 6-month-old male wild type (left) and MS/MTHFR double null mouse (right).

Brain lipids from 6-month-old male wild type and MS/MTHFR double null mouse were separated and analyzed by two-dimension thin-layer chromatograph, results showed no significant difference found between the mutant and wild type mouse (Figure 1-24).

MTHFR null or MS/MTHFR double null effects on gene expression in mouse liver and brain

Two cDNA microarray studies were performed to better understand the underlying mechanisms behind the phenotypes. Postnatal day (P)1 mouse brain and liver from MTHFR null, MS/MTHFR double null and wild type mice were used. The data revealed up-regulation and down-regulation of a significant number of genes over a broad range of expression levels in MTHFR null and MS/MTHFR double null liver and brain. There two mutant mice showed very similar gene expression profile differences when compared to wild type mice; the differentially expressed genes were very common in these two mutant mice. When we hybridize cDNA from single and double null mice, there were only a few genes which showed differential expression (see Table 1-6 and 1-7).

	Double null vs single null Log2 ratio	**Double null vs WT Log2 ratio**
ATPase, class I, type 8B, member 4	1.44	0.40
myosin VIIa	1.68	0.61
midline 1	1.85	2.07
DNA binding protein with his-thr domain	1.06	0.78

Table 1-6. List of differentially expressed genes in brain of MS/MTHFR double null comparing to MTHFR null and wild type.

	Double null vs single null Log2 ratio	Double null vs WT Log2 ratio
Splicing factor, arginine/serine-rich 8	1.10	1.41
Forkhead box O6	1.18	1.86
Zinc finger, MYND domain containing 19	0.93	1.94
SCAN domain-containing 1	1.25	1.27
Midline 1	1.86	2.61

Table 1-7. List of differentially expressed genes in liver of MS/MTHFR double null comparing to MTHFR null and wild type.

We then focused on those genes which showed common alteration in single and double null mice, and their complete lists are shown in Table 1-8 and 1-9. Among many categories of differentially expressed genes, of particular interest are the following groups: the iron-related genes hepcidin and H-ferritin; the lipid metabolism genes apolipoprotein A-IV, B and LDL receptor-related protein 1 (Lrp1); the ubiquitin related genes ubiquitin carboxy-terminal hydrolase L1 and ubiquitin-conjugating enzyme E2I (ubc9); growth hormone and insulin-like growth factor binding protein 1; and acute phase proteins orosomucoid 1 and 2, etc.

	Double null vs WT Log2 ratio	Single null vs WT Log2 ratio
Amino acid biosynthesis		
Asparagine synthetase	1.04	0.63
Cellular transportation		
Solute carrier family 7 (cationic amino acid transporter, y+ system), member 3	1.42	0.89
Folate metabolism and transportation		
Methylenetetrahydrofolate dehydrogenase (NAD+ dependent), methenyltetrahydrofolate cyclohydrolase	1.29	1.17
GH-IGF signaling		
Insulin-like growth factor binding protein 1	-1.25	-1.12
Growth hormone	-0.84	-1.14
CAMP signal transduction		
CAP, adenylate cyclase-associated protein 1 (yeast)	1.39	1.79
Translation factor		
Eukaryotic translation initiation factor 4E binding protein 1	1.24	1.15

Transmethylation		
Methionine adenosyltransferase II, alpha	1.24	0.89
Lipid metabolism		
Insulin induced gene 1	-1.11	-0.86
Carbohydrate metabolism		
Enolase 3, beta muscle	1.92	1.17
Brain structure		
Glial fibrillary acidic protein	-0.68	-0.77
Iron homeostasis		
Ferritin heavy chain 1	0.88	0.91
Hepcidin antimicrobial peptide	1.51	1.48
Proteinase inhibitor		
Serine (or cysteine) proteinase inhibitor, clade A, member 1e	-1.06	-0.68
Membrane structure		
Procollagen, type IV, alpha 6	0.49	1.35

Table 1-8. List of differentially expressed genes in brain of MS/MTHFR double null and MTHFR null compared with wild type.

	Double null vs WT Log2 ratio	**Single null vs WT Log2 ratio**
Lipid metabolism		
Apolipoprotein A-IV	-2.10	-1.21
Low density lipoprotein receptor- related protein 1	1.67	1.6
SUMOlytion		
Ubiquitin-conjugating enzyme E2I	-1.68	-1.17
Ubiquitin carboxy-terminal hydrolase L1	0.91	2.26
Iron homeostasis		
Ferritin heavy chain 1	0.89	1.51
Hepcidin antimicrobial peptide	2.16	1.95
Cell cycle		
Cyclin E1	0.64	2.11

Folate metabolism and transportation		
Mitochondrial folate transporter/carrier	1.7	2.51
Melanogenesis		
Dopachrome tautomerase	1.97	1.12
Transcription regulation		
H6 homeo box 3	-1.76	-1.71
Mitogen-activated protein kinase 8 interacting protein 3	1.51	1.45
SRY-box containing gene 1	2.48	1.81
G protein-coupled receptor 123	1.52	0.83
Homeo box B9	-1.63	-0.61
Myogenic differentiation 1	-1.68	-1.46
Protein phosphatase 1, regulatory subunit 10	1.72	0.93
Hormone biosynthesis		
Deiodinase, iodothyronine type III	-1.94	-0.90
Cellular transportation		
Solute carrier family 23 (nucleobase transporters), member 2	-1.69	-0.80
Solute carrier organic anion transporter family, member 4C1	1.71	0.74
Solute carrier organic anion transporter family, member 4C1	1.95	0.70
Solute carrier family 39 (zinc transporter), member 14	1.60	0.54
Solute carrier family 25, member 30	-1.51	-1.02
Solute carrier family 15 (H+/peptide transporter), member 2	-2.51	-2.14
Cell adhesion		
Cadherin 11	-2.08	-1.05
Immune response		
Interleukin 17 receptor D	1.51	0.55
Chemokine (C-X-C motif) ligand 1	2.52	2.91
Signal transduction		
G protein-coupled receptor 1	-1.62	-0.76
G protein-coupled receptor 100	1.81	1.69
Rho-related BTB domain containing 2	2.19	1.76
Adrenergic receptor, alpha 2a	-1.53	-0.73
G-protein coupled receptor 88	1.34	1.64

G protein-coupled receptor 48	1.64	0.99
CAP, adenylate cyclase-associated protein 1 (yeast)	2.97	1.86
One-carbon metabolism		
Carbonic anhydrase 3	1.97	0.92
Carbohydrate metabolism		
Glucuronidase, beta	1.52	1.42
Enolase 3, beta muscle	1.75	1.78
Acute response		
Orosomucoid 2	2.32	2.11
Orosomucoid 1	2.18	2.36
Oxygen transport		
Hemoglobin Y, beta-like embryonic chain	0.48	1.28
Exocytosis		
Synaptotagmin-like 3	1.60	1.54
Unclassified		
Abhydrolase domain containing 1	-1.86	-1.18
3-ketoacyl-CoA thiolase B	-1.55	-1.42
Murinoglobulin 1	1.70	1.04
Up-regulated in Myc liver	2.17	1.55
t-complex protein 10a	-1.68	-0.64

Table 1-9. List of differentially expressed genes in liver of MS/MTHFR double null and MTHFR null compared with wild type.

We then picked up several genes from the list and further confirmed the changes of expression levels by real-time PCR (Table 1-10 and 1-11).

Decrease---liver		cDNA microarray result (log2 ratio)		RT-PCR result (folds)	
		w/homo vs wt	homo/homo vs wt	w/homo vs wt	homo/homo vs wt
apoa4	apolipoprotein A-IV	1.21	2.10	3.87	6.97
ubc9	ubiquitin-conjugating enzyme E2I	1.17	1.68	2.69	3.76
Increase---liver					
frtH	ferritin heavy chain 1	1.51	0.89	3.94	3.32
uchl1	ubiquitin carboxy-terminal hydrolase L1	2.26	0.91	3.97	2.07
ccne1	cyclin E1	2.11	0.64	6.11	2.86
Lrp1	low density lipoprotein receptor- related protein 1	1.60	1.67	4.08	4.69
mft	mitochondrial folate transporter/carrier.	2.51	1.70	7.73	3.10
hamp	hepcidin antimicrobial peptide	1.95	2.16	6.13	5.26

Table 1-10. Comfirmation of hepatic microarray data by RT-PCR. Some of the genes which were differentially expressed in the liver of P(1) MTHFR null (w/homo) or MS/MTHFR double null (homo/homo) mice and confirmation of cDNA microarray results by RT-PCR.

Decrease-brain		cDNA microarray result (log2 ratio)		RT PCR result (folds)	
		w/homo vs wt	homo/homo vs wt	w/homo vs wt	homo/homo vs wt
gfap	glial fibrillary acidic protein	0.77	0.68	4.14	4.92
gh	growth hormone	1.14	0.84	5.50	2.45
igfbp1	insulin-like growth factor binding protein 1	1.11	1.25	2.99	5.03
Increase---brain					
frtH	ferritin heavy chain 1	0.91	0.88	2.45	2.01
mthfd2	methylenetetrahydrofolate dehydrogenase (NAD^+ dependent), methenyltetrahydrofolate cyclohydrolase	1.17	1.29	2.85	4.69
hamp	hepcidin antimicrobial peptide	1.48	1.51	4.78	4.93

Table 1-11. Comfirmation of brain microarray data by RT-PCR. Some of the genes which were differentially expressed in the brain of P(1) MTHFR null (w/homo) or MS/MTHFR double (homo/homo) null mice and confirmation of cDNA microarray results by RT-PCR.

DISCUSSION

MTHFR/MS double null mice survive and displayed a phenotype similar to that of MTHFR null mice, which confirmed that MS null mice die from extreme folate deficiency caused by a "methyl folate trap" and MS does not have additional unknown functions during development.

The only histological abnormalities of the single or the double knockout mice occurred in brains and testes. Among them, the testicular injury and impaired fertility of MS/MTHFR double null may most likely be explained by an impaired methylation, especially a hypo-methylation of DNA. The SAM/SAH level was significantly lower in MS/MTHFR double null mice and this ratio had been shown to be critical for testicular function in a study using Dnmt3L-/- mouse model (Webster. 2005). In another study, methionine supplementation seemed to reduce the testicular injury in rats fed on a Cbl-deficient diet (Yamada. 2007).

MTHFR null and MS/MTHFR double null mice showed a series of neuropathology, including a dramatic reduction in cerebellar size, the inner granule layer (IGL) diffusing in the rostral cerebellum, clusters of Purkinje cells intermingling with granule cells and dilated ventricular spaces (Chen. 2001). The underlying mechanism of the neuropathy is still unclear, although it might be related to defective DNA methylation and Reelin signaling pathway (Chen. 2005).

As expected, there was no myelin sheath loss like SCD seen in the brain or the spinal cord of single or double knockout mice. Considering the very low SAM/SAH ratio in the null brains, it is unlikely that defective methylation is responsible for this B12 deficiency neuropathy. Another possibility that elevated homocysteine causes demyelination was also ruled out for the same reason. Homocysteine was recently considered as a neurotoxin because several epidemiological studies have linked it to some CNS disorders of aging brain, such as cognitive decline, cerebrovascular disease and stroke, dementia and Alzheimer's disease (Obeid. 2006).

Impaired methylation is a critical phenomenon in MTHFR null or MS/MTHFR double null mice and it was postulated that the methylation of phosphatidylethanolamine (PE) to phosphatidylcholine (PC) would be interrupted under such a circumstances and result in a change of brain lipid composition. However, brain lipid motif in MS/MTHFR double null mice was similar to wild type mice, which implied that the conversion from PE to PC was not very sensitive to insufficient methyl group availability.

Methionine synthase is a low abundence protein. In adult mouse tissues, methionine synthase mRNA levels are expressed at the highest levels in pancreas, skeletal muscle, and heart, while hepatic and brain levels are much lower. However, methionine synthase is widely distributed and expressed in fetal development with the highest levels in nonhepatic tissue (Chen, 1997). Methionine synthase is expressed in the brain at twice the level as in the liver in adult mouse and such expression starts in early development. MS is postulated to have an important role in the brain: first, the main form of folate in the circulation is methyl-THF, which can not be readily retained in the cell until it is converted to THF by MS, at the same time, MTHFR is ubiquitously and highly expressed in the brain, the product methyl-THF from MTHFR must be reused locally; second, it is well known that brain folate level does not change significantly in

peripheral folate deficiency, MS is important to maintain brain folate levels; last, MS is relatively highly expressed in the olfactory bulb and hippocampus, the two regions where active neurogenesis had been observed, which implies MS is necessary for cell proliferation in adult brain.

MS protein levels were significantly decreased in MTHFR null and MS heterozygous mice. A surprising result is that there was no MS protein detected in primary cultured wild type mouse astrocytes. Reactive astrogliosis or "activated" astrocytes was considered as a common characteristic in the Cbl-deficient CNS of patients or various animal models (Scalabrino, 2001). Studies also showed that astrocytes efficiently uptake cobalamin, and methionine synthase activity was detected in the human transformed astrocyte cell line (TIN) and the human astrocytoma cell line (SIT) (Pezacka et al., 1992). It is still unclear whether this conflict resulted from the difference between primary cell cultures versus a transformed cell line or between species.

The similarity of MTHFR null and MS/MTHFR null was directly confirmed by the similarity of their gene expression profile. An Affymetrix array has been performed by Rozen group (Chen, 2002) to detect changes in gene expression in the brain of day 14 MTHFR null mice. However, other than increased MTHFD2, we did not see similarities between our differentially expressed genes and those obtained using the Affymetrix data. Because we used day 1 brains while the Rozen group used day 14 brains, the above difference may be explained by the dramatic dynamic change of gene expression pattern in neonates. For example, the Rozen group has found that the down-regulation of En2, Reln and Itpr1 expression in P7 MTHFR null brain did not occur in P2 brain (Chen, 2005).

The microarray data provide us with many clues to better understand the underlying mechanism of the abnormality in the null mice, as well as their cellular and biochemical changes. For example, compared with the wild type, growth hormone mRNA level is apparently low in MTHFR null and MS/MTHFR double null mice, which may be related to their retarded growth.

Several proteins involved in mitochondrial folate transportation and metabolism were found to be differentially expressed in the mutant mice compared to wild-type in our microarray data, for example, methylenetetrahydrofolate dehydrogenase (NAD^+ dependent), methenyltetrahydrofolate cyclohydrolase (MTHFD2) and mitochondrial folate transporter/carrier (MFT) mRNA were found significantly up-regulated in both single and double knockout mice. Folates interconversion and transport between cytosol and mitochondria is essential for the proper functioning of mammalian folate metabolism. In mitochondria, reduced folates are particularly necessary for the synthesis of glycine from serine and the glycine cleavage system, which in turn generates 10-formyltetrahydrofolate (Cook, 1979). A point mutation in MFT has been identified as the cause of the auxotrophy for glycine in a mutant Chinese hamster ovary cell line, glyB (McCarthy, 2004). The MTHFD2 mutation is embryonic lethal at about E12 and the fibroblast cell lines acquired from MTHFD2 knockout embryos are glycine auxotrophs (Patel, 2003). The up-regulation of MFT and MTHFD2 expression in MTHFR null or MS/MTHFR double null may be a result of elevated folylpolyglutamates in the cytosol. The above suggest that further study on MS/MTHFR mutant mice would help us to better understand the role of compartmentalization of folate cofactors in mammalian cells.

Folate compartmentalization in mammalian cells, primarily between the cytoplasm and mitochondria has been widely known (Christensen, 2006). However, recent studies demonstrated that cSHMT, thymidylate synthase, and dihydrofolate reductase, the three folate-dependent enzymes involved in de novo thymidylate synthesis, all contain SUMO modification consensus sequences and may be translocated into the nucleus by a ubiquitin-conjugating enzyme E2I (UBC9) catalyzed SUMOylation during S and G2/M phases of the cell cycle in MCF-7 cells (Woeller, 2007). In our microarray data, UBC9 and another SUMOylation related protein, ubiquitin carboxy-terminal hydrolase L1 (UCHL1) were found to be differentially expressed in mutant liver, which suggested that defective MTHFR might affect the nuclear translocation of enzymes involved in thymidylate synthesis.

There have been previously several reports on the interaction of folate and iron metabolism (Pellis, 2007). It was shown that Fe deficiency resulted in folate deficiency in animals and human subjects. Also a direct interaction of Fe on folate metabolism has been shown; reduction of free Fe by chelation of Fe by either the chemical chelator mimosine or the biological chelator ferritin heavy chain resulted in up-regulation of the translation of rat cytoplasmic serine hydroxylmethyltransferease (cSHMT) and increased folate catabolism (Oppenheim, 2001). Here, our microarray date once again demonstrate that interrupted folate metabolism induced abnormal expression of iron related proteins in the liver and brain. We also noticed that some of the up-regulated iron proteins, such as hepcidin, ferritin heavy chain 1, were up-regulated in acute-phase response (Sheikh, 2007). Combined with the discovery of up-regulation of other acute-phase proteins, orosomucoid 1 and 2, etc, it is very likely that the knockout mice were under stress.

There was a large variation among some MS/MTHFR double null mice. For example, their 12-month-old body weight varied from less than 30 grams to over 40 grams, the severity of their testicular injury and brain abnormality was also diverse.

I postulate that the different methylation patterns among the littermates is related to the variation among the mutant mice, also, different betaine-homocysteine- methyltransferase (BHMT) or cystathionine β-synthase (CBS) activities may involved and need further examination. BHMT and CBS are enzymes involved in another hepatic homocysteine remethylation pathway and the homocysteine transsulfuration pathway respectively. These two enzymes may become more important when MTHFR and MS are defective.

The variation among mutant mice was also expected to relate with their mix genetic background, although the effect of background has been minimized by comparison of siblings. The fact that MS/MTHFR double mutant mice could not be backcrossed to a pure C57BL/6 background also strongly suggested the genetic background dramatically influenced the phenotype of such mutations. Similar phenomenon had been found in many other gene knockout projects and has received widely attention. For example, on the mixed backgrounds (129/Sv X CF-1or 129/Sv X C57BL/6, etc), approximately half of TGFβ1 null mice survived and developed an inflammatory disorder; while there was only about 1% of TGFβ1 null animals live to birth on the C57BL/6 inbred background (Bonyadi, 1997).

To further understand the effect of genetic background on MS/MTHFR knockout phenotypes, we examined the genetic variation of folate-related biochemical parameters between inbred strains of mice. These studies are described in Chapter IV.

Chapter II: Effect of Vitamin B12 deficiency on the methylenetetrahydrofolate reductase null and the methionine synthase heterozygous mouse

Many studies in animals and human have shown that vitamin B12 deficiency is associated with retarded growth and weight loss. As mentioned previously, monkeys, fruit bats and pigs showed a similar neuropathy to human SCD on an extreme B12 deficient diet. However, rats, an extensively used animal model for B12 deficiency metabolic effects, do not show anemia or neuropathy, when deficiency is induced by dietary means or with N_2O. Only a few studies have been done using the mouse as a model for B12 deficiency and the results obtained resembled those from rats (McGing, 1981). Researchers did find elevated MMA, homocysteine and other biochemical changes in rodents fed on a B12 deficient diet, so the reason why B12 deprivation did not lead to pathologies in rodents remains unclear at present.

We studied the effects of a vitamin B12 deficient diet on mice for several reasons. First, the mouse is the only animal in which genetic mutations in folate enzymes are available. Although some of the symptoms of vitamin B12 deficiency which are normally observed in humans have been reproduced in one or more other animal models, none of these models can be used to study the effect of vitamin B12 deficiency when one of the enzymes in folate metaboliam is defective, such as has been observed with some human polymorphisms or inherited genetic disease. Using the MTHFR null and the MS mouse heterozygous for deletion of the enzymes, our studies provide the first data on the interactions of severe vitamin B12 deficiency with genetic folate metabolism defects.

The absence of detectable neuropathy in B12 deficient rodents does not categorically exclude a possible effect of B12 deprivation on myelin turnover. By using a sensitive quantitative test, such as isotope labeled galactocerebroside analysis as described below, such effects may be detected, especially when they may be aggravated by the genetic disturbances.

The stable isotope labeled galactocerebroside kinetics method was developed by Dr. Hellerstein (UCB) and KineMed Inc. (US Patent: 20050202406A1). Galactocerebroside (GalC) is a glycosphingolipid specific for myelin and myelin forming cells. GalC accounts for over 20% of the total myelin lipid and its concentration in the adult brain closely correlates with myelin content. When ^2H_2O is administered to animals, the isotopic enrichment in GalC reflects the *in vivo* myelin synthesis rate.

Applying this method, myelin status at two ages was measured to investigate the effect of vitamin B12 deficiency on myelin turnover. Initially, we studied myelin formation in postnatal pups. In the mouse, myelination starts at birth in the spinal cord and is complete in most areas of the brain 45–60 days postnatally (Nave, 1994). Myelination in the mouse brain occurs at two stages. The first stage (occurring approximately 5-15 days after birth) involves the proliferation of oligodendroglial cells, cell enlargement, and plasma membrane formation and is characterized by a distinct absence of myelin. During the second stage (approximately 16-30 days after birth) recognizable myelin can be observed in the brain and the maximum rate of deposition occurs at about 20 days of age (Baumann, 2001).

Secondly, myelin degradation and oligodendrocytes neogenesis was investigated in the adult or aged phase. Myelin degradation is very common in the cortex of old monkeys and it correlates well with decreased performance on cognitive tasks (Peters, 2002). However, it also parallels the addition of new oligodendrocytes. This balance between degradation and glial neogenesis is likely the reason that only low-level loss of oligodendrocytes is found throughout the life in the adult CNS. In normal situations, both myelin degradation and neogenesis are very slow. However, after an induced demyelination, an accelerated remyelination occurs, and we used this to compare differences among mice with genetic defects and the effects of a B12-deficient diet.

METHOD AND MATERIALS

Diet and animals

The diet used in this study was a soy-based AIN-93G diet (Dyets), which is the same as the AIN-93G diet described in earlier studies except soy protein was used to replace casein and the concentration of methionine, folate and vitamin B12 were redefined. The methionine, choline, folate and B12 content of the experimental diets are listed in Table 2-1. 1% succinyl sulfathiazole was added to both control and B12-deficient diets.

Table 2-1. Methionine, choline, folate and B12 content of experimental diets

Diet	L-methionine g/kg	choline bitartrate g/kg	folic acid mg/kg	B12 ug/kg
Control(with B12)	3.6	2.5	0.5	25
Without B12	3.6	2.5	0.5	0

Animals used in this study included MTHFR null, MS heterozygote and wild type mice. They were kept on +B12 or –B12 diets during breeding, lactation and growth.

2.1. Biochemical disruptions

Plasma homocysteine and methyl-malonyl CoA levels were measured as previously described.

2.2. Plasma lipid profile

2.2.1. Plasma Triglyceride

Plasma triglyceride (TG) concentrations were determined by enzymatic assays (Sigma serum triglyceride determination kit TR0100).

2.2.2. Plasma cholesterol

Plasma total cholesterol concentrations were determined by enzymatic assay (Sigma Infinity total cholesterol enzymatic assay kit).

2.3. Real-time quantitative PCR

Real-time PCR was performed as described in Part I. Mouse liver RNA was extracted and reverse-transcripted to cDNA. Expression of several apolipoprotein genes in MTHFR null, MS heterozygote and wild type liver treated with +/- B12 was compared because of their direct effect on lipid metabolism. GAPDH was used as a control house-keeping gene.

Table 2-2. Primer sequences of apolipoproteins used in real-time quantitative PCR.

Glyceraldehyde 3-phosphate dehydrogenase (GAPDH) F 5'-TTGATGGCAACAATCTCCAC-3' R 5'-CGTCCCGTAGACAAAATGGT-3'
Apolipoprotein A-I (Apoa1) F 5'- CCAGAGTGTCCCAGTTTTCC -3' R 5'- TATGTGGATGCGGTCAAAGA -3'
Apolipoprotein A-IV (Apoa4) F 5'-TAGCATCCCCAAGTTTGTCC -3' R 5'-ACCCAGCTAAGCAACAATGC -3'
Apolipoprotein C-I (Apoc1) F 5'- AAATGCCTCTGAGAACCAGG -3' R 5'- GGAGTTTGGGAACACTTTGG -3'
Apolipoprotein C-III (Apoc3) F 5'- TGCTCCAGTAGCCTTTCAGG -3' R 5'- GGTCCAGGATGCGCTAAGTA -3'
Apolipoprotein H (Apoh) F 5'- AGCAGGAATATCTGGGCTCC -3' R 5'- TCCCAAGAACATCAGTTTTGC -3'

2.4. Myelin formation and turnover as measured by galactocerebroside kinetics

Galactocerebroside (GalC) is a glycosphingolipid specific for myelin and myelin forming cells and it is the major component of myelin lipid. KineMed Inc. developed a GC/MS stable isotope methodology to measure GalC kinetics, which provided an ideal quantitative biomarker for myelin synthesis. The process included labeling the animals with heavy water ($^2H_20$), isolating brain GalC, analyzing the galactose moiety of GalC by GC/MS and determining the deuterium isotopic enrichment.

2.4.1. $^2H_20$ Labeling

Mice were injected with sterile 99.9% $^2H_20$ in 0.9% NaCl intra-peritoneally at a dose rate of 0.03 ml/gm body weight to achieve 5% body water enrichment. The mice were subsequently maintained on 8% $^2H_20$ in their drinking water, which maintains a body enrichment of about 5% due to dilution by metabolic water.

2.4.2. Brain lipid extraction and TLC

Mouse brain lipid was extracted as described in section 1.5.1. 100 ml 65:25:4 chloroform-methanol-H_2O was added to a TLC chamber and lined with filter paper (equilibrated a minimum 1hr prior to loading samples). 13.3µl brain extract and 10 µg (10 µl of 1mg/ml) cerebroside standard was warmed to room temperature to ensure complete solubilization and spotted on TLC plates. The TLC plate was developed with 65:25:4 chloroform-methanol-H_2O until 0.5 inch from the top. The plate was then removed from the chamber and air dried for 15 minutes. Plates were put into an iodine chamber at 80°C until spots were visible. Spots representing cerebroside bands were marked with a pencil and scraped into vials. The silica was wet with 50 µl water and extracted twice with 2 ml of 5:1 chloroform:methanol with intermediate vortexing and centrifugation. The supernatant was transferred to a 13mm vial and dried under nitrogen.

2.4.3. Galactocerebroside derivatization

100 µl of 20 mg/ml pentafluorobenzyl hydroxylamine hydrochloride (PFBHA) in water and 75µl of acetic acid were added to the above TLC products. The 13mm vials were capped, vortex, and incubated at 120°C for 120 min. After cooling, 1 ml acetic anhydride and 100µl methyl imidazole were added. The reaction proceeded for 15 minutes until then the vials were cooled. 2ml water and 1 ml dichloromethane were added. After vortexing and centrifugation, the bottom layer was transferred to a new vial containing 2ml water. This step was repeated twice, and the bottom layer after the third centrifugation was then transferred to a new vial containing sodium sulfate. After mixing and centrifugation, the supernatant from above vial was transferred to a GC vial and dried. 0.5 ml dichloromethane was added to sodium sulfate, vortexed, centrifuged, and the supernatants were combined to GC vials from last step. When drying was completed under nitrogen, galactocerebroside derivative was resolubilized in 100µl ethyl acetate.

2.4.4. NCI GC-MS analysis of galactocerebroside

The galactose-penta fluoride acetate derivatives ($C_{23}H_{24}O_{11}N_1F_5$) were analyzed by GC-MS (DB-17 HT column, J & W Scientific, Folsom, CA; HP 5890 GC and 5971 MS, Hewlett-Packard). Abundances of ions at m/z 585 and 586 were monitored.

2.4.5. Plasma $^2H_20$ enrichment determination with tetrabromomethane

The plasma $^2H_20$ enrichment was measured to calculate the theoretical maximum deuterium enrichment into GalC and then the GalC fractional synthesis. It was determined by a tetrabromomethane method (Macallan, 1998).

Calcium carbide was added to GC vials under helium atmosphere with no more than 20% relative humidity. CCl_4/Br_2 vial was prepared as follows: add 400 µl CCl_4 to a GC vial, add 10µl concentrated bromine solution and cap the vial with a Teflon cap immediately. One 10ml syringe with needle was used to evacuate 10ml air from above Teflon-capped vial and 10ml air/helium from the vial containing calcium carbide. Then the needle was placed back into the calcium carbide-containing vial. 20µl water distilled from plasma or $^2H_20$ enriched water standard was drawn up using a 1ml syringe and quickly injected into the evacuated vial containing calcium

carbide. The reaction was very rapid and the acetylene gas produced filled the 10ml syringe which stuck in the vial. 10ml gas was drawn up and injected into the Teflon-capped vial containing CCl_4/Br_2, and white smoke appeared in the vial. The acetylene was allowed to react with bromine for at least 2 hours. The vials were then uncapped and 20µl cyclohexene was added to each vial. When the solution turned clear, the vials were recapped immediately with a Teflon cap.

Derivative tetrabromoethane was then analyzed using a DB-225 fused silica column, and m/z 265 and 266 (M0 and M1 masses of the $^{79}Br^{79}Br^{81}Br$ [parent-OAc] isotopomer) was monitored. Standard curves of known $^2H_20$ enrichment were run before and after samples to calculate isotope enrichment.

2.4.6. Myelin formation in young mouse

MS heterozygote and wild type mice were treated with +/-B12 diets through breeding. Immediately after weaning on P21, mice were given a ^2H_2O bolus i.p. and 8% ^2H_2O was administered via drinking water *ad lib* to maintain 5% body water enrichment. Mice from each group were randomly chosen and sacrificed at P35, P50 and P65, and their brain GalC deuterium fraction was measured as described.

2.4.7. Demyelination/remyelination mouse model using diets supplemented with cuprizone

Cuprizone, a copper chelater, is known to result in synchronous and anatomically reproducible demyelination with recovery of myelination after removal of the agent (Jurevics, 2001). Cuprizone was purchased from Sigma (St. Louis, MO) and mixed well into powdered +/-B12 diet at a final concentration as 0.2% w/w. MTHFR null, MS heterozygote and wild type mice were first treated with +/-B12 diets since breeding. From postnatal week 8, mice were maintained on +/- B12 diets containing 0.2% cuprizone (w/w) for 6 weeks. Cuprizone was then removed from the diet; ^2H_2O treatment was administered immediately and continued for another 3 weeks. At the end of week 17, mice were sacrificed and the brains were dissected and used to analyze the fractional synthesis of ^2H –galC.

We also used various control groups to determine normal rates of myelin turnover. Control group were MTHFR null, MS heterozygous and wild type mice fed on +/- B12 diet which did not undergo cuprizone treatment but received 3-week ^2H_2O administration right before sacrifice at the end of week 17. The true myelin synthesis after induced demyelination by cuprizone was calculated by apparent fractional synthesis deducting normal fractional synthesis.

2.5. Histological staining of myelin

Brain sections of each group were stained with LFB as described in Part I. We focused on the corpus callosum region because it is one of the most widely studied regions in this model of demyelination.

RESULTS

B12-deficiency had no significant effects on body weight of wild type male mice at 3 months of age, but it did affect male MS heterozygous mice. The MS heterozygotes on the vitamin B12-deficient diet had a significantly higher body weight compared with their siblings fed a B12 sufficient diet (Figure 2-1). On the other hand, MTHFR null mice had a significant lower body weight compared to MS heterozygote and wild type, and their body weight were not affected by dietary B12 content.

MS heterozygotes and wild type mice had higher plasma cholesterol and triglyceride levels when fed a vitamin B12 deficient diet, and this trend was observed with both genders; MTHFR null mice had a significantly lower plasma cholesterol and triglyceride levels compared to the MS heterozygote and wild type, and their plasma lipid profiles were not affected by dietary B12 content (Figure 2-2 to 2-5). This was unexpected because it had been reported that MTHFR deficiency caused hyperhomocysteinemia which had a positive correlation with hypertriglyceridemia.

B12 deprivation caused significant increases in plasma homocysteine levels in wild type and MS heterozygous mice, 4.3 and 5.1 fold compared with their siblings fed a B12 sufficient diet, respectively, as shown in Figure 2-6. Dietary B12 did not affect plasma homocysteine in MTHFR null mice; with or without B12, those mice maintained their plasma homocysteine at an extremely high level.

Some epidemiological studies found an association between hyperhomocysteinemia and hypertriglyceridemia, as well as a low serum HDL level (Harjai, 1999). However, the MTHFR null mice with higher plasma homocysteine had lower plasma cholesterol and triglyceride levels compared to wild type or MS heterozygotes. This study strongly supports the idea that hyperhomocysteinemia was merely an independent risk factor for CVD; it may appear along with hypertriglyceridemia or other conventional risk factors, but there is not a causative relationship between them.

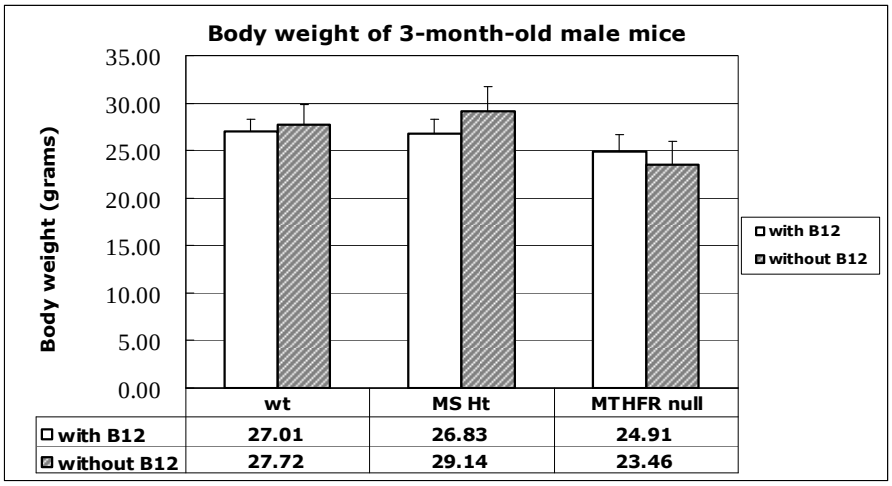

Figure 2-1. Dietary vitamin B12 affected 3-month-old male body weight in wild type, MS heterozygote and MTHFR null mice. Each bar represented data from 6-8 mice.

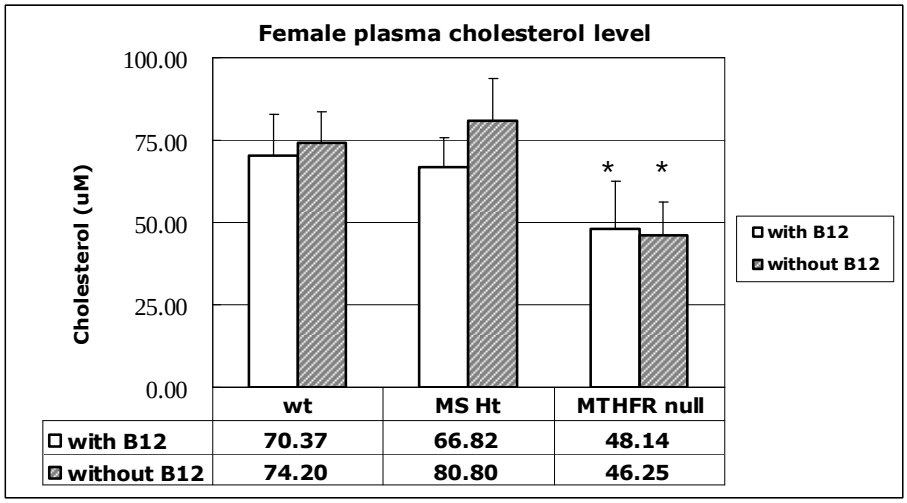

Figure 2-2. Dietary vitamin B12 affected female plasma cholesterol level in wild type, MS heterozygote and MTHFR null mice. Each bar represented data from 6-8 mice. * $P < 0.05$ for comparison of mutant mice with the WT mice on B12 sufficient diet (student's *t*-test).

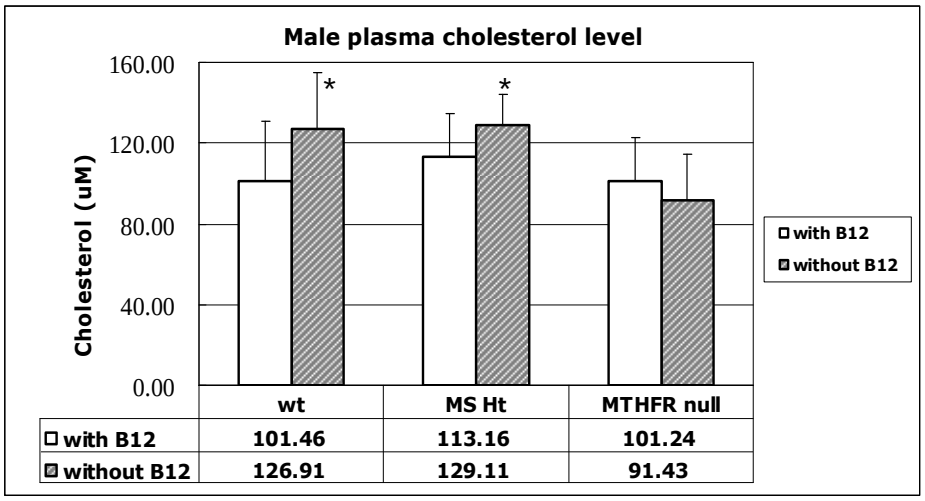

Figure 2-3. Dietary vitamin B12 affected male plasma cholesterol level in wild type, MS heterozygote and MTHFR null mice. Each bar represented data from 6-8 mice. * $P < 0.05$ for comparison of mutant mice with the WT mice on B12 sufficient diet (student's *t*-test).

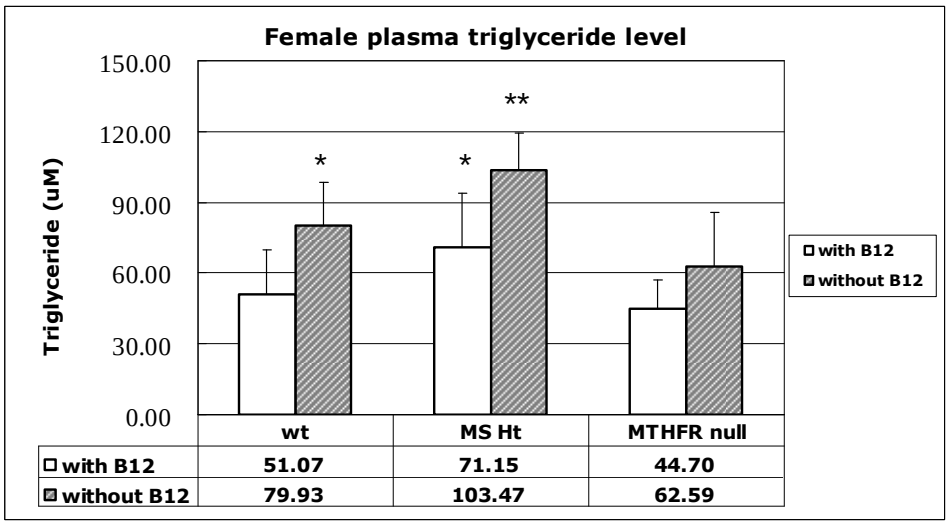

Figure 2-4. Dietary vitamin B12 affected female plasma triglyceride level in wild type, MS heterozygote and MTHFR null mice. Each bar represented data from 6-8 mice. * $P < 0.05$, ** $P < 0.01$ for comparison of mutant mice with the WT mice on B12 sufficient diet (student's *t*-test).

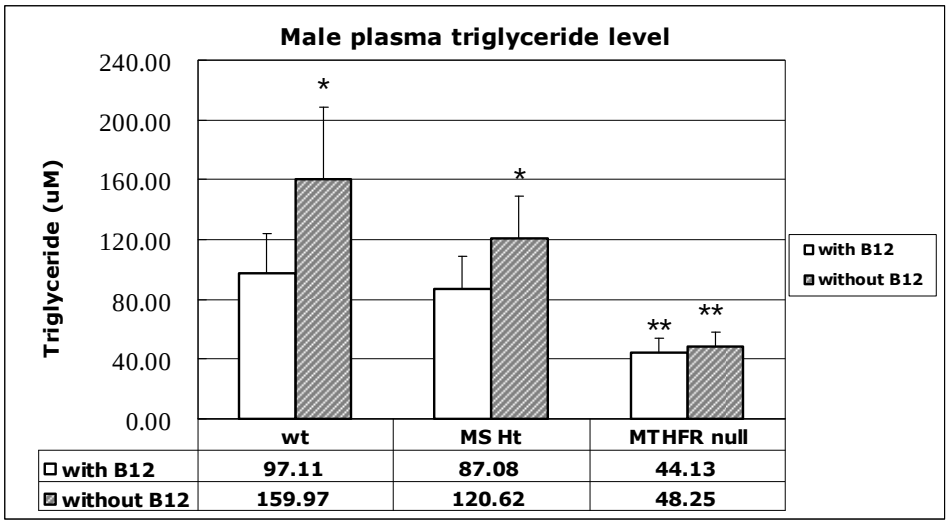

Figure 2-5. Dietary vitamin B12 affected male plasma triglyceride level in wild type, MS heterozygote and MTHFR null mice. Each bar represented data from 6-8 mice. * $P < 0.05$, ** $P < 0.01$ for comparison of mutant mice with the WT mice on B12 sufficient diet (student's *t-test*).

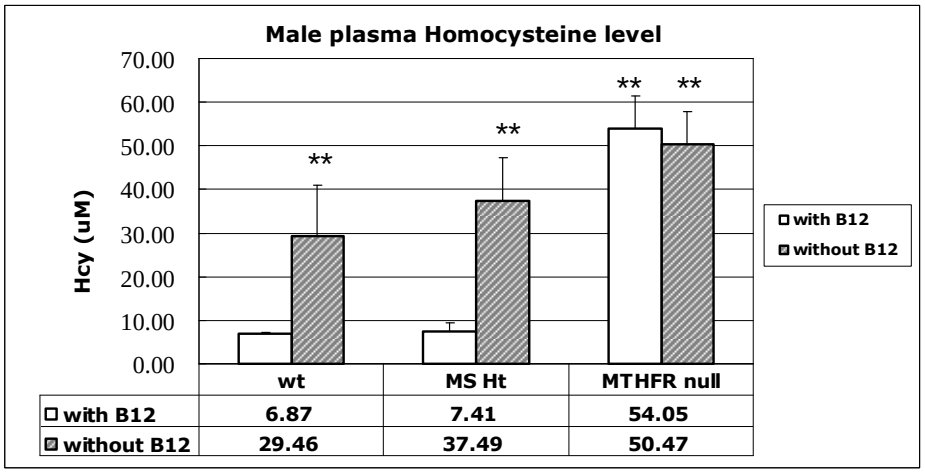

Figure 2-6. Dietary vitamin B12 affected male plasma homocysteine level in wild type, MS heterozygote and MTHFR null mice. Each bar represented data from 6-8 mice. ** $P < 0.01$ for comparison of mutant mice with the WT mice on B12 sufficient diet (student's *t-test*).

As shown in figure 2-7, plasma methylmalonyl CoA increased very significantly (over 300 fold) when vitamin B12 was deprived from the diet and this increase was not affected by genotype.

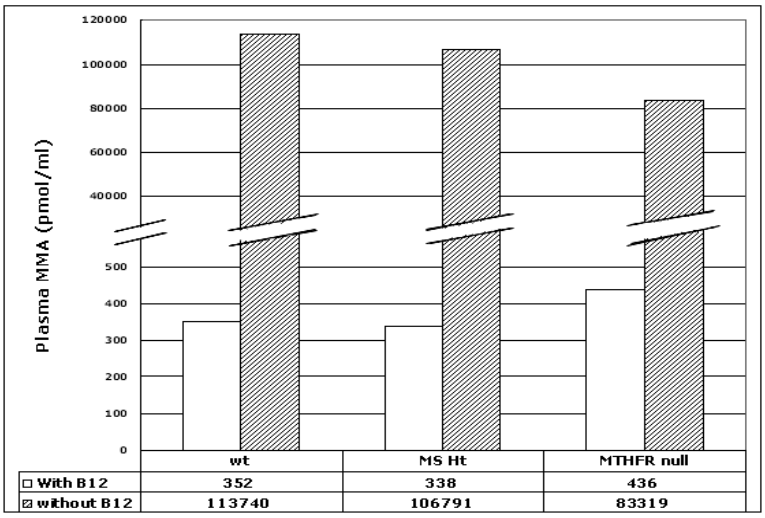

Figure 2-7. Diet vitamin B12 affected plasma methyl-malonyl CoA. Plasma MMA of mice increased very significantly (over 300 folds) when vitamin B12 was deprived from the diet.

ApoC1	Diet	Genotype	Fold change
	+B12	WT	1
		MS Ht	-1.6
		MTHFR null	-8.87
	-B12	WT	3.41
		MS Ht	2.55
		MTHFR null	-5.99
ApoC3	+B12	WT	1
		MS Ht	1.02
		MTHFR null	-6.15
	-B12	WT	16.02
		MS Ht	20.11
		MTHFR null	-1.88

Table 2-3. Real-time PCR showed that B12 deficiency affected ApoC1 and ApoC3 expression.

Real-time PCR results showed that B12 deficiency significantly alter the expression of several apolipoproteins which might in turn affect the plasma lipid profile. As shown in Table 2-3, B12 deficiency dramatically up-regulated hepatic ApoC1 and ApoC3 expression in MS heterozygotes and wild type mice, while MTHFR null mice maintained its ApoC1 and ApoC3 expression at a very low level regardless of the dietary B12.

Demyelination is a major neuropathological symptom of vitamin B12 deficiency in human. To compare myelin synthesis under circumstances of B12 deprivation was of great interest in our study. We measured GalC kinetics using GC/MS stable isotope labeling which provided a

quantitative method for studying myelin synthesis. This study included two aspects, first, to observe the role of vitamin B12 on initial myelination in young mice; second, to determine how B12 affected remyelination after an induced demyelination.

Vitamin B12 deficiency significantly decreased initial myelination rates in MS heterozygote and wild type young mice. Synthesis of GalC from whole brains (including cerebellum and brainstem) was measured. As shown on Figure 2-8 and Table 2-4, the MS heterozygote mice or wild type mice on vitamin B12 deficient diet had a significant lower GalC synthesis rate than those on vitamin B12 sufficient diet (deuterium fraction = 0.473 or 0.5 versus 0.552 or 0.562 individually) at day 35; however, those mice on the vitamin B12 deficient diet showed more rapid myelination in the following 30 days which made their overall GalC synthesis comparable to those on vitamin B12 sufficient diet (deuterium fraction = 0.76 or 0.729 versus 0.649 or 0.713 individually) at day 65. This retardation-catch up phenomenon was more obvious for MS heterozygote than wild type mice on vitamin B12 deficient diet.

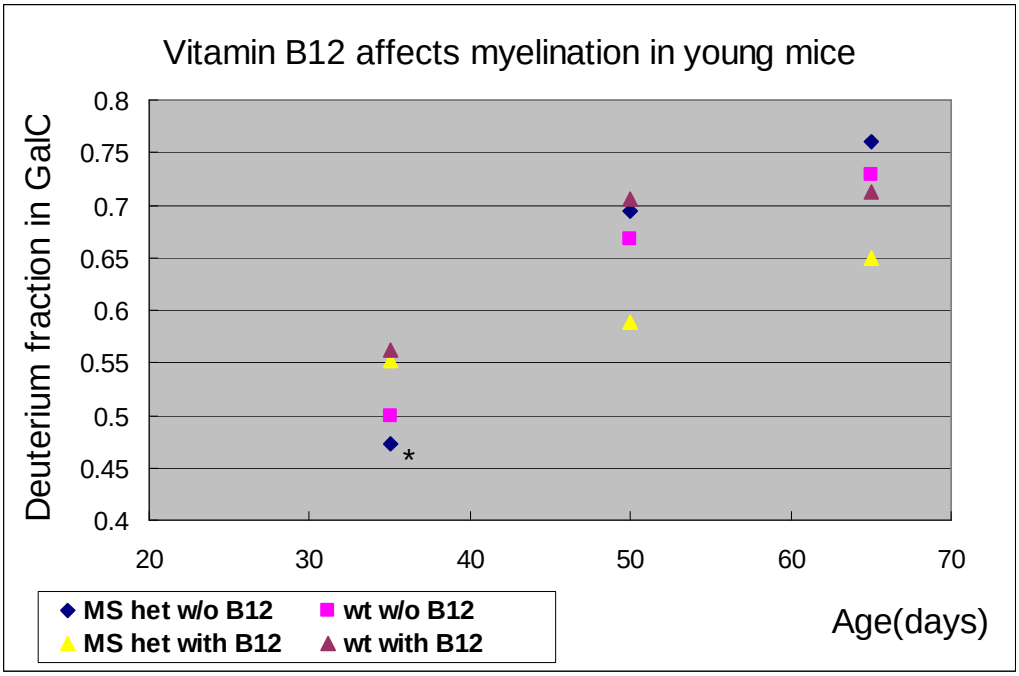

Figure 2-8. Vitamin B12 affected initial myelination in young mice. Time course of label incorporation into the galactose moiety of brain galC during 8% $^{2}H_2O$ administration in mice that were 21 days old until sacrificed at day 35, 50 or 65 (n=5 per group per time point). Mice were maintained on soy-based AIN-93G diet with or without vitamin B12. * $p < 0.05$ for comparison of mutant mice with the WT mice at the same age (One-way ANOVA).

		Day 35	Day 50	Day 65
Deuterium fraction in brain Galactocerebroside (SD)	with B12 wild type	0.562 (0.085)	0.706 (0.128)	0.713 (0.054)
	with B12 MS Heterozygote	0.552 (0.091)	0.588 (0.073)	0.649 (0.075)
	without B12 wild type	0.500 (0.048)	0.668 (0.080)	0.729 (0.074)
	without B12 MS Heterozygote	0.473* (0.030)	0.694 (0.098)	0.760 (0.065)

Table 2-4. Dietary vitamin B12 affected initial myelination in young mice. Numbers represented data from 5-7 mice of each group. * $p < 0.05$ for comparison of mutant mice with the WT mice at the same age (One-way ANOVA).

In the demyelination/remyelination experiment, Luxol Fast Blue staining of brains from each group provided a basic insight of myelin status. Corpus callosum is the major region in the brain where oligodendrocytes as well as oligodendrocyte progenitor cells accumulate. It is also the major part affected by cuprizone induced demyelination. As shown on Figure 2-9, at the beginning of the experiment, mice of all genotypes regardless of whether fed with the + or - B12 diet had well myelinated corpus callosum. Also, we did not detect any myelopathy in the white

matter of the upper spinal cord in these mice, even in the B12 deficient ones (data not shown). The observation that vitamin B12 deficiency did not result in demyelination in adult mice of each genotype was consistant with previous studies that there was no demyelination observed in rodents fed on a B12 deficient diet. After 6 weeks of cuprizone ingestion the mice exhibited patches of myelin loss in the corpus callosum. Different degrees of remyelination were observed in Luxol fast blue slices of the recovery group. In wild type animals, both B12 sufficient and deficient groups showed some remyelination in the corpus callosum, but B12 deficient mice still lost the laminar structure partially (Figure 2-9 c and f). B12 deficiency significantly impaired the remyelination ability of MS heterozygous mice; compared to the one fed on a B12 sufficient diet, those fed on a B12 deficient diet still had most of the myelin missing (Figure 2-9 i and l). Surprisingly, based on the histological staining result, MTHFR null mouse recovered better on a B12 deficient diet than on a B12 sufficient diet (Figure 2-9 o and r). Again, we did not find histological abnormalities in the white matter of the upper spinal cord in the cuprizone treated mice, no matter what genotypes they were or what diet they were fed on (data not shown).

Three weeks of control diet after 6 weeks of cuprizone treatment resulted in a rebound in myelin synthesis with a fractional synthesis rate greater than that found in the control animals in all groups by significantly different degrees. We determined GalC fractional synthesis in the groups without cuprizone treatment as controls which represented the natural myelin turnover and those with cuprizone treatment as samples which represented the true remyelination after induced demyelination. As shown in Figure 2-10 and Table 2-5, vitamin B12 deprivation significantly inhibited remyelination in MS heterozygote and wild type mice (Deuterium fraction of true remyelintion = 0.013 and 0.018, respectively, compared with 0.067 and 0.047 on the vitamin B12 sufficient diet). Remyelination in MTHFR null mice was not affected by vitamin B12 deprivation (0.017 without B12 and 0.015 with B12).

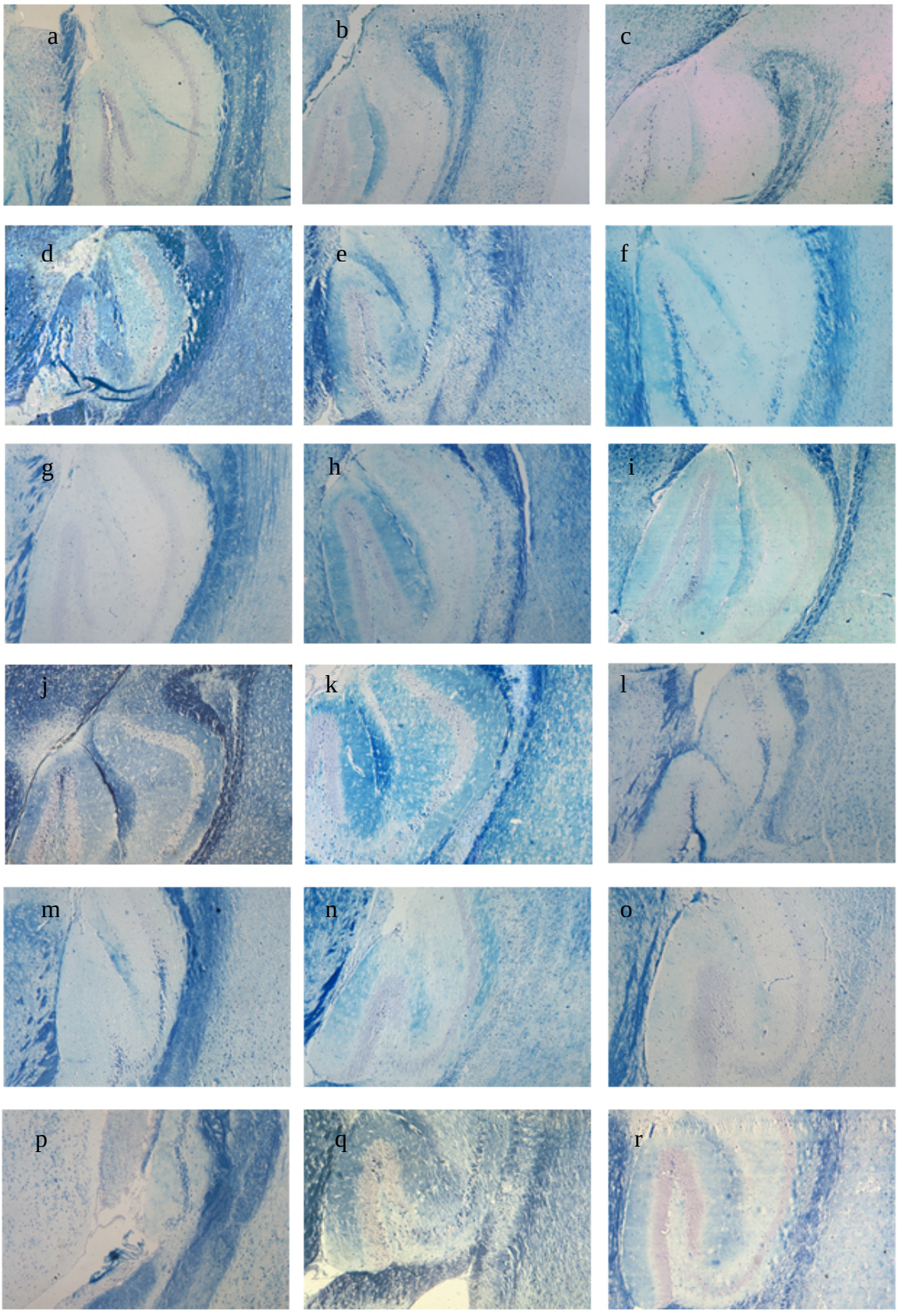
a
b
c
d
e
f
g
h
i
j
k
l
m
n
o
p
q
r

Figure 2-9. Myelin of corpus callosum at sagittal slices of brain stained by Luxol Fast Blue. Left column: control mice of each genotype fed on a soy-based AIN-93G diet with or without vitamin B12; middle column: mice maintained on a diet added with 0.2% cuprizone for 6 weeks; right column: mice back-fed to original diet for three weeks after 6 weeks of cuprizone diet. First row (a, b and c): wild type mice on a vitamin B12 sufficient diet; second row (d, e and f): wild type mice on a vitamin B12 deficient diet; third row (g, h and i): MS heterozygous mice on a vitamin B12 sufficient diet; fourth row (j, k and l): MS heterozygous mice on a vitamin B12 deficient diet; fifth row (m, n and o): MTHFR null mice on a vitamin B12 sufficient diet; sixth row (p, q and r): MTHFR null mice on a vitamin B12 deficient diet.

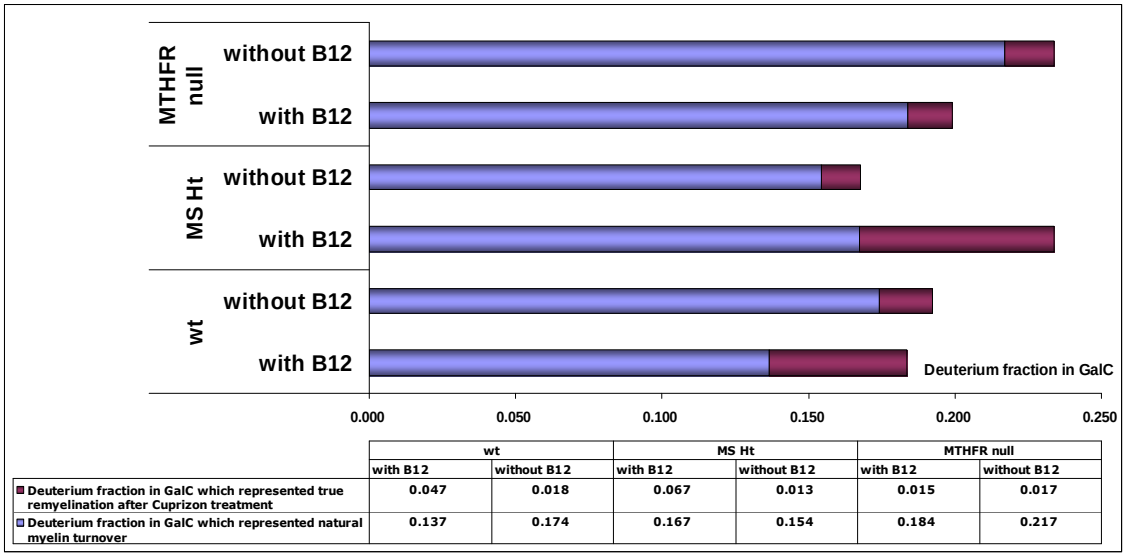

	wt		MS Ht		MTHFR null	
	with B12	without B12	with B12	without B12	with B12	without B12
Deuterium fraction in GalC which represented true remyelination after Cuprizon treatment	0.047	0.018	0.067	0.013	0.015	0.017
Deuterium fraction in GalC which represented natural myelin turnover	0.137	0.174	0.167	0.154	0.184	0.217

Figure 2-10. Dietary vitamin B12 affected remyelination after cuprizon treatment. Effect of cuprizone administration and its cessation on brain myelin synthesis rates in vivo in mice were measured. Controls which represented natural myelin turnover were groups with no cuprizone given; experiment which represented true remyelination after Cuprizon treatment were groups received cuprizone for 6 weeks followed by control diet for 3 weeks. All mice drank 8% $^{2}H_2O$ drinking water for 3 weeks before euthanasia. Each bar represents data from 4-6 mice of each group.

		Natural myelin turnover	Apparent remyelination	True remyelination (Average)
Deuterium fraction in brain GalC (SD)	with B12 wild type	0.137 (0.030)	0.184 (0.037)	0.047
	with B12 MS Heterozygote	0.167 (0.034)	0.234 (0.039)	0.067
	with B12 MTHFR Nullizygote	0.184 (0.013)	0.199 (0.066)	0.015
	without B12 wild type	0.174 (0.025)	0.192 (0.030)	0.018
	without B12 MS Heterozygote	0.154 (0.017)	0.168 (0.042)	0.013
	without B12 MTHFR Nullizygote	0.217 (0.054)	0.234 (0.059)	0.017

Table 2-5. Dietary vitamin B12 affected remyelination after cuprizon treatment.

DISCUSSION

Animal models for subacute combine degeneration have been intensely studied for many years. The only available rodent models resembling human SCD were rats with Cbl deficiency induced by means of total gastrectomy (lack of intrinsic factor which is necessary for Cbl absorption) or a chronic Cbl-deficient diet (over 9 months) (Scalabrino et al., 1995). Based on observations from these animal models, a new "cytokine-growth factor theory" was raised to explain the Cbl-deficiency neuropathy. The dysregulated cytokines and growth factors included increased cytokine (TNF-α) and growth factor (NGF), and the decreased cytokine (IL-6) and growth factor (EGF). In addition, an increased activity of NF-κB was induced by elevated TNF-α and NGF. The researchers pointed out Cbl had a non-coenzymic neurotrophic function by regulating the cytokines and growth factors and it was this recently discovered function that caused the neuropathy of Cbl deficiency.

The above theory brought current studies of Cbl-deficiency into a broader view. However, it still poses many questions. The first concern was the complexity of the consequences of a total gastrectomy. After a total gastrectomy (TGX), the release of secretin and CCK, as well as the pancreatic enzymes all decrease, which in turn result an inadequate bile emulsification and pancreatic digestion of food. Other than cobalamin, iron, calcium, fat, carotene and other nutrients may also be deficient because of malabsorption. For example, over 70% patients with TGX suffer from iron-deficient anemia (Toffolon, 1974). Also, acquired copper deficiency after TGX has received wide attention because severe neuropathy similar to SCD had been observed among these patients (Tan, 2006).

In addition, the "cytokine-growth factor theory" also faced following uncertainties and controversies: (a) Cbl-deficiency-induced dysregulated cytokines and growth factors pattern have also be seen in some other organs (e.g. kidneys and liver), but no well-defined morphological lesions were detected (Veber, 2008). (b) NF-κB is involved in signaling of inflammation and immunity; in neurons, NF-κB activates the expression of the class I major histocompatibility complex (MHC I) and results in the immune removal of the neuron (Gobin, 2001). However, NF-κB was activated but did not stimulate any immunological or inflammatory consequences in Cbl-deficient rats. (c) Oligodendrocytes were much less affected than astrocytes in Cbl-deficiency rats, while EGF, a strong trophic factor toward oligodendrocytes, was found dramatically decreased in these rats.

To sum up, studies on TGX rats showed a close relationship between Cbl-deficiency and dysregulated cytokine/growth factors. However, there was not enough evidence to draw the conclusion that such a relationship is irrelevant to cobalamin's coenzyme functions.

Although rodents fed on Cbl-deficient diet did not develop pathological symptoms, they did show significant changes in biomarkers such as MMA and homocysteine. Also, in view of the extreme slow course of development of SCD, we decided to examine the more subtle quantitative myelin changes in Cbl-deficient animals. The stable isotope labeled GalC GC-MS method, which is much more sensitive than other methods to measure myelin turnover, gave us a good tool to accomplish this goal.

As expected, when cobalamin was deficient, mice showed a slower initial myelin formation and impaired remyelination after an artificial induced demyelination, and such a tendency was more obvious in MS heterozytes than wild-type animals. Our results agreed with observations in Cbl-deficient patients: in newborns with Cbl-deficiency, retarded myelination is very common (Lövblad. 1997); clinical reports showed that a large subgroup of patients with multiple sclerosis, an auto-immune inflammatory demyelination disease, had coexisting vitamin B12 deficiency, which suggested that Cbl-deficiency might aggravate the symptoms of multiple sclerosis or delay the recovery from the disease (Reynolds. 1992).

At the same time, plasma MMA increased as over 300 fold when mice were fed on a vitamin B12 deficient diet regardless of their genotypes. That mice did not undergo a spontaneous demyelination in CNS under such conditions strongly supported that a mutase defect is not responsible for B12 neuropathy.

In addition to myelin status, the general growth and the lipid profiles of these mice were also examined. I found that both wild-type and MS heterozygous mice grew well on a Cbl-deficient diet, which is conflict with previous results. In rats, many studies showed that a markedly reduced body weight was observed in rats fed *ad libitum* on a B12-deficient diet for 90 days. It was reported that when BALB/C mice were fed with a B12-deficient diet for 90 days, they showed slightly retarded growth (Kawata, 2004). In a previous study from our lab, when fed usung the same Cbl-deficient diet as used here, the wild type growth was little affected, however, MS heterozygotes showed retarded growth. The only difference in my recent experiments compared the previous one was the different genetic background of the mice. I used a mix background versus C57BL/6, so the genetic background may be the explanation for the difference.

However, coincident with my results, several recent clinical reports suggest an association between an increased risk of vitamin B12 deficiency and obesity in children and adolescents (Pinhas-Hamiel, 2006). While our results do not agree with their suggestion that the hyperhomocystinemia resultng from B12 deprivation was the key factor, because MTHFR null mice maintained an extremely high plasma homocysteine no matter which diet they were fed on, however, they had significantly lower body weight and plasma cholesterol or triglyceride.

Our previous microarray data showed that multiple lipoprotein genes were differentially expressed in B12-deficient mouse brain. Many of them belong to two known lipoprotein gene clusters. One includes ApoAI, ApoAV and ApoCIII; the other one includes ApoCI, ApoCII and ApoCIV. The differential expression of some of these genes, including ApoCI and ApoCIII, was confirmed in my study by RT-PCR.

Other than their functions in lipid metabolism, abnormal expressions of lipoproteins are also associated with high instances of neurological diseases. For example, ApoAI and ApoAII are considered as amyloidogenic apolipoproteins and they are major components of amyloid fibrils (Ge, 2007). Amyloid fibril deposition is associated with Alzheimer's disease, familial amyloid polyneuropathy. ApoCI may also be a risk factor for cognitive impairment in the elderly (Serra-Grabulosa, 2003). Consequently, we can not exclude the possibility that dysregulated apolipoproteins are involved in B12 neuropathy development.

Chapter III: The effect of 5-methyl THF in the diet of the MS/MTHFR double null

MS has been widely considered as the pivotal enzyme involved in vitamin B12 deficiency-induced neuropathology. However, as previously described, the homozygous MS knockout is early embryonic lethal and can not be rescued by nutritional supplementation during pregnancy, while the heterozygote is basically normal except for slightly elevated plasma homocysteine. Therefore, a MS conditional knockout mouse, such as an adult inducible or tissue-specific MS deletion which may help bypass the embryonic lethality of MS defect, would be the best model to investigate B12 neuropathy.

However, before we get the conditional mutant MS mice, the current mouse models can be manipulated to mimic the complicated situation of an MS defect to some degree. The approach we used was to observe the effect of a 5-methyl-THF diet on mice double null for MS and MTHFR. As described in Chapter I, when the MS/MTHFR double null were fed on a diet containing folic acid, the MTHFR knockout blocks formation of the "methyl folate trap", which makes dietary folate retainable and functional, so MS/MTHFR double null mice survive and have a phenotype similar to MTHFR single null mice. However, when fed on a diet with 5-methyl-THF as the only source of folate, such a double knockout can simulate the real condition of a MS defect, including both defective methylation and functional folate deficiency cause by the "methyl folate trap", and maybe more importantly, an accumulation of 5-methyl-THF.

The accumulation of 5-methyl-THF is the most significant difference between cobalamin deficiency and folate deficiency. In B12 deficiency, when all folate coenzymes are trapped as the methyl form, other biofunctional forms of folate, such as 10-formyl-THF and methylene-THF, which are important one-carbon donors for purine and thymidylate synthesis respectively, are extremely deficient. In addition, the 5-methyl-THF that accumulates is a potential inhibitor for multiple enzymes, for example, glycine-N-methyl transferase (GNMT) (Wagner, 1985) and serine hydroxymethyltransferase (SHMT) (Stover, 1991).

Because the neurological manifestation of Cbl-deficiency is so unique, the question is whether the existence of a methyl-folate trap may fully or partially be responsible for the Cbl deficiency-induced lesions was of great interest. Thus, we simulated such a condition by feeding the MS/MTHFR double null mice with a diet containing no folic acid but containing 5-methyl-THF diet at a high concentration. This study should be very useful to help us study the underlying mechanism of B12 neuropathy.

MATERIAL AND METHODS

Powdered folate deficient AIN-93G diet containing 1% succinyl sulfathiazole was mixed well with folic acid or 5-methyl THF at a final concentration of 2mg/kg. These diets were administered *ad libitum* to randomly chosen two groups of MS/MTHFR double null or wild type mice at age 12 months. Body weights were recorded every 3 days and mice were sacrificed after two months after over-night fasting and the following procedures were performed on the samples.

3.1. Complete blood count

Blood (200 μL) was obtained from heart and collected into ethylene diaminetetraacetic acid (EDTA)-coated tubes (Sarstedt, Numbrecht, Germany). Subsequently, the complete blood profile was analyzed using an Advia 120 Automated Hematology Analyzer at the Center for Sickle Cell Disease & Thalassemia of Children's Hospital Oakland Research Institute (CHORI).

3.2. Blood smear histological stain

Blood smear films were fixed in absolute methanol and stained with Wright-Giemsa hematology stain kit (Volu-Sol, Inc) according to the manufacture’s instruction.

3.3. Histological examination of myelin by Luxol fast blue staining

Demyelination was determined histochemically by examining standard 7 μm paraffin sagittal brain or coronal T3 spinal cord sections stained with Luxol fast blue (LFB).

3.4. Real-time quantitative PCR

RT-PCR of several genes reported to be dysregulated in a TGX induced Cbl-deficient rat brain (Scalabrino, 1990) was performed as previously described in Chapter I and primers were listed in table 3-1.

Table 3-1. RT-PCR Primer sequences for cytokines and growth factors.

Gene	**Sequence (5'-3')**
NGF	
Forward	TCTGTGTACGGTTCTGCCTG
Reverse	CAGCTTTCTATACTGGCCGC
EGF	
Forward	TCTGGGTCAATCCGAGAGAT
Reverse	TCGAGAGAAGCGAGAGAAGC
TNFα	
Forward	CAG CCG ATG GGT TGT ACC TT
Reverse	GGC AGC CTT GTC CCT TGA
NFκB	
Forward	GAGCGTGATAAATGACGTGG
Reverse	CACAGGACGAGAACGGAGAC
IL6	
Forward	TGGTACTCCAGAAGACCAGAGG
Reverse	AACGATGATGCACTTGCAGA

RESULTS

Surprisingly, MS/MTHFR double null mice fed on a diet containing 2mg/kg 5-methyl-THF did not lose weight (Δ body weight <= 1.2 ± 0.4 grams) nor showed any apparent weakness during the 2-month administration, nor did the wild type mice on the same diet or mice on a control diet containing 2mg/kg folic acid diet.

	2mg/kg 5-methyl-THF diet		2mg/kg folic acid diet	
	MS/MR double null	Wild type	MS/MR double null	Wild type
WBC (x 10^3 cells/uL)	5.50 ± 1.48*	7.59 ± 0.81	6.09 ± 0.90*	7.92 ± 1.31
RBC (x 10^6 cells/uL)	6.82 ± 1.22**	9.79 ± 0.84	9.07 ± 0.36	9.36 ± 0.51
HGB (g/dL)	11.0 ± 2.0*	14.5 ± 0.9	14.0 ± 0.7	13.8 ± 0.5
HCT (%)	32.9 ± 5.7**	44.6 ± 2.3	42.2 ± 2.1	42.4 ± 1.7
MCV (fL)	48.4 ± 0.9**	45.6 ± 1.7	46.5 ± 2.0	45.4 ± 1.2
RDW (%)	16.1 ± 2.1*	13.7 ± 1.3	12.8 ± 0.8	13.4 ± 0.9
MCH (pg)	16.2 ± 0.7**	14.8 ± 0.4	15.5 ± 0.9	14.8 ± 0.3
MCHC (g/dL)	33.4 ± 1.0*	32.6 ± 0.4	33.2 ± 0.9	32.6 ± 0.3
Retic (x 10^9 cells/L)	125.1 ± 40.5**	253.0 ± 29.2	278.5 ± 74.0	272.2 ± 59.4
CHr (pg)	17.7 ± 0.7**	15.4 ± 0.5	15.7 ± 0.9	14.9 ± 0.6
PLT (x 10^3 cells/uL)	445 ± 555	1013 ± 991	730 ± 1197	685 ± 407
Neut (x 10^3 cells/uL)	0.97 ± 0.16*	1.84 ± 0.89	2.35 ± 1.75	2.41 ± 1.25
Lymph (x 10^3 cells/uL)	3.16 ± 2.00	5.05 ± 0.38	2.80 ± 1.10*	4.79 ± 1.09
Mono (x 10^3 cells/uL)	1.01 ± 0.76*	0.24 ± 0.06	0.56 ± 0.53	0.25 ± 0.09

Table 3-2. Hematologic parameters of murine blood. WBC: white blood cell, RBC: red blood cell, HGB: hemoglobin, HCT: hematocrit, MCV: mean corpuscular volume, RDW: Red blood cell distribution width, MCH: mean corpuscular hemoglobin, MCHC: Mean corpuscular hemoglobin concentration, Retic: reticulocyte, CHr: reticulocyte hemoglobin content, PLT: platelet, Neut: neutrophil, Lymph: lymphocyte, Mono: monocyte. Mean ± standard deviation was given for 4-6 mice of each group. *p<0.05, **p<0.01 unpaired student's *t-test* compared with WT mice on a folic acid diet.

Although the mice did not show dramatic physical abnormalities, MS/MTHFR double null fed on the methyl-THF diet did develop anemia. Table 3-2 describes the complete blood counts

and red blood cell indices of MS/MTHFR double knockout and controls maintained on the 2mg/kg 5-methyl-THF or folic acid diets for 2 months beginning at 12 months of age. The anemia is moderately severe, with the hemoglobin reduced by at least one third in the MS/MTHFR double null on the 5-methyl-THF diet. Clinically, the mean corpuscular volume (MCV) is used as an essential diagnostic index lead to judge the type on anemia with relevant biochemical changes. In this case, red blood cells are macrocytic (MCV increased), and hyperchromic (MCHC increased) (Figure 3-1).

As predicted, the absolute reticulocyte count of double null mice fed on the methyl-THF diet was markedly reduced to half that of the control, indicating an anti-proliferative anemia, likely with a component of decreased cell survival. Also, the reticulocytes formed in experimental mice might be significantly larger than those from control, because of their significant elevated hemoglobin contents (Figure 3-2).

Platelet counts were consistently decreased to various degrees in the mutant mice fed on the 5-methyl-THF diet, and there was a significant trend toward a decreased white blood cell count. What is particularly noteworthy is that compared to decreased neutrophils and lymphocytes, the number of monocytes increased dramatically, as shown in Figure 3-3.

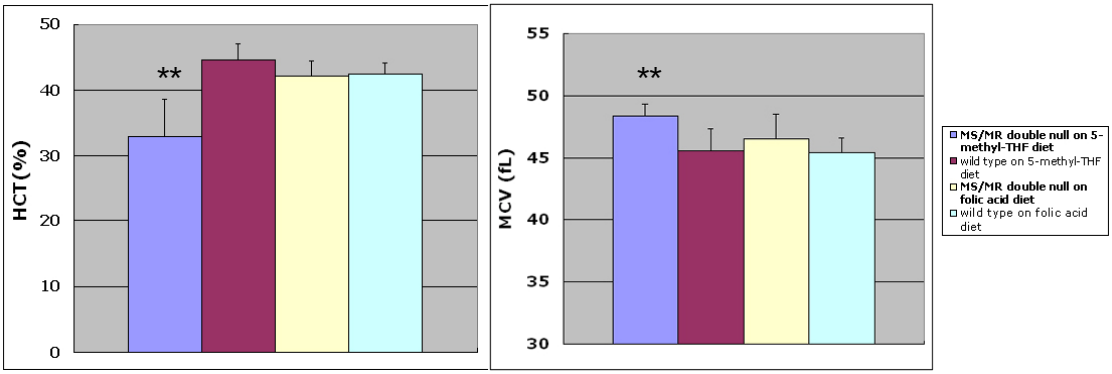

Figure 3-1. Comparison of HCT and MCV of wild type and MS/MTHFR double null mice fed on a modified AIN-93G diet containing 2mg/kg folic acid or 2mg/kg 5-methyl-THF. Each bar represented data from 4-6 mice. ** $P < 0.01$ for comparison other groups of mice with WT mice on a folic acid diet (student's *t*-test).

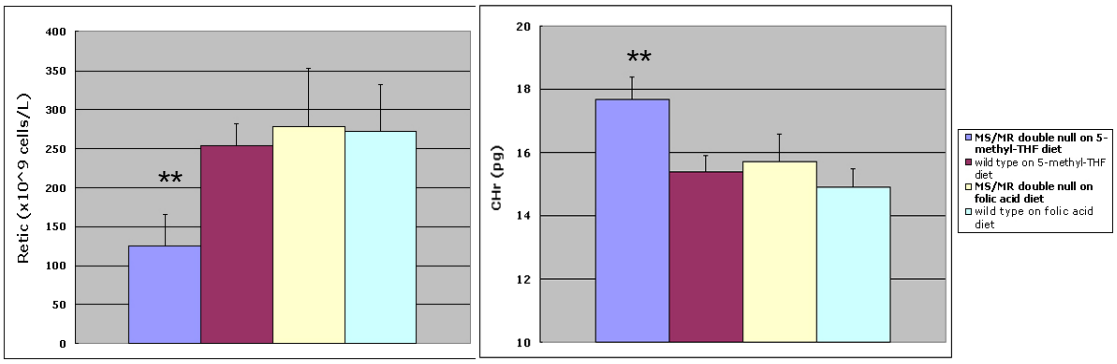

Figure 3-2. Comparison of Retic and CHr of wild type and MS/MTHFR double null mice fed on a modified AIN-93G diet containing 2mg/kg folic acid or 2mg/kg 5-methyl-THF. Each bar represented data from 4-6 mice. ** $P < 0.01$ for comparison other groups of mice with WT mice on a folic acid diet (student's *t*-test).

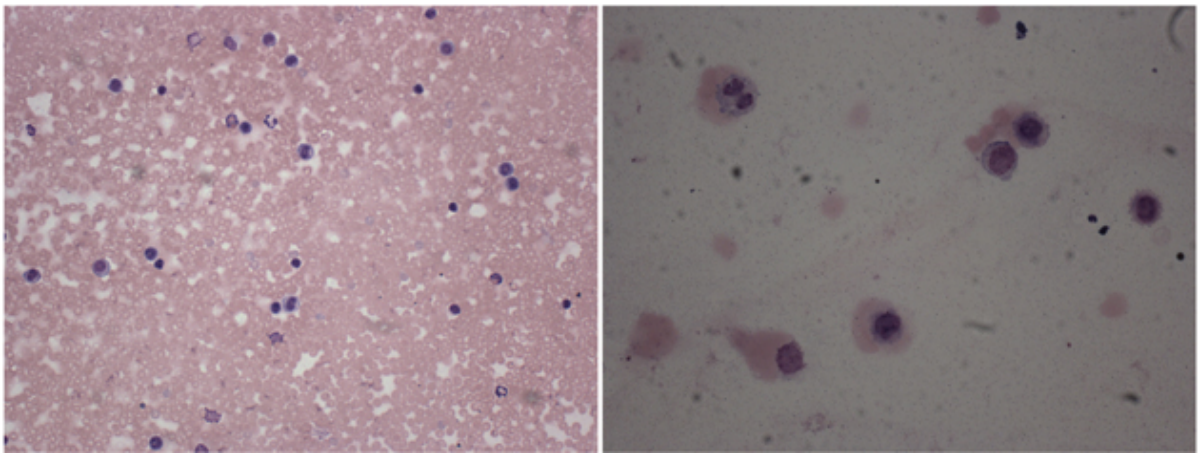

Figure 3-3. Wright-Giemsa stain of blood smear from MS/MTHFR double null mouse fed on a modified AIN-93G diet containing 2 mg/kg 5-methyl-THF. Left: 20X. Right: 40X.

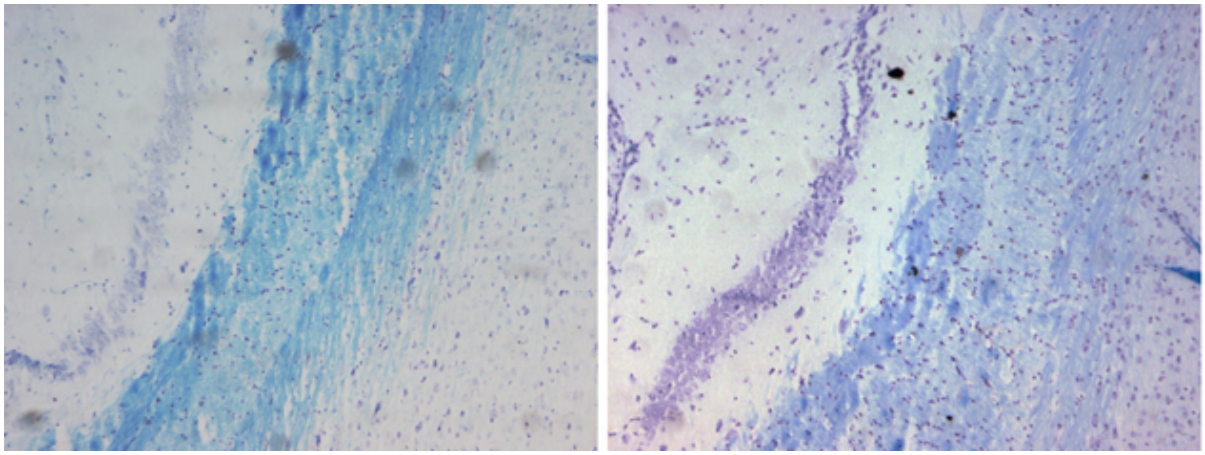

Figure 3-4. Mild myelin defect in brain of MS/MTHFR double null mouse fed on a 5-methyl-THF diet. Myelin at corpus callosum was stained by Luxol Fast Blue. Left: MS/MTHFR double null mouse on a folic acid diet; right: MS/MTHFR double null mouse on a 5-methyl-THF diet.

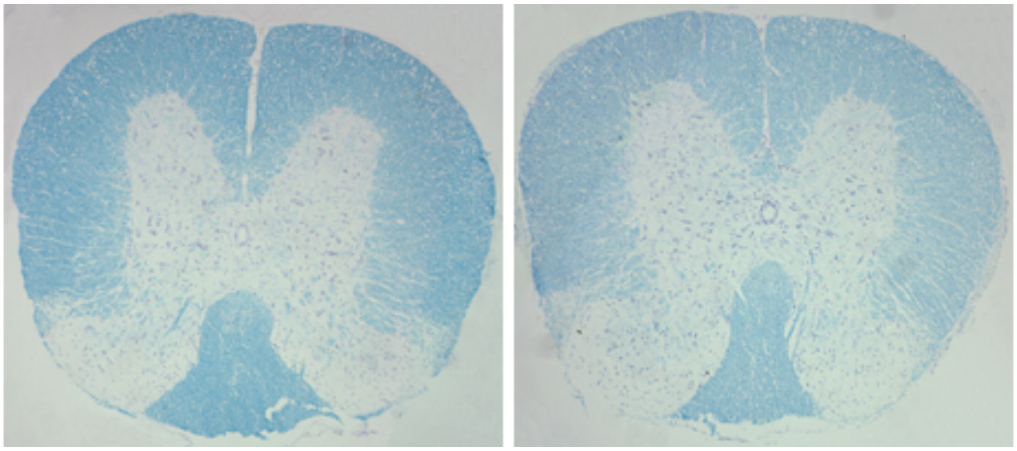

Figure 3-5. Histology of double mutant spinal cord. Myelin at T3 spinal cord was stained by Luxol Fast Blue. Left: MS/MTHFR double null mouse on a folic acid diet; right: MS/MTHFR double null mouse on a 5-methyl-THF diet.

In total five double knockout mice fed on 5-methyl-THF diet, CNS white matter in three of five seemed normal, while the other two showed a mild myelopathy by histological staining. Their white matter in corpus callosum showed a paler color and lost its structural integrity, which was reflected in its dilated diameter and sparse sheath bundle. Accordingly, the white matter in the upper spinal cord of double mutant mice fed on the methyl-THF diet was less stained. However, we did not observe a spongy or "vacuolar" degeneration of CNS myelin. One possibility is that the myelopathy we found was still in its early stage, while the vacuolation is the late and ultimate stage of myelin loss.

Coincidently, the two mice with mild myelopathy were those with the worst hematological manifestations (with HCT as low as 28.6% and 31.9%, respectively). This suggested that the

hematological and neuropathological manifestation of Cbl-deficiency is closely related, at least in this mouse model.

Dysregulated cytokines and growth factors were detected in the TGX induced Cbl-deficient rats, so we performed RT-PCR to determine their expression. These cytokines and growth factors included TNF-α, NGF, IL-6, EGF and NF-κB. Among them, NGF, IL-6 and EGF expression was similar among all mice. We found increased expression of TNF-α and NF-κB, but only in those two mice with the worst anemia and myelopathy. The mean fold increase of TNF-α and NF-κB in these two mice was 5.82 and 8.40, respectively. The other three double null mice fed on 5-methyl-THF diet had indistinguishable gene expression patterns to the control group.

The coexistence of anemia, myelopathy and elevated TNF-α/NF-κB can not be simply explained by coincidence. With these preliminary observations, the relationship between above three needs further investigation. Another unresolved question was why some of the double null mice developed a myelopathy while others did not; it may imply that the occurrence of B12 deficiency neuropathy needs some other contributor which is currently unknown.

DISCUSSION

When fed on a 5-methyl-THF diet, MS/MTHFR double null showed a severe macrocytic anemia, although they did not lose weight or show apparent weakness. Previous experimental Cbl-deficient animal models did not show peripheral blood or bone marrow pathology, although megaloblastic macrocytic anemia could be observed in monkeys fed on a folate-deficient diet (Rasmussen, 1982). In an early study, rhesus monkeys fed on a Cbl-deficient diet for five years did not show morphological or quantitative change on peripheral blood and bone marrow (Agamanolis, 1976). Results from other animals (monkeys, fruit bats, rats, etc) fed on Cbl-deficient diet or treated with N_2O were similar. These studies had led to a theory that the Cbl deficient anemia is unique to humans (Toohey, 2006). Our findings suggested that the hematologic manifestations of Cbl deficiency can be detected in an animal model.

Some double mutant mice treated with 5-methyl-THF also showed myelopathy in CNS, but the main locus was the corpus callosum, not the spinal cord as we expected. On one hand, the ultrastructural features of CNS white matter (myelin in spinal cord, corpus callosum, optic nerve and cerebellum) need further examination by electron microscope scanning. On the other hand, Cbl neuropathy can exist in multiple sites in humans. It has been reported that in adult Cbl-deficient patients, lesions predominately damaged the SC and peripheral nerves, while cerebral damage was rare (Healton, 1991); on the other hand, maternal deficiency is the direct cause of neonates deficiency and it usually results in lesions in brain and retarded myelination, while SC lesions and peripheral neuropathy are unusual effects (Whitehead, 2006).

Therefore, my conclusion is that vitamin B12 deficiency-induced neuropathy is mediated by defective methionine synthase and the formation of methyl folate trap. Although this theory is very convincing to us, we still need data from more animals to verify it, and whether 5-methyl-THF is a potential neurotoxin will be tested in vitro by its effect on primary cultured CNS cells from double knockout mice.

The Federal Drug Administration has required folic acid fortification of all enriched cereal-grain products in the U.S. since January 1998. On one hand, this fortification has reduced the incidence of abnormally low plasma folate from 21% to < 2% in nonsupplement takers, the incidence of mild hyperhomocysteinemia dropped from 21% to 10% after the fortification, and there was a 19% drop in the rate of NTD in the United States (Rader, 2002). On the other hand, it also raises some concerns (Solomons, 2007). First, folate fortification was suggested to correlate with an increased colorectal cancer rates in an ecologic analysis of folic acid supplementation in the United States and Canada. Both animal and human studies showed that high level of folate supplement may promote growth of pre-existing tumors. Also, it has been reported that high folic acid intake may exacerbate the clinical neurological manifestations of vitamin B12 deficiency, and possible biochemical explanations for this phenomenon are of interest to us. The existence of megaloblastic macrocytic anemia and an early-phase neuropathy in MS/MTHFR double null mice fed on 5-methyl-THF implies that the formation of a methyl folate trap is fully or at least mainly responsible for the symptoms of pernicious anemia. Also, such a theory helps explain the exacerbation effect of folate supplementation on B12 deficient neuropathy: for Cbl-deficient patients, more folate intake only elevates 5-methyl-THF which inhibits multiple enzymes and

may be potentially toxic, while other folate derivatives, especially those necessary for DNA synthesis, do not increase.

As previously mentioned, in the "cytokine-growth factor theory" raised by Dr. Scalabrino and colleagues, the neurotrophic action of Cbl was considered as a non-coenzyme function of Cbl mainly based on the following observation: in the spinal cord myelin of TGX rats, the severity of the vacuolation was not proportionally related to the accumulation of MMA and Hcy in CSF and serum; also, the spongy vacuolation appeared much earlier than the accumulation of Hcy and MMA (Scalabrino, 1997). However, all current evidence can not rule out the possibility that the cytokine and growth factor changes are still the consequences of altered coenzyme-related biochemical parameters. Moreover, what is noteworthy is that disrupted biochemical factors related to the impaired coenzyme functions of Cbl do not just include MMA and Hcy, but also folate derivatives. Rapid accumulation of 5-methyl-THF and decrease of all other form of folates may play an important role in the Cbl-deficiency neuropathy, as confirmed by our present study. The coexistence of the anemia, the neuropathy and the elevated cytokines TNF-α/NF-κB also support our theory that the methyl folate trap causes pernicious anemia and does not conflict with the previous observations from Cbl-deficient rats.

Other evidences also showed that long-term CNS local low folate may have a significant influence on the demyelination process, and moreover, it may be a prerequisite for SCD. First, thymidylate synthase (TS) is widely and highly expressed in adult mouse brain (Suleiman, 1982), which implies DNA synthesis may be more active than has been thought, while TS is highly sensitive to impaired folate metabolism. Also, long term research in humans suggested that new oligodendrocytes are born and added slowly throughout life (McTigue, 2008), and low folate status may directly impact oligodendrocytes neogenesis.

Although the study of MS/MTHFR double knockout mice fed on 5-methyl-THF diet showed a very exciting and promising prospect on the vitamin B12 deficiency neuropathy research, the better and more suitable animal model would still be a conditional knockout of MS, such as a global inducible knockout in adulthood or a tissue specific deletion. Many unresolved questions about one carbon and B12 metabolism can be answered using these conditional MS knockout mice: for example, what are the interactions between peripheral and brain cobalamin and folate; how does the methionine remethylation cycle change in MS deficient mice; does MS involve the reduction of inactive form cob(II)alamin catalyzed by methionine synthase reductase (MSR); and most importantly, what is the real cause of B12 neuropathy.

Finally, although it is very likely that the B12 neuropathy is related to a defective MS activity, the possibility that B_{12} plays a role in some other currently unrecognized metabolic reaction distinct from MS and the mutase reactions can not be excluded.

Chapter IV: Approaches to understanding genetic variation in folate metabolism in mice

The use of mice (Mus musculus) in scientific research is of long standing. Mice are easy to handle and manipulate, and as mammals, they share a high degree of similarity with humans. Inbreeding in mice was initiated by Dr C. C. Little in 1909 and he generated the first inbred mouse strain, DBA, which was separated into two widely distributed substrains DBA/1 and DBA/2 in 1930 (Strong, 1942). Inbred mice strains were obtained by mating siblings for twenty or more consecutive generations. At the twentieth generation, about 98.6% of the genetic loci were homozygous in each mouse (Beck, 2000). Dr. Little also founded the Roscoe B. Jackson Memorial Laboratory (now The Jackson Laboratory) at Bar Harbor, Maine, in 1929, which has become the repository of strains of inbred mice. The Jackson Laboratory has produced and/or housed the most common strains of inbred mice used nowadays in biomedical research: A, BALB/c, CBA, C57BL, C57BR, C57L, C58, DBA, N, and I , etc (Hoag, 1964).

Since the 1980s, genetic modified mouse models, such as transgenic mice and knockout mice, have become powerful tools to address important biomedical and physiological questions. It has become increasingly important to consider the genetic background of these mice when selecting experiment controls and interpreting results, because inbred mouse strains have a tremendous variety of physiological characteristics, from appearance and basic blood chemistry to complicated behavior and disease susceptibility.

In regard to folate metabolism, however, studies comparing inbred mouse strains have been rare. In a recent study by the Rozen group (Knock, 2008), the C57Bl/6 strain was found to be more resistant to tumorigenesis induced by folate deficiency than the BALB/c strain; only the latter showed global DNA hypomethylation, increased DNA damage and increased dUTP:dTTP ratios when fed on a low-folate diet, which suggested that genetic variations might play a role in either folate absorption and utilization, or DNA methylation patterns. In another study (Finnell, 1997), after the injection of a teratogenic reagent (valproic acid) on gestational day 8.5, the frequency of neural tube defects in the embryos from the SWV strain was significantly greater than the rate observed in the LM/Bc strain. It was demonstrated that higher expression of the MTHFR gene in LM/Bc embryos was related to these different responses following teratogenic exposure. Despite these insightful observations, the discrete differences in folate-related metabolites among strains have never been investigated in any large scale study of inbred mice, and no studies have investigated folate metabolism-related modifier genes.

Modern genetic methods, such as quantitative trait locus (QTL) analyses, make it possible to define regions that are different or identical between inbred mouse strains, and thus to relate specific chromosomal regions to inheritable phenotypes. A QTL is a region of the genome that harbors one or more genes affecting a quantitative trait, which is complex, continuous, and regulated by multiple genes interacting with each other and the environment (Korstanje, 2002). QTL mapping is the statistical study to locate and estimates the effect of QTLs and it has become a very important tool for finding the genes that relate to certain characteristic or regulate complex human diseases. Successful QTL mapping requires a densely spaced set of polymorphic markers which can be efficiently assayed. In the early days, QTL mapping was mainly based on restriction fragment length polymorphisms (RFLPs); later, SSR (simple sequence repeat), also known as single strand length polymorphisms (SSLPs) were largely used (Moore, 2000).

Currently, single nucleotide polymorphisms (SNPs) have become the basis of most QTL mapping practice.

The inbred mouse is an ideal model organism for QTL mapping because genetic resources are plentiful. The mouse genome of several strains has been sequenced: C57BL/6J was sequenced by the publicly-funded Mouse Genome Sequencing Consortium, 129X1/SvJ, DBA/2J, and A/J were sequenced by Celera; and importantly, an increasingly large number of SNPs for the mouse genome are available (Flint, 2005).

In the current study, we took advantage of recent advances in SNP mapping in mice to identify candidate loci underlying the differences in folate-related metabolite levels between inbred strains.

METHODS AND METERIALS

4.1. Mouse samples

Mouse livers and plasma were generously supplied by Dr. Seung-min Lee (Vulpe lab), UC Berkeley, CA. The mouse husbandry was as follows. 4-week-old mice from the following inbred strains were obtained from The Jackson Laboratory, Bar Harbor, ME: 129S1/SvImJ(Catalog No.2448), A/HeJ(645), A/J(646), AKR/J(648), B10.D2-*Hc*^{0}*H2*^{d}*H2-T18*^{c}/oSnJ(461), BALB/cByJ(1026), BALB/cJ(651), C3H/HeJ(659), C57BL/6J(664), CAST/EiJ(928), DBA/2J(671), MRL/MpJ(486), NZB/BlNJ(684), SM/J(687), LG/J(675), and LP/J(676). Mice were fed *ad libitum* an AIN-93G diet to 8 weeks of age. At the time of sacrifice, mice were euthanized by carbon dioxide gas without fasting. Plasma and tissues were collected, snap-frozen in liquid nitrogen and stored at -70°C. Samples from 6 male mice of each strain were used for this study.

4.2. Folate-related biochemical parameters analysis

Mouse brain and liver SAM/SAH, plasma homocysteine/cysteine, liver and plasma total folate were measured as previously described in Part I.

4.3. Candidate folate metabolism related gene identification

The candidate gene identification analysis was performed by Dr. Stela Masle (Vulpe lab), UC Berkeley, CA.

4.3.1. Descriptive measurements setting

Standard descriptive measurements of each of 9 traits (brain SAH, brain SAM, brain SAH/SAM ratio, liver SAH, liver SAM, liver SAH/SAM ratio, plasma Hcy, plasma Cys and liver folate) were reported for each strain. These measures included Mean, Standard Error (of the Mean), Median, Standard Deviation, Sample Variance, Kurtosis, Skewness, Range, Minimum, Maximum and Count. Among them, Kurtosis and Skewness were measures of “normality” of the data, which means how well the data is following the Normal distribution. Outlier (Grubb’s) test was performed to detect any outliers in the data.

4.3.2. SNP selection

The SNP data were obtained from the Broad Institute (http://www.broad.mit.edu/personal/claire/MouseHapMap/Inbred.html). This data set contains 138,793 SNPs from 49 commonly used inbred strains. The average interlocus distance for the autosomal markers is 17.5 kb. The SNP genotyping accuracy reported by the Broad Institute is over 99.8%. In this SNP set, 136,832 SNPs were informative in the 13 strains used in this study: 129S1/SvImJ, A/J, AKR/J, BALB/cByJ, BALB/CJ, C3H/HeJ, C57BL/6J, DBA/2J, LG/J, LP/J, MRL/MpJ, NZB/BlNJ, SM/J. Genotype file included both actual SNPs as well as imputed SNPs.

4.3.3. QTL Mapping

QTL mapping was performed to find candidate DNA regions or genes associated with the 9 folate-related traits using web based haplotypes association mapping program SNPster (version_3.3), available at http://snpster.gnf.org. The haplotype method used was previously described by Pletcher and McClurg (Pletcher, 2004; McClurg, 2007). Briefly, haplotypes are inferred looking over sliding 3-SNP-window and inferred haplotypes are used as the independent factor in one-factor ANOVA. Single strain haplotypes are omitted. F-test was performed for a given phenotype and a haplotype group. Significance of F-statistic is estimated from background distribution simulated non-parametrically. Significance cutoff of $-\log_{(10)}$ p-value is arbitrarily chosen to be at 2.5 [$-\log_{(10)}$ p-value = association score (AS)]. To account for possible population structure, "weighted' bootstrap was used and set as exponent of 3 (default values).

QTL mapping results were depicted in Manhattan plots using GWAS_GUI_v0.0.2 program (Chen, 2009).

RESULTS

Difference in hepatic SAM SAH levels between mouse strains

We measured hepatic SAM and SAH in 16 inbred strains of mice. There was a dramatic difference in hepatic SAM and SAH content between mouse strains. The 129S1/SvImJ and CAST/EiJ mice have the lowest liver SAM with the highest liver SAH levels, which resulted in the lowest SAM/SAH ratio; while DBA/2J and C3H/HeJ strains have the lowest SAH and the highest SAM level, respectively, which resulted in the highest SAM/SAH ratio among these inbred strains (Fig 4-1).

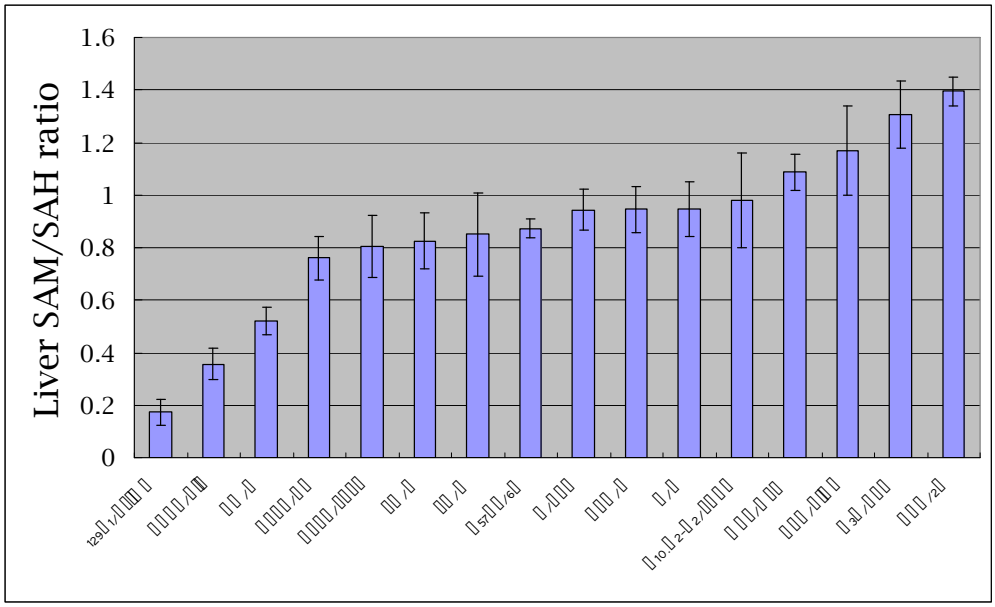

Figure 4-1. Average hepatic SAM/SAH ratio of inbred mouse strains. Mouse strains are ordered in terms of average hepatic SAM/SAH ratio from the lowest to the highest.

It was very interesting that the 129S1/SvImJ mice have the highest liver iron level while the DBA/2J and C3H/HeJ mice have the lowest iron levels according to a previous study done by Dr. Seung-min Lee, which suggests the strains with high hepatic SAM/SAH ratios have lower hepatic iron, and vice versa. This finding prompted us to further investigate the relationship between the SAM/SAH ratio and iron level. A regression analysis showed a significant negative linear correlation between individual liver SAM/SAH ratio and iron level (P=0.00003), as shown in Figure 4-2.

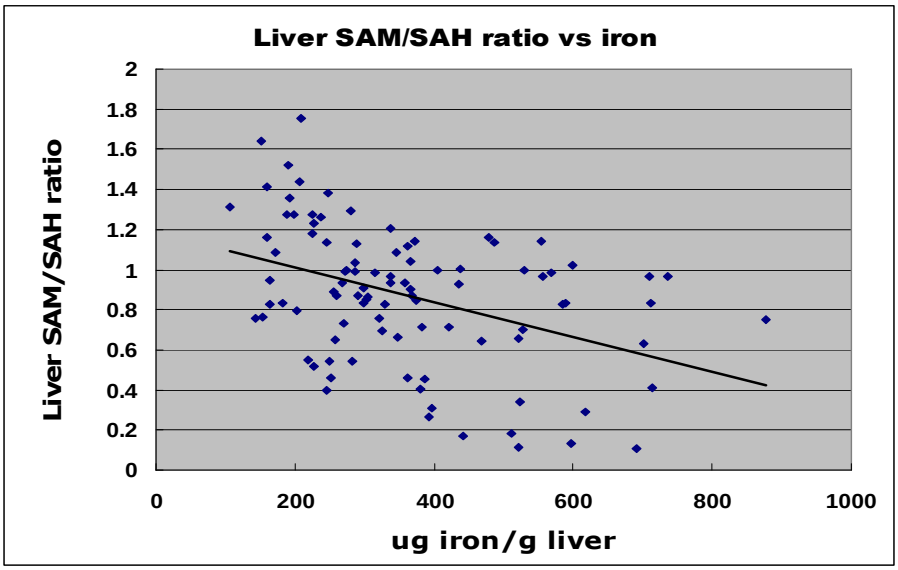

Figure 4-2. Liver SAM/SAH ratio is correlated with liver iron level. (P=0.00003)

Difference in hepatic folate levels between mouse strains

We measured hepatic folate levels in 16 inbred strains of mice (Fig 4-3). There was a clear difference in hepatic folate between mouse strains with a wide range from 15 nmol/g in the BALB/cByJ mice to 28 nmol/g in the AKR/J mice. A regression analysis was also performed to determine the relationship between hepatic folate and hepatic iron, but no statistically significant correlation was found (P= 0.38, data not shown).

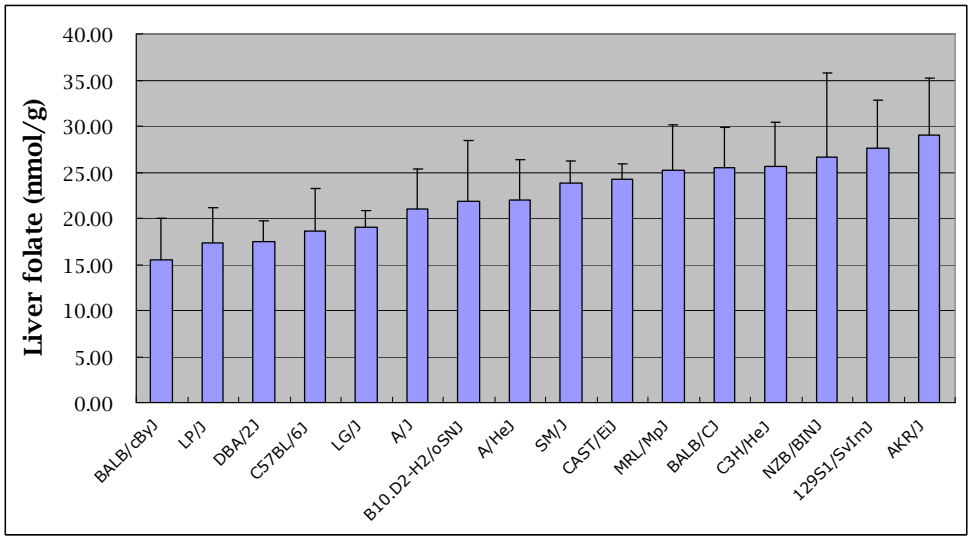

Figure 4-3. Average hepatic total folate of inbred mouse strains. Mouse strains are ordered in terms of average hepatic total folate from the lowest to the highest.

Difference in brain SAM and SAH levels between mouse strains

We measured brain SAM and SAH in 16 inbred strains of mice. There was a clear difference in brain SAM and SAH content between mouse strains. However, brain SAM and SAH levels tended to be positively correlated, with higher SAM level in mice with higher SAH level. For example, as was found for liver, the 129S1/SvImJ mice have the lowest brain SAM, but they also have a rather low brain SAH, which result in their SAM/SAH ratio being similar to other strains. This trend led to a fairly narrow range of brain SAM/SAH ratios (from 1.0 to 1.5) among these inbred strains (Fig 4-4).

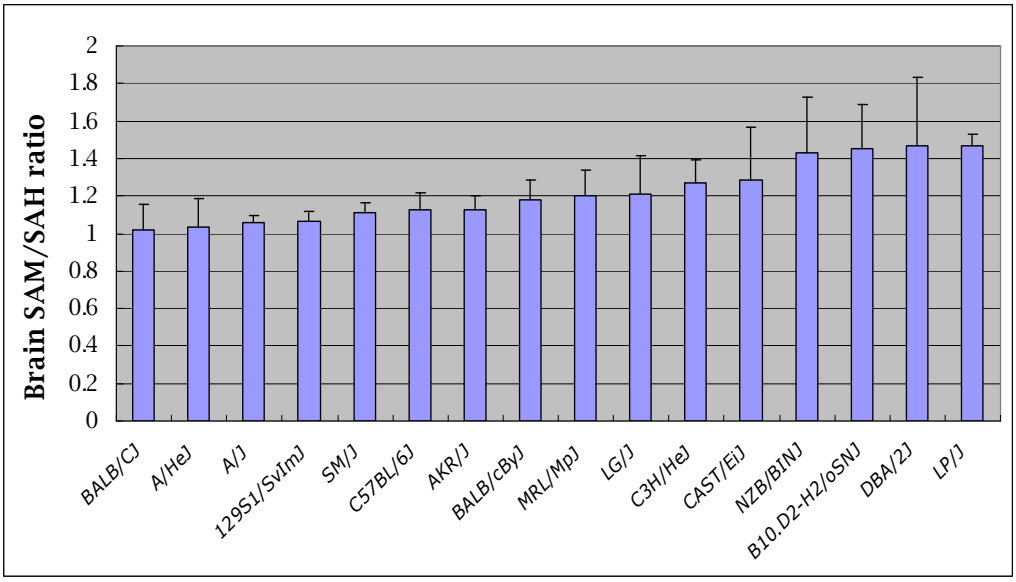

Figure 4-4. Average brain SAM/SAH ratio of inbred mouse strains. Mouse strains are ordered in terms of average brain SAM/SAH ratio from the lowest to the highest.

Difference in plasma homocysteine and cysteine levels between mouse strains

We measured plasma homocysteine and cysteine in 16 inbred strains of mice, and found large differences between the strains. Plasma cysteine varied from 125 μM in the BALB/CJ mice to 219 μM in the C3H/HeJ mice, as shown in Figure 4-5. Plasma homocysteine varied from 2.5 μM in the BALB/CJ mice to 6.3 μM in the 129S1/SvImJ mice, as shown in Figure 4-6.

As a summary of the above data, Table 4-1 shows a complete list of folate-related metabolites in the inbred mouse strains.

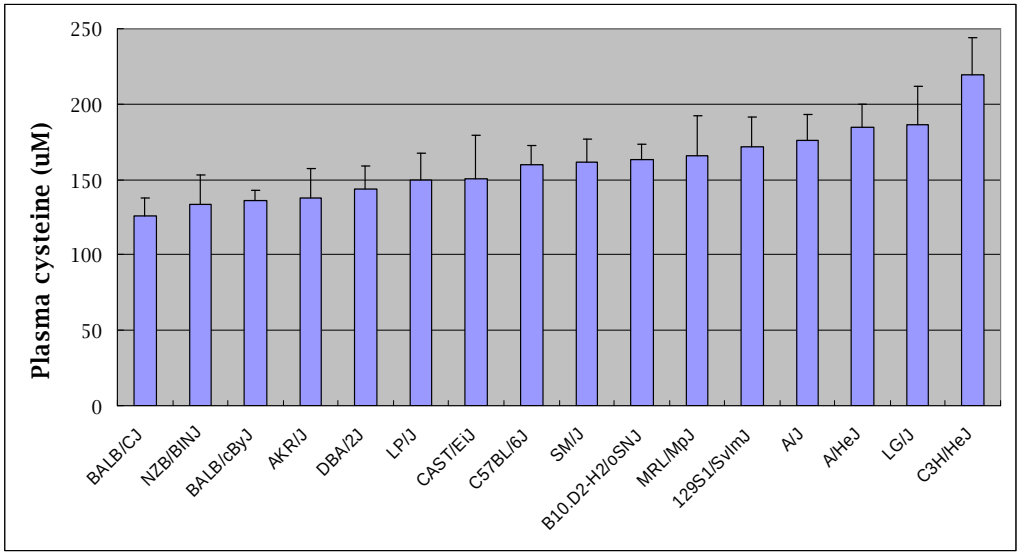

Figure 4-5. Average plasma cysteine levels of inbred mouse strains. Mouse strains are ordered in terms of average plasma cysteine levels from the lowest to the highest.

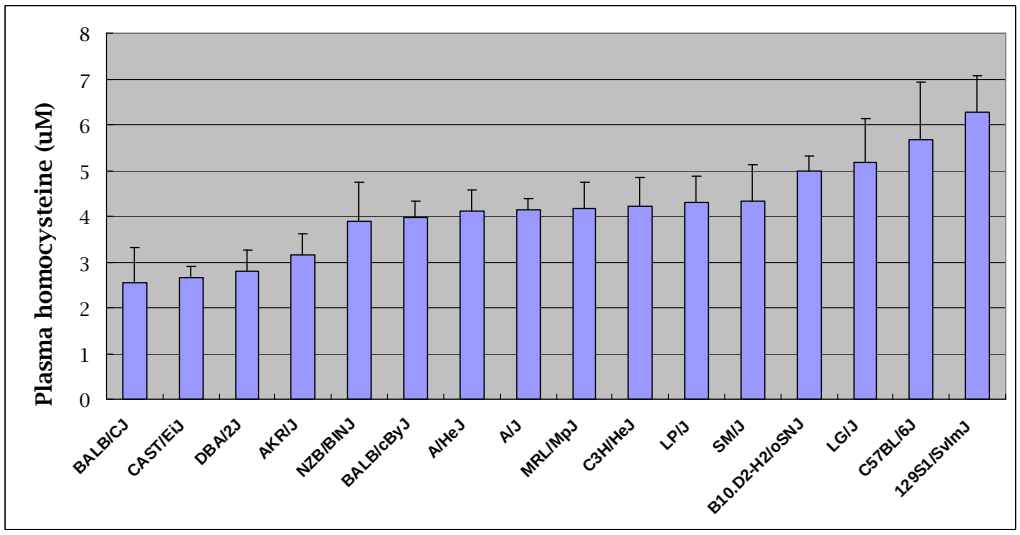

Figure 4-6. Average plasma homocysteine levels of inbred mouse strains. Mouse strains are ordered in terms of average plasma homocysteine levels from the lowest to the highest.

Strain name	Liver folate (nmol/g)	Plasma Cys (uM)	Plasma Hcy (uM)	Brain SAM (nmol/g)	Brain SAH (nmol/g)	Brain SAM/SAH	Liver SAM (nmol/g)	Liver SAH (nmol/g)	Liver SAM/SAH
129S1/SvImJ	27.6 ± 5.3	171.6 ± 19.6	6.3 ± 0.8	6.3 ± 1.1	5.9 ± 0.9	1.1 ± 0.1	6.7 ± 3.5	39.3 ± 10.0	0.2 ± 0.1
A/HeJ	22.0 ± 4.4	184.2 ± 15.2	4.1 ± 0.5	8.5 ± 0.5	8.3 ± 0.9	1.0 ± 0.2	20.1 ± 9.3	20.7 ± 8.0	0.9 ± 0.1
A/J	21.0 ± 4.3	175.7 ± 17.3	4.1 ± 0.3	9.0 ± 0.7	8.5 ± 0.9	1.1 ± 0.0	24.2 ± 5.5	26.1 ± 7.3	0.9 ± 0.1
AKR/J	29.0 ± 6.2	137.7 ± 19.6	3.1 ± 0.5	8.1 ± 1.1	7.3 ± 1.3	1.1 ± 0.1	25.1 ± 1.3	27.0 ± 3.7	0.9 ± 0.1
B10.D2-H2/oSNJ	21.8 ± 6.7	163.5 ± 10.2	5.0 ± 0.3	8.5 ± 0.8	5.9 ± 0.8	1.5 ± 0.2	22.2 ± 7.6	23.6 ± 10.6	1.0 ± 0.2
BALB/cByJ	15.5 ± 4.6	136.4 ± 6.7	4.0 ± 0.3	8.7 ± 0.7	7.5 ± 1.0	1.2 ± 0.1	23.2 ± 2.7	29.7 ± 5.3	0.8 ± 0.1
BALB/CJ	25.5 ± 4.4	125.5 ± 12.6	2.5 ± 0.8	8.8 ± 1.4	8.8 ± 2.1	1.0 ± 0.1	22.1 ± 2.6	29.4 ± 4.7	0.8 ± 0.1
C3H/HeJ	25.6 ± 4.9	219.0 ± 25.2	4.2 ± 0.6	7.7 ± 0.5	6.1 ± 0.8	1.3 ± 0.1	30.6 ± 3.5	23.5 ± 1.4	1.3 ± 0.1
C57BL/6J	18.6 ± 4.7	159.8 ± 13.1	5.7 ± 1.3	8.8 ± 0.5	7.8 ± 0.7	1.1 ± 0.1	28.1 ± 7.7	32.1 ± 7.9	0.9 ± 0.0
CAST/EiJ	24.2 ± 1.7	150.1 ± 29.0	2.7 ± 0.2	9.4 ± 0.6	7.5 ± 1.2	1.3 ± 0.3	12.3 ± 2.7	35.9 ± 12.5	0.4 ± 0.1
DBA/2J	17.5 ± 2.2	143.4 ± 15.6	2.8 ± 0.5	8.7 ± 0.6	6.2 ± 1.6	1.5 ± 0.4	24.3 ± 2.6	17.4 ± 1.4	1.4 ± 0.1
LG/J	19.0 ± 1.9	186.5 ± 25.3	5.2 ± 1.0	8.8 ± 0.7	7.4 ± 0.7	1.2 ± 0.2	25.7 ± 5.1	31.7 ± 7.3	0.8 ± 0.1
LP/J	17.3 ± 3.9	149.4 ± 18.0	4.3 ± 0.6	7.9 ± 0.5	5.4 ± 0.5	1.5 ± 0.1	25.4 ± 7.5	30.0 ± 5.7	0.9 ± 0.2
MRL/MpJ	25.2 ± 4.9	165.7 ± 26.8	4.2 ± 0.6	8.6 ± 0.6	7.2 ± 1.1	1.2 ± 0.1	25.4 ± 3.4	23.3 ± 1.8	1.1 ± 0.1
NZB/BINJ	26.6 ± 9.3	133.9 ± 18.8	3.9 ± 0.8	9.1 ± 1.3	6.7 ± 2.3	1.4 ± 0.3	26.7 ± 4.0	23.4 ± 4.0	1.2 ± 0.2
SM/J	23.8 ± 2.4	161.4 ± 15.1	4.3 ± 0.8	8.5 ± 1.0	7.7 ± 0.9	1.1 ± 0.1	17.0 ± 3.5	33.3 ± 7.4	0.5 ± 0.1

Table 4-1. Folate-related metabolites of inbred mouse strains.

Candidate gene identification

	Chr	Locus pos	-$\log_{10}$ P	Ref Seq	Possible Candidate Genes	Gene Symbol
Brain SAH	4	150189677	2.506378	NM_001081557	calmodulin binding transcription activator 1	**Camta1**
	7	46131980	2.638248	NM_013624	Otogelin	**Otog**
	18	65796254	2.628527	NM_207255	zinc finger protein 532	**Zfp532**
Brain SAM	4	150017483	2.119476	NM_001081557	calmodulin binding transcription activator 1	**Camta1**
	16	59876076	2.017381	NM_007938	Eph receptor A6	**Epha6**
Brain SAM/SAH	7	90226340	2.487707	NM_031394	synaptotagmin-like 2	**Sytl2**
	7	91018730	2.477615	NM_011807	discs, large homolog 2 (Drosophila)	**Dlg2**
	7	92630857	2.543373	NM_029494	RAB30, member RAS oncogene family	**Rab30**
	11	119885427	2.414834	NM_001109658	5-azacytidine induced gene 1	**Azi1**
Liver folate	11	6980681	2.280085	NM_009622	adenylate cyclase 1	**Adcy1**
	17	83126185	2.216386	NM_134117	protein kinase domain containing, cytoplasmic	**Pkdcc**
Liver SAH	1	23866357	2.533552	NM_028534	stromal membrane-associated protein 1	**Smap1**
	1	24195132	2.514326	NM_007740	collagen, type IX, alpha 1	**Col9a1**
	1	25057739	2.61805	NM_175642	brain-specific angiogenesis inhibitor 3	**Bai3**
	11	29037368	2.778504	NM_027869	polyribonucleotide nucleotidyltransferase 1	**Pnpt1**

Table 4-2. List of part of the genes in candidate regions found by SNP associated QTL mapping study. One SNP of one candidate gene for each region is shown.

QTL mapping was performed as described for each of 9 traits. Results are shown only for SNPs that exceed an arbitrarily set cutoff of association score (AS) >2.5 (or AS >2.0 if results showed no value above 2.5). Several genes in candidate regions are shown in Table 4-2. None of these has been previously identified as being relating to folate metabolism.

DISCUSSION

As previously described, there was a large phenotypic variation among MS/MTHFR double null mice in a mix background, even within siblings. In addition, difficulties were encountered when trying to backcross MS/MTHFR double mutant mice onto a pure C57BL/6 background. These evidences strongly suggested that genetic background has significant effects on folate metabolism, and this hypothesis was verified by this study. Mouse brain and liver SAM and SAH, plasma homocysteine and cysteine, liver and plasma total folate were measured in 16 inbred strains, and most of these 9 traits showed significant differences among strains.

Among the strains used in this study, 129S1/SvImJ mice are unique in folate metabolism; they have the highest hepatic folate, plasma homocysteine, hepatic SAH and the lowest SAM both in the brain and the liver, as well as the lowest hepatic SAM/SAH ratio and the differences between 129S1/SvImJ mice and the average levels of the other strains are very large. 129S1/SvImJ is a substrain of 129 mice, which were particularly important in creating gene knockout and other targeted mutant mice as these mice are often maintained on a mixture of C57BL/6 and a 129 strain. According to Jackson Laboratory Mouse Phenome Database, the 129S1/SvImJ mouse is exceptional in the following phenotypes among inbred strains: high levels of 3 major white blood cells, eosinophils, monocytes and neutrophils, high hematocrit and hemoglobin, high plasma HDL cholesterol, low serum phosphorous and sodium, etc. It is still unclear if any of these exceptions is related to the unique folate metabolism in 129S1/SvImJ mouse, but it is possible that this strain has a higher ability to absorb and store dietary folate which may results in the higher counts of hemocytes. On the other hand, historically, all 129 inbred mice are known for their higher incidence of spontaneous testicular teratomas (Simpson, 1997), which is possibly related to impaired methylation, as suggested by their extremely low SAM and SAM/SAH ratio.

A considerable variance was found in n hepatic SAM/SAH ratios among inbred strains, by contrast, brain SAM/SAH ratios fell into a relatively narrow range. Apparently, mouse brain has the ability to maintain stable methylation, which might be critical for its normal functions.

As previously stated, MTHFR and MS/MTHFR knockout mice had significantly greater levels of H-ferritin and hepcidin gene expression compared to wild type mice, which implies more iron storage in their body. This change in iron-related gene expression after knocking out folate-related genes led me to discover a relationship between iron and folate metabolism among inbred mouse strains. A regression analysis showed a significant negative linear correlation between individual liver SAM/SAH ratios and iron levels, but I did not find any correlation between liver folate and iron level, which suggests that iron homeostasis may be only related to methylation status but not folate storage.

We performed SNP associated QTL mapping of divergent folate metabolites between different mouse strains and identified some candidate regions associated with each trait. There were no well-known major genes involved in folate metabolism found in the study, which was not surprising because similar phenomena have been observed by other researches in different areas, for example, the loci that harbor known iron metabolism genes did not correlate with hepatic iron, according to a study by Dr. Seung-min Lee (unpublished data). The genes found here in candidate regions were not directly related to folate absorption, storage, conversion or utilization, which means they are more likely to be modifier genes of

folate metabolism. These results of QTL mapping need to be confirmed and further investigated by other approaches, such as microarray analysis and RT-PCR.

REFERENCES

Agamanolis, D.P., Chester, E.M., Victor, M., Kark, J.A., Hines, J.D., Harris, J.W. (1976) Neuropathology of experimental vitamin B12 deficiency in monkeys. *Neurology*. 26(10):905-14.

Amur, S.G., Shanker, G., Cochran, J.M., Ved, H.S., Pieringer, R.A. (1986) Correlation between inhibition of myelin basic protein (arginine) methyltransferase by sinefungin and lack of compact myelin formation in cultures of cerebral cells from embryonic mice. *J Neurosci Res.* 16(2):367-76.

Anand, P., Awasthi, S., Mahdi, A., Tiwari, M., Agarwal, G.G. (2009) Serum homocysteine in Indian adolescents. *Indian J Pediatr.* 76(7):705-9.

Baik, H.W., Russell, R.M. (1999) Vitamin B12 deficiency in the elderly. *Annu Rev Nutr.* 19:357-77.

Bailey, L.B., Gregory, J.F. (1999) Polymorphisms of methylenetetrahydrofolate reductase and other enzymes: metabolic significance, risks and impact on folate requirement. *J Nutr.* 129(5):919-22.

Barth, J.L., Argraves, W.S. (2001) Cubilin and megalin: partners in lipoprotein and vitamin metabolism. *Trends Cardiovasc Med.* 11(1):26-31.

Baumann, N., Pham-Dinh, D. (2001) Biology of oligodendrocyte and myelin in the mammalian central nervous system. *Physiol Rev.* 81(2):871-927.

Beck, J.A., Lloyd, S., Hafezparast, M., Lennon-Pierce, M., Eppig, J.T., Festing, M.F., Fisher, E.M. (2000) Genealogies of mouse inbred strains. *Nat Genet.* 24(1):23-5.

Bird, A. (1992) The essentials of DNA methylation. *Cell.* 70(1):5-8.

Blount, B.C., Ames, B.N. (1994) Analysis of uracil in DNA by gas chromatography-mass spectrometry. *Anal Biochem.* 219(2):195-200.

Bonyadi, M., Rusholme, S.A., Cousins, F.M., Su, H.C., Biron, C.A., Farrall, M., Akhurst, R.J. (1997) Mapping of a major genetic modifier of embryonic lethality in TGF beta 1 knockout mice. *Nat. Genet.* 15(2): 207–11.

Bottiglieri, T. (2005) Homocysteine and folate metabolism in depression. *Prog Neuropsychopharmacol Biol Psychiatry.* 29(7):1103-12.

Bottiglieri, T., Hyland, K. (1994) S-adenosylmethionine levels in psychiatric and neurological disorders: a review. *Acta Neurol Scand Suppl.* 154:19-26.

Brattstrom, L., Wilcken, D.E., Ohrvik, J., Brudin, L. (1998) Common methylenetetrahydrofolate reductase gene mutation leads to hyperhomocysteinemia but not to vascular disease: the result of a meta-analysis. *Circulation.* 98(23):2520-6.

Bunge, M.B., Schilling, R.F., Schloesser, L.L. (1956) Intrinsic factor studies. IV. Selective absorption and binding of cyanocobalamin by gastric juice in the presence of excess pseudovitamin B12 or 5, 6-dimethylbenzimidazole. *J Lab Clin Med.* 48(5):735-44.

Butler, M.G., Joseph, G.M., Rames, L.J., Cacheiro, N., Lozzio, C.B. (1988) Chromosome breakage in control and fragile X subjects using folate-deficient culture conditions. *Hum Genet.* 78(4):383.

Butterworth, C.E. Jr, Bendich, A. (1996) Folic acid and the prevention of birth defects. *Annu Rev Nutr.* 16:73-97.

Chen, L., Qi, H., Korenberg, J., Garrow, T.A., Choi, Y.J., Shane, B. (1996) Purification and properties of human cytosolic folylpoly-gamma-glutamate synthetase and organization, localization, and differential splicing of its gene. *J Biol Chem.* 271(22):13077-87.

Chen, L.H., Liu, M.L., Hwang, H.Y., Chen, L.S., Korenberg, J., Shane, B. (1997) Human methionine synthase. cDNA cloning, gene localization, and expression. *J Biol Chem.* 272(6):3628-34.

Chen, Z., Ge, B., Hudson, T.J., Rozen, R. (2002) Microarray analysis of brain RNA in mice with methylenetetrahydrofolate reductase deficiency and hyperhomocysteinemia. *Brain Res Gene Expr Patterns.* 1(2):89-93.

Chen, Z., Karaplis, A.C., Ackerman, S.L., Pogribny, I.P., Melnyk, S., Lussier-Cacan, S., Chen, M.F., Pai, A., John, S.W., Smith, R.S., Bottiglieri, T., Bagley, P., Selhub, J., Rudnicki, M.A., James, S.J., Rozen, R. (2001) Mice deficient in methylenetetrahydrofolate reductase exhibit hyperhomocysteinemia and decreased methylation capacity, with neuropathology and aortic lipid deposition. *Hum Mol Genet.* 10(5):433-43.

Chen, Z., Schwahn, B.C., Wu, Q., He, X., Rozen, R. (2005) Postnatal cerebellar defects in mice deficient in methylenetetrahydrofolate reductase. *Int J Dev Neurosci.* 23(5):465-74.

Christensen, K.E., MacKenzie, R.E. (2006) Mitochondrial one-carbon metabolism is adapted to the specific needs of yeast, plants and mammals. *Bioessays.* 28(6):595-605.

Cook, R.J., Blair, J.A. (1979) The distribution and chemical nature of radioactive folates in rat liver cells and rat liver mitochondria. *Biochem J.* 178(3):651-9.

Cooper, D.N., Krawczak, M. (1989) Cytosine methylation and the fate of CpG dinucleotides in vertebrate genomes. *Hum Genet.* 83(2):181-8.

Devlin, A.M., Ling, E.H., Peerson, J.M., Fernando, S., Clarke, R., Smith, A.D., Halsted, C.H. (2000) Glutamate carboxypeptidase II: a polymorphism associated with lower levels of serum folate and hyperhomocysteinemia. *Hum Mol Genet.* 9(19):2837-44.

Dinn, J.J., McCann, S., Wilson, P., Reed, B., Weir, D., Scott, J. (1978) Animal model for subacute combined degeneration. *Lancet.* 2(8100):1154.

Duffield, M.S., Phillips, J.I., Vieira-Makings, E., Van der Westhuyzen, J., Metz, J. (1990) Demyelinisation in the spinal cord of vitamin B12 deficient fruit bats. *Comp Biochem Physiol C.* 96(2):291-7.

Durand, P., Fortin, L.J., Lussier-Cacan, S., Davignon, J., Blache, D. (1996) Hyperhomocysteinemia induced by folic acid deficiency and methionine load--applications of a modified HPLC method. *Clin Chim Acta.* 252(1):83-93.

Fell, D., Benjamin, L.E., Steele, R.D. (1985) Determination of adenosine and S-adenosyl derivatives of sulfur amino acids in rat liver by high-performance liquid chromatography.J *Chromatogr.* 345(1):150-6.

Festen, H.P. (1991) Intrinsic factor secretion and cobalamin absorption: Physiology and pathophysiology in the gastrointestinal tract. *Scand J Gastroenterol Suppl.* 188:1-7.

Finnell, R.H., Wlodarczyk, B.C., Craig, J.C., Piedrahita, J.A., Bennett, G.D. (1997) Strain-dependent alterations in the expression of folate pathway genes following teratogenic exposure to valproic acid in a mouse model. *Am J Med Genet.* 70(3):303-11.

Flint, J., Valdar, W., Shifman, S., Mott, R. (2005) Strategies for mapping and cloning quantitative trait genes in rodents. *Nat Rev Genet.* 6(4):271-86.

Foo, S.K., Shane, B. (1982) Regulation of folylpoly-gamma-glutamate synthesis in mammalian cells. In vivo and in vitro synthesis of pteroylpoly-gamma-glutamates by Chinese hamster ovary cells. *J Biol Chem.* 257(22): 13587-92.

Frenkel, E.P., Kitchens, R.L., Hersh, L.B., Frenkel, R. (1974) Effect of vitamin B12 deprivation on the in vivo levels of coenzyme A intermediates associated with propionate metabolism. *J Biol Chem.* 249(21):6984-91.

Frenkel, E.P., Prough, R., Kitchens, R.L. (1980) Measurement of tissue vitamin B12 by radioisotopic competitive inhibition assay and quantitation of tissue cobalamin fractions. *Methods Enzymol.* 67:31-40.

Ge, F., Yao, J., Fu, X., Guo, Z., Yan, J., Zhang, B., Zhang, H., Tomozawa, H., Miyazaki, J., Sawashita, J., Mori, M., Higuchi, K. (2007) Amyloidosis in transgenic mice expressing murine amyloidogenic apolipoprotein A-II (Apoa2c). *Lab Invest.* 87(7):633-43.

Gobin, S.J., Montagne, L., Van Zutphen, M., Van Der Valk, P., Van Den Elsen, P.J., De Groot, C.J. (2001) Upregulation of transcription factors controlling MHC expression in multiple sclerosis lesions. *Glia.* 36(1):68-77.

Goode, E.L., Potter, J.D., Bigler, J., Ulrich, C.M. (2004) Methionine synthase D919G polymorphism, folate metabolism, and colorectal adenoma risk. *Cancer Epidemiol Biomarkers Prev.* 13(1):157-62.

Gregory, J.F., Cuskelly, G.J., Shane, B., Toth, J.P., Baumgartner, T.G., Stacpoole, P.W. (2000) Primed-constant infusion with [2H3]serine allows in vivo measurement of serine turnover, homocysteine remethylation, and transsulfuration processes in human one-carbon metabolism. *Am J Clin Nutr.* 72(6):1535-41.

Gueant, J.L., Gueant-Rodriguez, R.M., Anello, G., Bosco, P., Brunaud, L., Romano, C., Ferri, R., Romano, A., Candito, M., Namour, B. (2003) Genetic determinants of folate and vitamin B12 metabolism: a common pathway in neural tube defect and Down syndrome? *Clin Chem Lab Med.* 41(11):1473-7.

Harjai, K.J. (1999) Potential new cardiovascular risk factors: left ventricular hypertrophy, homocysteine, lipoprotein(a), triglycerides, oxidative stress, and fibrinogen. *Ann Intern Med.* 131(5):376-86.

Healton, E.B., Savage, D.G., Brust, J.C.M., Garrett, T.J., Lindenbaum, J. (1991) Neurologic aspects of cobalamin deficiency. *Medicine.* 70(4):229-45.

Herbert, V., Zalusky, R. (1962) Interrelations of vitamin B12 and folic acid metabolism: folic acid clearance studies. *J Clin Invest.* 41:1263-76.

Hitchings, G.H., Burchall, J.J. (1965) Inhibition of folate biosynthesis and function as a basis for chemotherapy. *Adv Enzymol Relat Areas Mol Biol.* 27:417-68.

Ho, H.Z., Glahn, T.J., Ho, J.C. (1988) The fragile-X syndrome. *Dev Med Child Neurol.* 30(2):257-61.

Hoag, W.G. (1964) Animal control for inbred mouse colonies of the Jackson Laboratory. *Lab Anim Care.* 14:253-9.

Hoffbrand, A.V., Weir, D.G. (2001) The history of folic acid. *Br J Haematol.* 113(3):579-89.

Jacobs, A. (1959) Evolution of modern medicine: pernicious anemia, 1822-1929. *AMA Arch Intern Med.* 103(2):329-33.

Jurevics, H., Hostettler, J., Muse, E.D., Sammond, D.W., Matsushima, G.K., Toews, A.D., Morell, P. (2001) Cerebroside synthesis as a measure of the rate of remyelination following cuprizone-induced demyelination in brain. *J Neurochem.* 77(4):1067-76.

Kawata, T., Funada, U., Wada, M., Matsushita, M., Sanai, T., Yamada, H., Kuwamori, M., Arai, K., Yamamoto, Y., Tanaka, N., Tadokoro, T., Maekawa, A. (2004) Breeding severely vitamin B12-deficient mice as model animals. *Int J Vitam Nutr Res.* 74(1):57-63.

Kim, J.S., Lee, H., Kim, H., Shim, Y.M., Han, J., Park, J., Kim, D.H. (2004) Promoter methylation of retinoic acid receptor beta 2 and the development of second primary lung cancers in non-small-cell lung cancer. *J Clin Oncol.* 22(17):3443-50.

Kim, Y.I. (2009) Role of the MTHFR polymorphisms in cancer risk modification and treatment. *Future Oncol.* 5(4):523-42.

Knock, E., Deng, L., Wu, Q., Lawrance, A.K., Wang, X.L., Rozen, R. (2008) Strain differences in mice highlight the role of DNA damage in neoplasia induced by low dietary folate. *J Nutr.* 138(4):653-8.

Korstanje, R., Paigen, B. (2002) From QTL to gene: the harvest begins. *Nat Genet.* 31(3):235-6.

Kutzbach, C., Stokstad, E.L. (1967) Feedback inhibition of methylene-tetrahydrofolate reductase in rat liver by S-adenosylmethionine. *Biochim Biophys Acta.* 139(1):217-20.

Lentz, S.R. (2005) Mechanisms of homocysteine-induced atherothrombosis. *J Thromb Haemost.* 3(8):1646-54.

Li, E., Beard, C., Jaenisch, R. (1993) Role for DNA methylation in genomic imprinting. *Nature.* 366(6453):362-5.

Locksmith, G.J., Duff, P. (1998) Preventing neural tube defects: the importance of periconceptional folic acid supplements. *Obstet Gynecol.* 91(6):1027-34.

Lövblad, K., Ramelli, G., Remonda, L., Nirkko, A.C., Ozdoba, C. Schroth, G. (1997) Retardation of myelination due to dietary vitamin B12 deficiency: cranial MRI findings. *Pediatr Radiol.* 27(2):155–8.

Lumb, M., Sharer, N., Deacon, R., Jennings, P., Purkiss, P., Perry, J., Chanarin, I. (1983) Effects of nitrous oxide-induced inactivation of cobalamin on methionine and S-adenosylmethionine metabolism in the rat. *Biochim Biophys Acta.* 756(3):354-9.

Macallan, D.C., Fullerton, C.A., Neese, R.A., Haddock, K., Park, S.S., Hellerstein, M.K. (1998) Measurement of cell proliferation by labeling of DNA with stable isotope-labeled glucose: studies in vitro, in animals, and in humans. *Proc Natl Acad Sci U S A.* 95(2):708-13.

Matthews, R.G., Elmore, C.L. (2007) Defects in homocysteine metabolism: diversity among hyperhomocyst(e)inemias. *Clin Chem Lab Med.* 45(12):1700-3.

McCarthy, E.A., Titus, S.A., Taylor, S.M., Jackson-Cook, C., Moran, R.G. (2004) A mutation inactivating the mitochondrial inner membrane folate transporter creates a glycine requirement for survival of chinese hamster cells. *J Biol Chem.* 279(32): 33829-36.

McGing, P.G., Scott, J.M. (1981) Evidence that the decreased liver folate status following vitamin B-12 inactivation in the mouse is due to increased loss rather than impaired uptake. *Biochim Biophys Acta.* 673(4):594-7.

McTigue, D.M., Tripathi, R.B. (2008) The life, death, and replacement of oligodendrocytes in the adult CNS. *J Neurochem.* 107(1):1-19.

Metz, J. (1992) Cobalamin deficiency and the pathogenesis of nervous system disease. *Annu Rev Nutr.* 12:59-79.

Metz, J., Kelly, A., Swett, V.C., Waxman, S., Herbert, V. (1968) Deranged DNA synthesis by bone marrow from vitamin B-12-deficient humans. *Br J Haematol.* 14(6):575-92.

Minot, G.R., Murphy, W.P. (1983) Landmark article (JAMA 1926). Treatment of pernicious anemia by a special diet. By George R. Minot and William P. Murphy. *JAMA.* 250(24):3328-35.

Mitchell, H.K., Snell, E.E., Williams, R.J. (1941) The concentration of “folic acid”. *J Am Chem Soc.* 63(8): 2284-5.

Moore, K.J., Nagle, D.L. (2000) Complex trait analysis in the mouse: The strengths, the limitations and the promise yet to come. *Annu Rev Genet.* 34:653-86.

Murao, K., Kubo, Y., Ohtani, N., Hara, E., Arase, S. (2006) Epigenetic abnormalities in cutaneous squamous cell carcinomas: frequent inactivation of the RB1/p16 and p53 pathways. *Br J Dermatol.* 155(5):999-1005.

Nave, K.A. (1994) Neurological mouse mutants and the genes of myelin. *J Neurosci Res.* 38(6):607-12.

Nockolds, C.K., Ramaseshan, S., Waters, T.N., Waters, J.M., Hodgkin, D.C. (1967) Structure of a monocarboxylic acid derivative of vitamin B12. Crystal and molecular structure from x-ray analysis. *Nature.* 214(5084):129-30.

Noronha, J.M., Silverman, M. (1962) On folic acid, vitamin B12, methionine, and formiminoglutamate metabolism. In *Vitamin B12 and Intrinsic Factor, 2nd Eur. Symp.*, ed. H. C. Heinrich, pp. 728-36. Stuttgart: Ferdinand Enke.

Obeid, R., Herrmann, W. (2006) Mechanisms of homocysteine neurotoxicity in neurodegenerative diseases with special reference to dementia. *FEBS Lett.* 580(13):2994-3005.

Oppenheim, E.W., Adelman, C., Liu, X., Stover, P.J. (2001) Heavy chain ferritin enhances serine hydroxymethyltransferase expression and de novo thymidine biosynthesis. *J Biol Chem.* 276(23):19855-61.

Ouerhani, S., Oliveira, E., Marrakchi, R., Ben Slama, M.R., Sfaxi, M., Ayed, M., Chebil, M., Amorim, A., El Gaaied, A.B., Prata, M.J. (2007) Methylenetetrahydrofolate reductase and methionine synthase polymorphisms and risk of bladder cancer in a Tunisian population. *Cancer Genet Cytogenet* . 176(1):48-53.

Patel, H., Di Pietro, E., MacKenzie, R.E. (2003). Mammalian fibroblasts lacking mitochondrial NAD -dependent methylenetetrahydrofolate dehydrogenase-cyclohydrolase are glycine auxotrophs. *J Biol Chem.* 278(21): 19436–41.

Pereira, T.V., Rudnicki, M., Pereira, A.C., Pombo-de-Oliveira, M.S., Franco, R.F. (2006) 5,10-Methylenetetrahydrofolate reductase polymorphisms and acute lymphoblastic leukemia risk: a meta-analysis. *Cancer Epidemiol Biomarkers Prev.* 15(10):1956-63.

Peters, A. (2002) The effects of normal aging on myelin and nerve fibers: a review. *J Neurocytol.* 31(8-9):581-93.

Pezacka, E.H., Jacobsen, D.W., Luce, K., Green, R. (1992) Glial cells as a model for the role of cobalamin in the nervous system: impaired synthesis of cobalamin coenzymes in cultured human astrocytes following short-term cobalamindeprivation. *Biochem Biophys Res Commun.* 184(2): 832–9.

Pinhas-Hamiel, O., Doron-Panush, N., Reichman, B., Nitzan-Kaluski, D., Shalitin, S., Geva-Lerner, L. (2006) Obese children and adolescents: a risk group for low vitamin B12 concentration. *Arch Pediatr Adolesc Med.* 160(9):933-6.

Quadros, E.V., Nakayama, Y., Sequeira, J.M. (2009) The protein and the gene encoding the receptor for the cellular uptake of transcobalamin-bound cobalamin. *Blood.* 13(1):186-92.

Rader, J.I. (2002) Folic acid fortification, folate status and plasma homocysteine. *J Nutr.* 132(8 Suppl):2466S-2470S.

Rasmussen, K.M., Hayes, K.C., Thenen, S.W. (1982) Megaloblastic anemia and the requirement for folic acid in the cebus monkey (Cebus albifrons). *Am J Primatol.* 2(1):87-97.

Reeves, P.G. (1997) Components of the AIN-93 diets as improvements in the AIN-76A diet. *J Nutr.* 127(5 Suppl):838S-841S.

Reidy, J.A. (1988) Role of deoxyuridine incorporation and DNA repair in the expression of human chromosomal fragile sites. *Mutat Res.* 200(1-2):215-20.

Reynolds, E.H., Bottiglieri, T., Laundy, M., Crellin, R.F., Kirker, S.G. (1992) Vitamin B12 metabolism in multiple sclerosis. *Arch Neurol.* 49(6):649-52.

Robscheit-Robbins, F.S., Whipple, G.H. (1929) Blood regeneration in severe anemia: XIV. A Liver fraction potent in pernicious anemia fed alone and combined with whole liver, liver ash and fresh bile. *J Exp Med.* 49(2):215-27.

Rosenberg, I.H. (1976) Absorption and malabsorption of folates. *Clin Haematol.* 5(3):589-618.

Rosenblatt, D.S., Cooper, B.A. (1989) Selective deficiencies of methyl-B12 (cblE and cblG). *Clin Invest Med.* 12(4):270-1.

Rosenblatt, D.S., Cooper, B.A. (1990) Inherited disorders of vitamin B12 utilization. *Bioessays.* 12(7):331-4.

Roth, J.R., Lawrence, J.G., Bobik, T.A. (1996) Cobalamin (coenzyme B12): synthesis and biological significance. *Annu Rev Microbiol.* 50:137-81.

Rozen, R. (1996) Molecular genetics of methylenetetrahydrofolate reductase deficiency. *J Inherit Metab Dis.* 19(5):589-94.

Russell-Jones, G.J., Alpers, D.H. (1999) Vitamin B12 transporters. *Pharm Biotechnol.* 12:493-520.

Salazar, M.D., Ratnam, M. (2007) The folate receptor: what does it promise in tissue-targeted therapeutics? *Cancer Metastasis Rev.* 26(1): 141-52.

Sanderson, P., Stone, E., Kim, Y.I., Mathers, J.C., Kampman, E., Downes, C.S., Muir, K.R., Baron, J.A. (2007) Folate and colo-rectal cancer risk. *Br J Nutr.* 98(6):1299-304.

Scalabrino, G., Monzio-Compagnoni, B., Ferioli, M.E., Lorenzini, E.C., Chiodini, E., Candiani, R. (1990) Subacute combined degeneration and induction of ornithine decarboxylase in spinal cords of totally gastrectomized rats. *Lab Invest.* 62(3):297-304.

Scalabrino, G., Buccellato, F.R., Tredici, G., Morabito, A., Lorenzini, E.C., Allen, R.H., Lindenbaum, J. (1997) Enhanced levels of biochemical markers for cobalamin deficiency in totally gastrectomized rats: uncoupling of the enhancement from the severity of spongy vacuolation in spinal cord. *Exp Neurol.* 144(2):258-65.

Schwahn, B.C., Laryea, M.D., Chen, Z., Melnyk, S., Pogribny, I., Garrow, T., James, S.J., Rozen, R. (2004) Betaine rescue of an animal model with methylenetetrahydrofolate reductase deficiency. *Biochem J.* 382(Pt 3):831-40.

Seetharam, B., Yammani, R.R. (2003) Cobalamin transport proteins and their cell-surface receptors. *Expert Rev Mol Med.* 5(18):1-18.

Selhub, J. (2008) Public health significance of elevated homocysteine. *Food Nutr Bull.* 29(2 Suppl):S116-25.

Sellers, T.A., Kushi, L.H., Cerhan, J.R., Vierkant, R.A., Gapstur, S.M., Vachon, C.M., Olson, J.E., Therneau, T.M., Folsom, A.R. (2001) Dietary folate intake, alcohol, and risk of breast cancer in a prospective study of postmenopausal women. *Epidemiology.* 12(4):420-8.

Serra-Grabulosa, J.M., Salgado-Pineda, P., Junqué, C., Solé-Padullés, C., Moral, P., López-Alomar, A., López, T., López-Guillén, A., Bargalló, N., Mercader, J.M., Clemente, I.C., Bartrés-Faz, D. (2003) Apolipoproteins E and C1 and brain morphology in memory impaired elders. *Neurogenetics.* 4(3):141-6.

Shane, B. (1989) Folylpolyglutamate synthesis and role in the regulation of one-carbon metabolism. *Vitam Horm.* 45:263-335.

Sheikh, N., Dudas, J., Ramadori, G. (2007) Changes of gene expression of iron regulatory proteins during turpentine oil-induced acute-phase response in the rat. *Lab Invest.* 87(7):713-25.

Simpson, E.M., Linder, C.C., Sargent, E.E., Davisson, M.T., Mobraaten, L.E., Sharp, J.J. (1997) Genetic variation among 129 substrains and its importance for targeted mutagenesis in mice. *Nat Genet.* 16(1):19-27.

Sirotnak, F.M., Tolner, B. (1999) Carrier-mediated membrane transport of folates inmammalian cells. *Annu Rev Nutr.* 19: 91-122.

Small, D.H., Carnegie, P.R., Anderson, R.M. (1981) Cycloleucine-induced vacuolation of myelin is associated with inhibition of protein methylation. *Neurosci Lett.* 21(3):287-92.

Smith, B.T., Mussell, J.C., Fleming, P.A., Barth, J.L., Spyropoulos, D.D., Cooley, M.A., Drake, C.J., Argraves, W.S. (2006) Targeted disruption of cubilin reveals essential developmental roles in the structure and function of endoderm and in somite formation. *BMC Dev Biol.* 6:30.

Solomons, N.W. (2007) Food fortification with folic acid: has the other shoe dropped? *Nutr Rev.* 65(11):512-5.

Sourial, N.A., Waters, A.H. (1992) Effect of pH on binding of B12 to IF and R-protein. *Br J Haematol.* 81(1):136-8.

Stover, P., Schirch, V. (1991) 5-Formyltetrahydrofolate polyglutamates are slow tight binding inhibitors of serine hydroxymethyltransferase. *J Biol Chem.* 266(3):1543-50.

Strong, L.C. (1942) The origin of some inbred mice. *Cancer Res.* 2: 531-9.

Suleiman, S.A., Spector, R. (1982) Identification, development, and regional distribution of thymidylate synthetase in adult rabbit brain. *J Neurochem.* 38(2):392-6.

Supić, G., Kozomara, R., Branković-Magić, M., Jović, N., Magić, Z. (2009) Gene hypermethylation in tumor tissue of advanced oral squamous cell carcinoma patients. *Oral Oncol.* Aug 7. [Epub ahead of print]

Swanson, D.A., Liu, M.L., Baker, P.J., Garrett, L., Stitzel, M., Wu, J., Harris, M., Banerjee, R., Shane, B., Brody, L.C. (2001) Targeted disruption of the methionine synthase gene in mice. *Mol Cell Biol.* 21(4):1058-65.

Tan, J.C., Burns, D.L., Jones, H.R. (2006) Severe ataxia, myelopathy, and peripheral neuropathy due to acquired copper deficiency in a patient with history of gastrectomy. *J Parenter Enteral Nutr.* 30(5):446-50.

Toffolon, E.P., Goldfinger, S.E. (1974) Malabsorption following gastrectomy and ileal resection. *Surg Clin North Am.* 54(3):647-53.

Toohey, J.I. (2006) Vitamin B12 and methionine synthesis: a critical review. Is nature's most beautiful cofactor misunderstood? *Biofactors.* 26(1):45-57.

Trabetti, E. (2008) Homocysteine, MTHFR gene polymorphisms, and cardio-cerebrovascular risk. *J Appl Genet.* 49(3):267-82.

van der Linden, I.J., Afman, L.A., Heil, S.G., Blom, H.J. (2006) Genetic variation in genes of folate metabolism and neural-tube defect risk. *Proc Nutr Soc.* 65(2):204-15.

Veber, D., Mutti, E., Tacchini, L., Gammella, E., Tredici, G., Scalabrino, G. (2008) Indirect down-regulation of nuclear NF-kappaB levels by cobalamin in the spinal cord and liver of the rat. *J Neurosci Res.* 86(6):1380-7.

Wagner, C., Briggs, W.T., Cook, R.J. (1985) Inhibition of glycine N-methyltransferase by folate derivatives: implications for regulation of methyl group metabolism. *Biochem Biophys Res Commun.* 127(3):746-52.

Webster, K.E., O'Bryan, M.K., Fletcher, S., Crewther, P.E., Aapola, U., Craig, J., Harrison, D.K., Aung, H., Phutikanit, N., Lyle, R., Meachem, S.J., Antonarakis, S.E., de Kretser, D.M., Hedger, M.P., Peterson, P., Carroll, B.J., Scott, H.S. (2005) Meiotic and epigenetic defects in Dnmt3L-knockout mouse spermatogenesis. *Proc Natl Acad Sci U S A.* 102(11):4068-73.

Weir, D.G., Keating, S., Molloy, A., McPartlin, J., Kennedy, S., Blanchflower, J., Kennedy, D.G., Rice, D., Scott, J.M. (1988) Methylation deficiency causes vitamin B12-associated neuropathy in the pig. *J Neurochem.* 51(6):1949-52.

Whitehead, V.M. (2006) Acquired and inherited disorders of cobalamin and folate in children. *Br J Haematol.* 134(2):125-36.

Whittingham, S., Mackay, I.R. (2005) Autoimmune gastritis: historical antecedents, outstanding discoveries, and unresolved problems. *Int Rev Immunol.* 24(1-2):1-29.

Wilson, S.D., Horne, D.W. (1984) High-performance liquid chromatographic determination of the distribution of naturally occurring folic acid derivatives in rat liver. *Anal Biochem.* 142(2):529-35.

Woeller, C.F., Anderson, D.D., Szebenyi, D.M., Stover, P.J. (2007) Evidence for small ubiquitin-like modifier-dependent nuclear import of the thymidylate biosynthesis pathway. *J Biol Chem.* 282(24):17623-31.

Yamada, K., Kawata, T., Wada, M., Mori, K., Tamai, H., Tanaka, N., Tadokoro, T., Tobimatsu, T., Toraya, T., Maekawa, A. (2007) Testicular injury to rats fed on soybean protein-based vitamin B12-deficient diet can be reduced by methionine supplementation. *J Nutr Sci Vitaminol.* 53(2): 95-101.

Zhao, R., Matherly, L.H., Goldman, I.D. (2009) Membrane transporters and folate homeostasis: intestinal absorption and transport into systemic compartments and tissues. *Expert Rev Mol Med.* 11:e4.